AB INITIO STUDIES OF PHOSPHOLIPID HEADGROUPS

WEN LI

AB INITIO STUDIES OF PHOSPHOLIPID HEADGROUPS

By

Wen Li

M. Sc., Memorial University of Newfoundland

A thesis submitted to the School of Graduate Studies in partial fulfillment of the requirements for the degree of Master of Physics

Department of Physics

Memorial University of Newfoundland

October, 1995

Abstract

The thesis consists of two distinct but closely related parts. In the first part we present a systematic conformational study of the stable headgroup structures for phospholipid single molecule using five model compounds: $CH_3PO_4^-CH_3$, $CH_3CH_2PO_4^-CH_2CH_3$, $CH_3CH_2PO_4^-CH_2CH_2NH_3^+$ (phosphorylethanolamine, PE, with methyl end group), glycerophosphorylethanolamine (GPE) and glycerophosphorylcholine (GPC). The potential energy scans and the fully geometry optimized structures were obtained using the molecular orbital program Gaussian 92. The changes in geometrical parameters and conformational energy differences due to the usage of different basis sets (STO-3G, 3-21G*, 6-31G* and 6-31+G*) were investigated. Since $3-21G^*$ and $6-31G^*$ basis sets gave similar results, $3-21G^*$ basis set was chosen for our calculations. The comparison was made between the phospholipid structural parameters (such as molecular area, thickness of the polar region, thickness of the headgroup and dipole) obtained for the model compounds. In the second part of the thesis, the hydrated PE and GPE are investigated. The results show that the structures of PE and GPE are strongly dependent upon the hydration force. We also investigated the effect of hydration on other model compounds. We have studied the following (hydrated) model systems: PE + $4H_2O$, GPE + $6H_2O$ and 2PE + $4H_2O$. Direct comparisons of the calculated geometry parameters of compounds in the presence of water with the crystallographic results has been also presented. The geometrical parameters for hydrated molecules are closer to the crystallographic experimental data than those obtained for isolated molecules.

Acknowledgments

I am greatly thankful to my supervisor, Dr. J. B. Lagowski, for her valuable guidance, generous help, knowledgeable instruction and kind encouragement during the M.Sc. program and also for her much patient corrections during the completion of the thesis.

I would like to thank Dr. M. Morrow for helpful discussions and in particular for his suggestion to focus the M.Sc. research on studying the behavior of the membrane in the presence of water. Also I would like to thank Dr. Poirier for his advise regarding some of the theoretical aspects of this research especially at the initial stage of this project.

I am grateful to Dr. B. J. Yuan and Dr. D. Lu for their very valuable help and very kind encouragement. I would like to thank my fellow graduate students Mr. R. Power and Mr. Y. R. Kuang for their useful help.

I also want to thanks to my family and friends who gave me support and encouragement.

The author acknowledges the financial support from the Natural Sciences and Engineering Research Council of Canada (NSERC).

Table of Contents

List of Tables

List of Figures

Chapter 1

Introduction

Approximately one century ago, Overton found that lipids readily diffused across cellular membranes. He suggested that the cellular membranes contain lipid molecules[1]. In subsequent years, using different techniques, the lipids have been studied extensively. In 1940, Gorter and Grendel suggested that membrane lipids were organized into bilayers, with polar headgroups facing outwards. They also indicated that proteins were major structural components of membranes. A schematic of a bilayer and protein is illustrated in Figure 1.1[34].

In the physiological temperature range, lipid bilayers have two distinct phases[34]. The lower temperature gel phase (L_β phase) is highly ordered, has a lower surface area and a lower lipid mobility. In this phase, the hydrocarbon chains of the lipids are almost fully extended in the all-trans conformation. At higher temperature, the bilayer enters the partially ordered liquid crystal phase (liquid-crystalline phase or L_α phase). The L_α phase is characterized by an increase in the surface area and in the lipid mobility. The L_β and L_α phases are shown schematically in Figure 1.2.

Physiologically active biomembranes are observed only in the L_α phase. Therefore, the studies of the L_α phase and the phase transition from L_β to L_α phase are of most interest to scientists.

The intermolecular packing in both L_β and L_α phases partially depends on the interactions between the headgroups and the water molecules, which in turn form a hydrogen bonded network[3]. Some water molecules are directly hydrogen bonded to the headgroups. And some water molecules are hydrogen bonded to other water

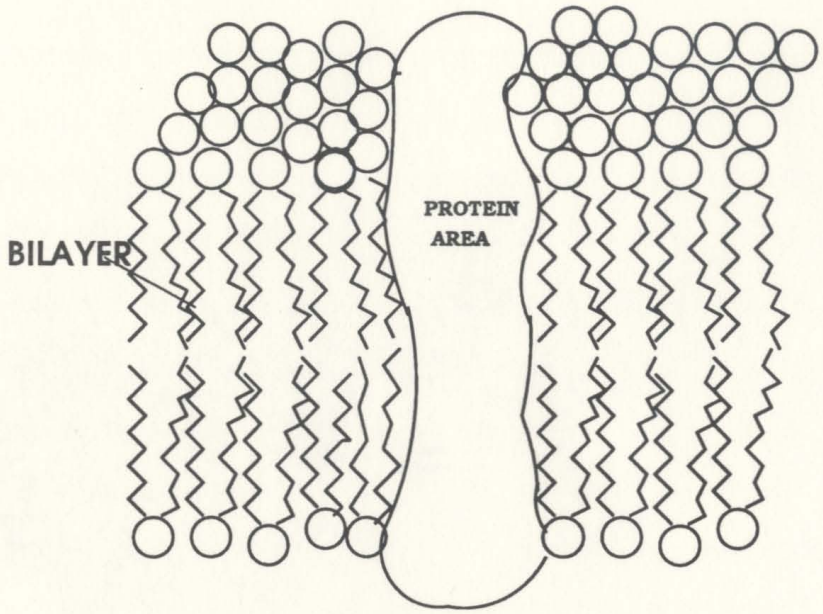

Figure 1.1 A qualitative model system containing bilayer and a protein.

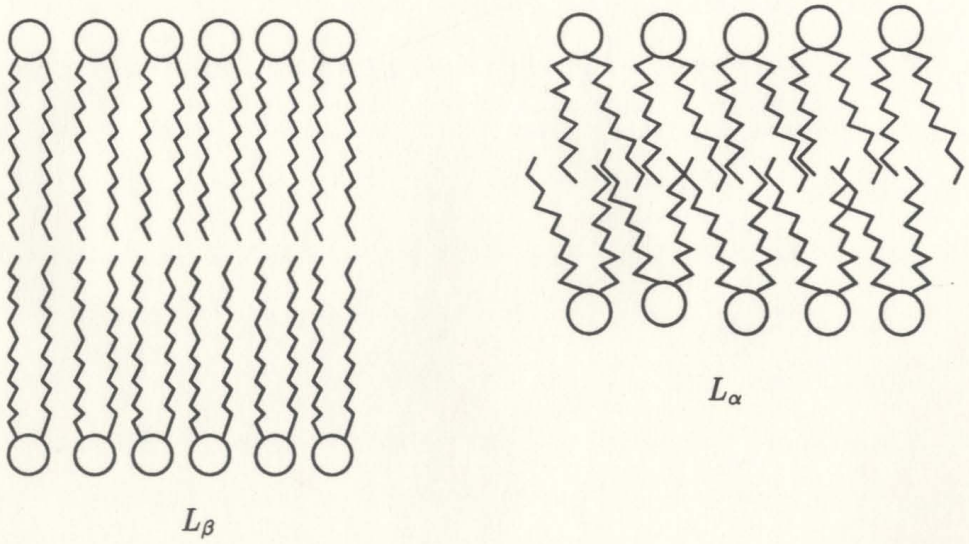

Figure 1.2 The membrane in L_α and L_β phases.

molecules in the interfacial regions in order to stabilize the linkages between the adjacent bilayers. The phase transition is determined by the structural characteristics of the lipids themselves, degree of hydration, temperature and other factors. The structural characteristics are in turn determined, in part, by the intrinsic conformational stability of single, isolated and hydrated phospholipid molecules and, in part, by the morphology of the larger scale assemblies (such as bilayers) that include the intermolecular interactions.

In this work, we focus on studying the structure and the intrinsic stability of single (or at most two), isolated or hydrated (with few water molecules) phospholipid molecules with two different headgroups using quantum mechanical methodology. In general, it is believed that the stable structure of a molecule is dominated by its intrinsic structure (that is, one that would be obtained for a single molecule in gas phase) even in the presence of other molecules. In other words, it is believed that, in most cases, the presence of intermolecular interactions would lead to small distortions in molecular structure relative to the isolated molecular structure. This work, in part, is an attempt to test this hypothesis for lipid systems with ab initio simulations. That is, one of the goals of this work is to determine whether ab initio calculations would model best possible conformations of phospholipids in real bilayers (liquid-crystalline state) or in crystals. We point out that calculated results can only be directly compared with crystalline structures since detailed liquid-crystalline structures are difficult to determined experimentally and are not readily available.

A chemical structure of phospholipids consists of two regions: hydrophobic polar headgroups and hydrophilic long hydrocarbon chains. The representative chemical structure of a typical phospholipid molecule is shown in Figure 1.3(a). Its structure is schematically displayed in Figure 1.3(b). The three dimensional (3D) structure is also shown in Figure 1.4. Following the notation in reference [4], the polar headgroup

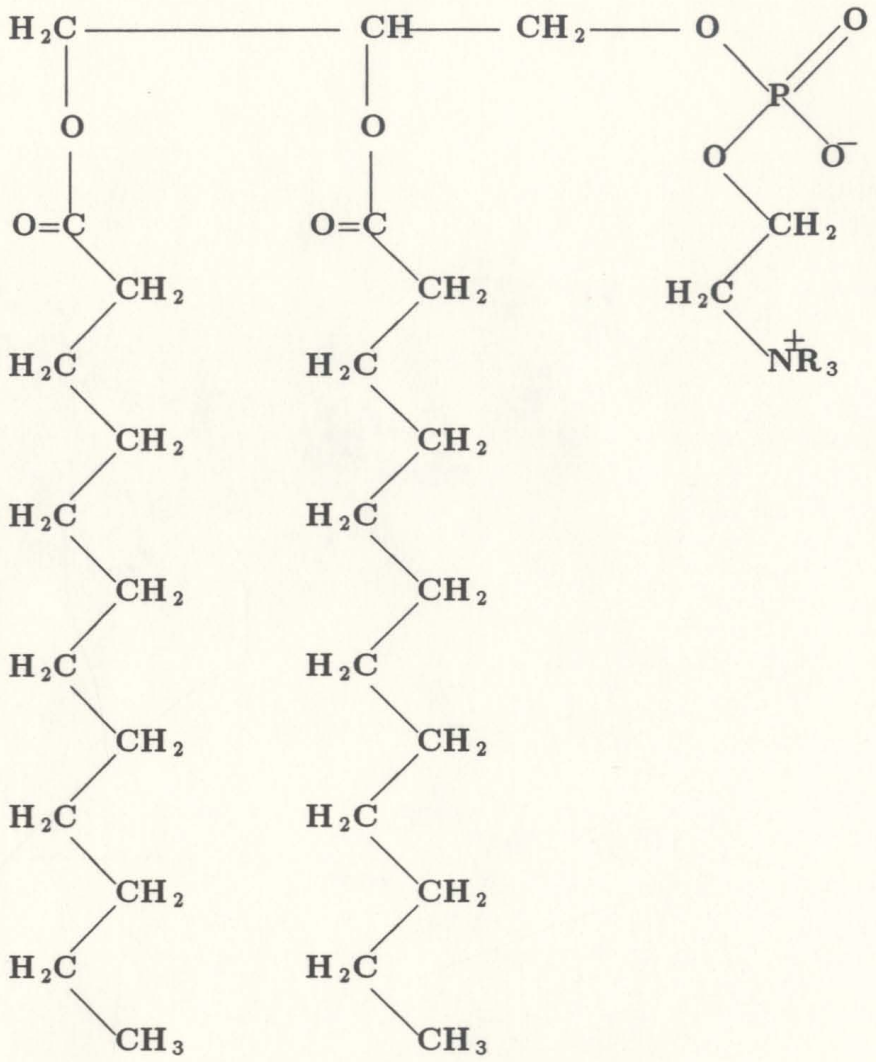

Figure 1.3(a)

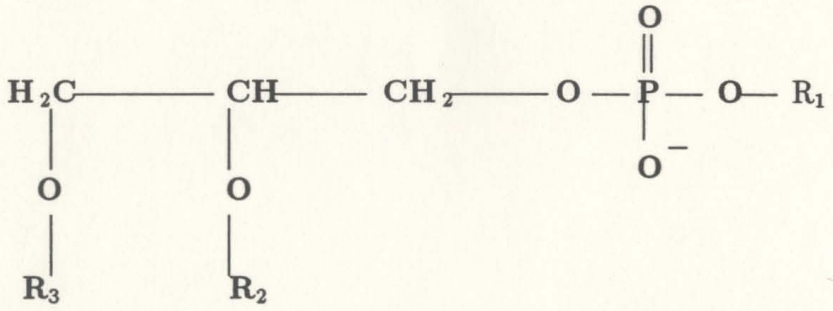

Figure 1.3(b)

Figure 1.3 The chemical structure of phospholipid.

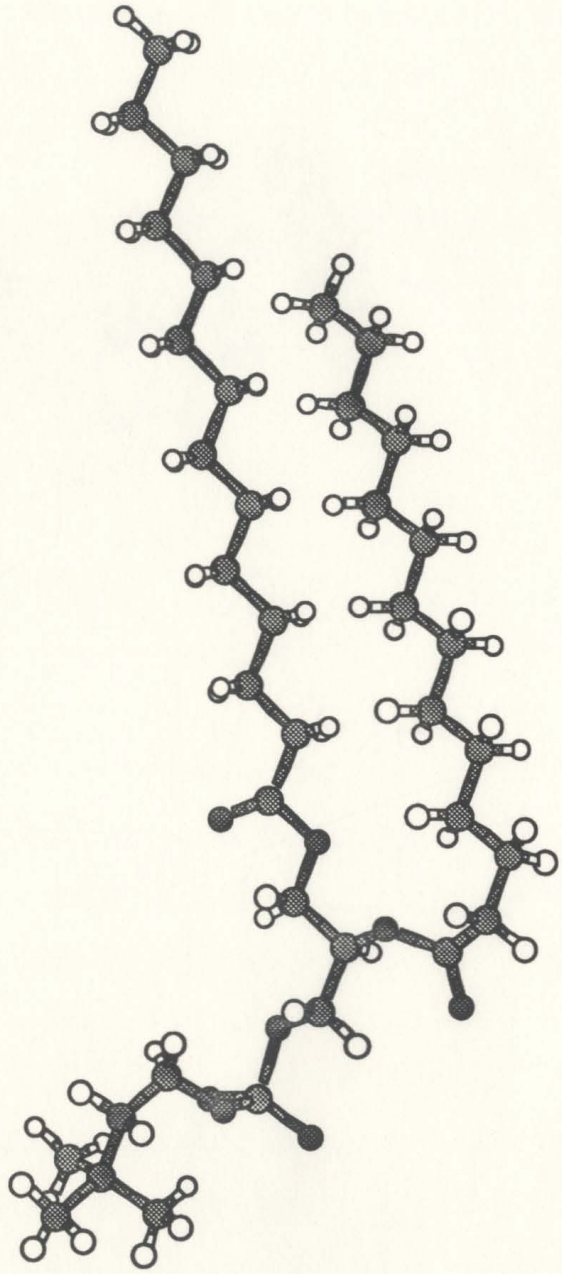

Figure 1.4 The conformation of a phospholipid molecule in a crystal.

is called the α-chain. It is attached to atom C(1) of the glycerol (see Figure 1.6). The fatty alcyl chains, β-chain and γ-chain are linked respectively to carbon atoms C(2) and C(3). In Table 1.1 we list some of the more common lipid molecules[1] used in model bilayers.

Table 1.1: The components of phospholipid molecules and their abbreviated names.

R1	R2, R3 (R2=R3)	abbreviation
-H	$CH_3(CH_2)_{14}COOH$	DPPA
$-CH_2-CH_2-NH_3$	$(CH_2)_{14}COOH$	DPPE
	$CH_3(CH_2)_{10}COOH$	DLPE
$-CH_2-CH_2-N^+-(CH_3)_3$	$CH_3(CH_2)_{14}COOH$	DPPC
	$CH_3(CH_2)_{10}COOH$	DLPC
	$CH_3(CH_2)_{12}COOH$	DMPC
$-CH_2-CH(NH_2)-C$	$CH_3(CH_2)_{14}COOH$	DPPS
$-CH_2-CH(OH)-CH_2-OH$	$CH_3(CH_2)_{14}COOH$	DPPG

It is should be noted that these molecules have principally two types of headgroups accompanied by different length of α, β and γ chains. The most common headgroups found in phospholipid component of biological membranes are phosphorylcholine (PC) and phosphorylethanolamine (PE). Their chemical structures are shown in Figure 1.5. In this work, the labeling of atoms in lipid molecules follows the convention as shown in Figure 1.6[4] (for dihedral angles – four atoms are listed from which two planes can be formed, the relative orientation of these planes define the actual value for a given dihedral angle).

The living cell is a dynamic system whose many functions include the energy capture, transfer and conversion. All living cells in nature are surrounded by external membranes. Biological membranes are involved in a large number of vital processes. They have such important functions as conduction of nervous impulse, conversion of light into chemical energy, conversion of light into electrical energy, oxidative

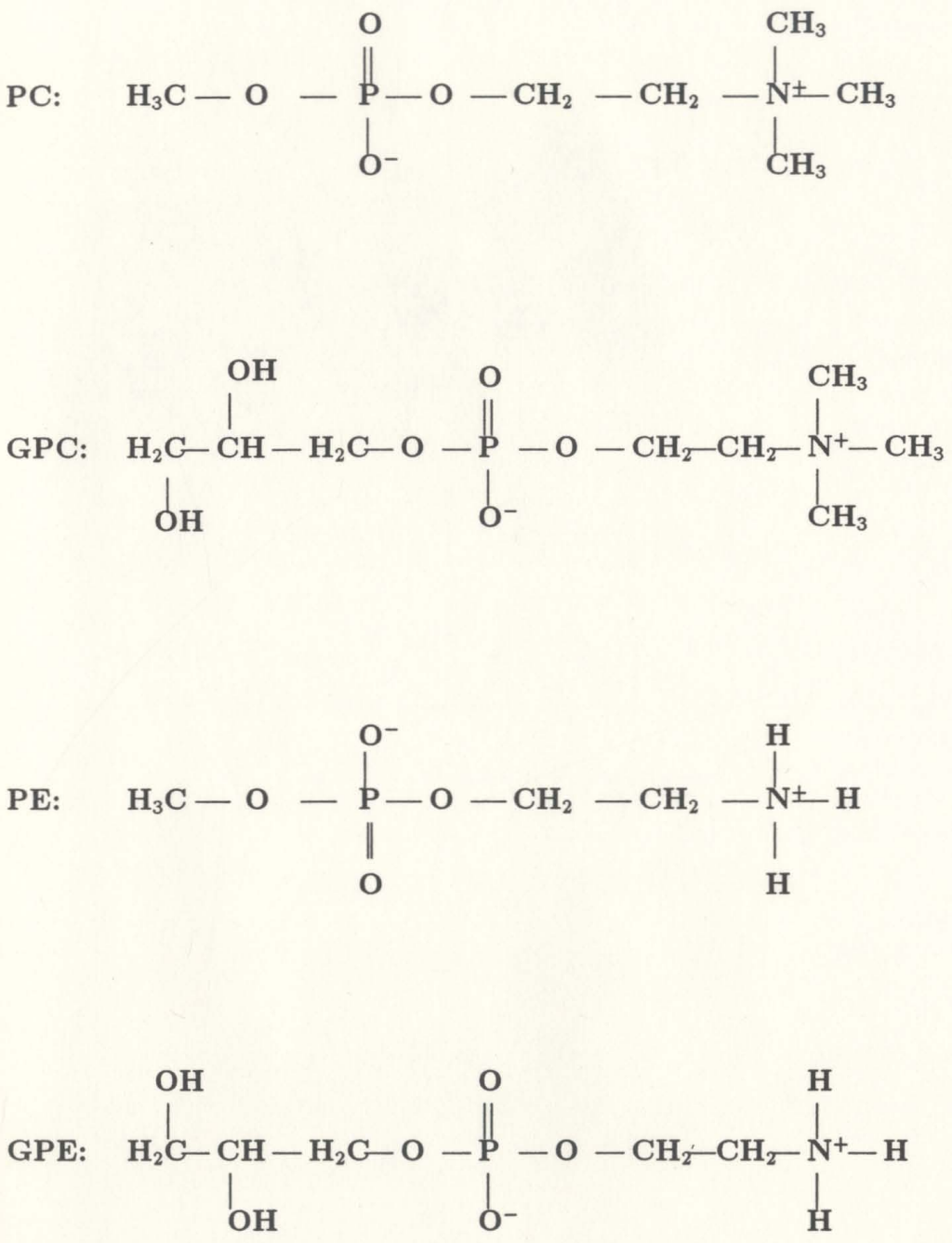

Figure 1.5: Chemical structures of PC (phosphorylcholine), GPC (glycerophosphorylcholine), PE (phosphorylethanolamine) and GPE (glycerophosphorylethanolamine).

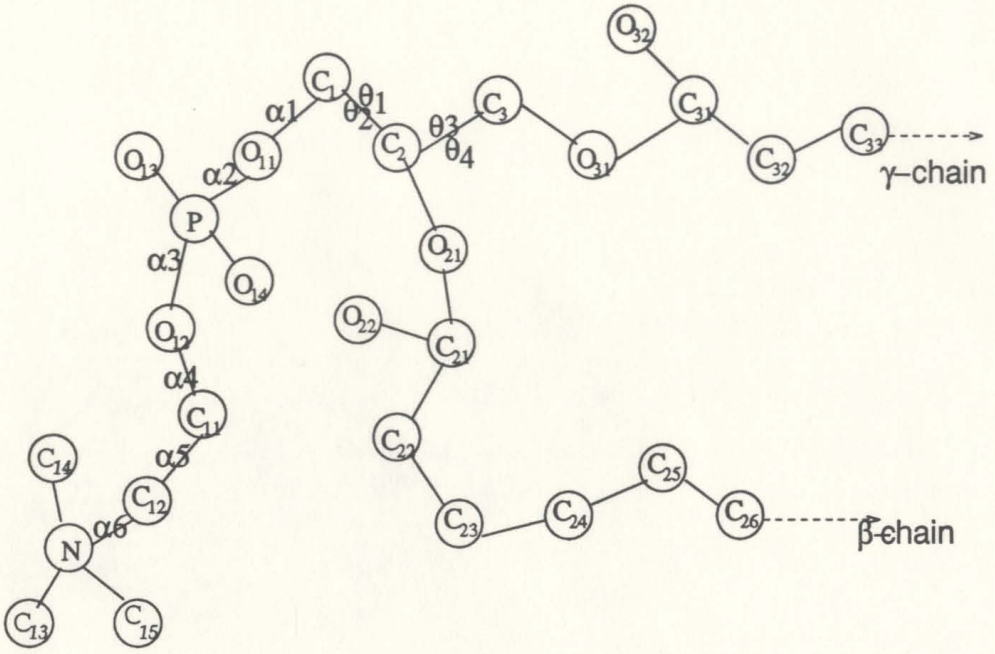

α_1	C(2)-C(1)-O(11)-P	θ_1	O(11)-C(1)-C(2)-C(3)
α_2	C(1)-O(11)-P-O(12)	θ_2	O(11)-C(1)-C(2)-O(21)
α_3	O(11)-P-O(12)-C(11)	θ_3	C(1)-C(2)-C(3)-O(31)
α_4	P-O(12)-C(11)-C(12)	θ_4	O(21)-C(2)-C(3)-O(31)
α_5	O(12)-C(11)-C(12)-N		
α_6	C(11)-C(12)-N-C(13)		

Figure 1.6 The conventional atom numbering and notation for the the dihedral angles for typical phospholipid molecule[2].

Notation of staggered and eclipsed torsion angles ranges:

sp: $0^o \pm 30^o$, $\pm sc : \pm 60^o \pm 30^o$,

$\pm ac : \pm 120^o \pm 30^o$, $ap : 180^o \pm 30^o$

and photo synthetic phosphorylation protein synthesis and so on. The molecular structures of biological membranes are very complex. The major difficulty in their studies is that the plasma membrane due to its thinness cannot be easily observed directly.

Table 1.2: The summary of experimental findings for phospholipid-water membrane systems.

method	model	results
x-ray diffraction[4]	DLPE DMPC LPPC GPE GPC	1. Single crystal data: (a) parameters of unit cell; (b) bilayer thickness; (c) molecular area; (d) hydrocarbon chain tilt and cross-sections. 2. Molecular conformations: (a) headgroup conformations; (b) headgroup orientation; (c) dialcylglycerol conformations. 3. Molecular packing: (a) space requirements of the headgroups; (b) headgroup interactions. 4. Space requirements of the hydrocarbon chains. 5. Behavior of phase transitions.
NMR[5] [6, 7]	phospholipid -water system	NMR works cover a wide range of experimental conditions e.g. crystal aqueous dispersions at different states of hydration and temperatures. Most of them focus on: (a) molecular conformations in aqueous dispersion; (b) measuring of the order parameter or time-average angular amplitude of motion of the chain segments.

Phospholipids commonly exist in biomembrane, their placements are strongly influenced by the interactions between them and other components in membrane. Their stable molecular structures tend to be the ones that are most energetically favorable. They minimize interactions between hydrocarbon residues of the lipid and the water molecules of the solvent. It is obvious that these structures vary with the external conditions: temperature, concentrations of lipids and water and so forth. Bilayers undergo a phase transition with the changes of temperature. Studies of the molecular structure revealed some properties and functions of biological membranes. A number of experimental techniques are used in the investigation of the structure of membranes such as x-ray diffraction, electron microscopy, nuclear magnetic resonance[4] and others. Computer simulation studies can also give detailed information about the structure, function, and dynamics of the lipid molecules at the atomic level. This approach employs both quantum and classical mechanics methodologies. The quantum mechanical computer simulations typically fall into two categories. They are the semi-empirical and the ab initio molecular orbital theory methods. We summarize the typical findings from the experimental and computational approaches for lipid systems in Tables 1.2 and 1.3. Table 1.2 focuses on the x-ray diffraction techniques and NMR methods. The former is normally used to determine the crystalline structure of the lipid solid state systems. The experimental investigations provide detailed structural information for phospholipid molecules and for their bulk properties in water.

Most of the ab initio calculations that involve torsional angle optimizations are carried out using the "rigid-rotor" approximation[12]: bond lengths and bond angles are held constant and usually only one or two dihedral angles are varied. Generally the results obtained using a rigid-rotor approximation exhibit large deviations from full geometry optimized values.

Table 1.3: The summary of previous theoretical calculations.

Model	method	results
$CH_3PO_4^-CH_3$ [8]	MD[1]	α_2-gauche
	semi-empirical	α_3-gauche
	ab initio(G70,G90)	
$CH_3CH_2CH_2PO_4^-CH_3$	ab initio	scans PES[2] of α_1, θ_1
		$\theta_1 = 59.4°$
		$\alpha_1 = 95.1°$
		$\alpha_2 = 76.9°$
		$\alpha_3 = 73.8°$
PE [9]	ab initio	$(\alpha_2 = -81°, \alpha_3 = -81°)$
		$(\alpha_6 = 165°)$
		$\alpha_4 = -60°, \alpha_5 = 90°$
		$\alpha_4 = 180°, \alpha_5 = 60°$
	MD	$\alpha_4 = 276°, \alpha_5 = 67°$
PC [10]	MD	$\alpha_4 = 249°, \alpha_5 = 67°$
hydrated PE[11] ($6H_2O$)	PCILO[3]	$\alpha_4 = 240°, \alpha_5 = 60°$
hydrated PC ($3H_2O$)	PCILO	$\alpha_4 = 120°, \alpha_5 = 300°$
hydrated PC ($5H_2O$)	PCILO	$\alpha_4 = 180°, \alpha_5 = 300°$

[1] MD stands for molecular dynamics calculations.
[2] PES stands for potential energy surface.
[3] PCILO stands for particular choice of the localized orbitals.

From this brief review of previous works, we note that many of the structural calculations focus on the phospholipid headgroup or the extended structure that includes part of the α-chain. This is, in part, due to the fact that α-chain lies in the interfacial region of the lipid-water system and the greatest susceptibility to conformational changes in phospholipid occurs mostly around the α-chain. It appears also that membrane permeability may be strongly correlated with the conformational changes in the α-chain[8]. Essential in this respect are the torsional angles α_4 and

α_5. These angles (α_4 and α_5) exhibit large differences depending on the computational method used and the environment around phospholipid molecules (see for example Table 1.3). In this work, we propose to overcome some of these difficulties with determining the stable conformations for phospholipids by systematically investigating their structure with the use of model compounds in a series of ab initio molecular orbital theory calculations. The results are presented in following chapters.

In chapter 2, the ab initio molecular orbital theory is reviewed. First, the Schrödinger equation for a molecular system is set up. Next the antisymmetric many-electron wavefunction is formulated which is followed by a brief outline of the derivation of Hartree-Fock and Roothaan equations. The types of basis functions employed in molecular calculations are listed. Finally, brief description of the Gaussian 92 software package is given.

In chapter 3 systematic calculations for five model compound are presented. We begin by analyzing compound I, $CH_3PO_4^-CH_3$, which is common to almost all phospholipid molecules and thus is a fundamental part of the phospholipid headgroup. The potential energy surface (PES) is scanned using the rigid-rotor approximation to find the stable geometrical structures corresponding to global and local minimum energies. The scan results are used as an initial starting point for the full geometry gradient optimizations. Our findings are consistent with experimental results and previous calculations. Next, an extended model compound II, $CH_3CH_2PO_4^-CH_2CH_3$, has been studied. Both the rigid-rotor scan of the PES and the full geometry optimizations have been performed again. Seven stable structure minimizing energy have been obtained for compound II. The compound III, $CH_3CH_2PO_4^-CH_2CH_2NH_3^+$, is an extended PE molecular compound. Rigid-rotor scanning of PES for (α_1, α_4), (α_1, α_5) identifies the referenced geometry structure

corresponding to the minimum energies. In this case, it is evident that the neglect of the molecule-water interactions (which in turn allows for the strong interaction between cation PO_4^- and anion NH_3^+) leads to optimization difficulties. Four stable structures have been found. They are compared with the experimental crystallographic results. It should be noted that in extending compound III to compound IV (GPC) we have used the starting geometry parameters from the x-ray experiment data. The final geometry displays a slight shift from the experimental structure but the conformation remains basically the same. Moreover, we note that the unit cell of phospholipid crystal consists of two molecules (as determined from the x-ray diffraction experiment[4]). Thus, full geometry optimization was also performed for two GPC molecules.

In chapter 4, the second part of our calculations, we have considered the lipid-water systems. In particular we study the structure of compound III in the presence of $4H_2O$. The stability of the system is observed. Also a system composed of two compounds III with four water molecules is investigated. This should mimic the bilayer system more closely. The region between the layers is taken up by the four water molecules. Hydrated GPE was also studied (GPE plus six water molecules were taken into account). Hydrogen bonds are discussed.

Finally in chapter 5, we summarize our results and present conclusions. We compare our results with experiment crystallographic data, other ab initio molecular dynamics (MD) and semi-empirical calculations. Conclusions regarding the importance of the hydrogen bonds in determining the structure of the phospholipid-water complexes will be presented.

Chapter 2

Theory – Hartree-Fock Approximation

Accurate structural properties of molecular systems such as phospholipid molecules can be determined with the use of quantum mechanical computational methods. In the quantum mechanical theory[33], the Schrödinger equation, in principle, gives an accurate description of the behaviour of microscopic particles (that constitute molecules) such as nuclei and electrons. However, the exact solution of the Schrödinger equation can only be obtained for one electron systems. Isolated phospholipid molecules and membrane systems composed of phospholipid and water molecules are complex multi-atom (thus multi-electron and multi-nuclei) systems. For these systems the Schrödinger equation cannot be solved exactly. Hence, a series of approximations must be introduced into the exact ab initio theory. In spite of these approximations, results obtained from this approach often show good agreement with empirically determined data.

The approximate ab initio molecular orbital theory requires that we address questions such as[32]: What approximation should be used for the Hamiltonian of the system?; What functional form should be chosen for the total wavefunction?; What is the appropriate basis set expansion for the one-electron molecular orbitals?; What is the most efficient self-consistent process for solving the approximate Schrödinger equation?. Various molecular properties (such as geometries, relative stabilities, vibrational spectra, dipole moments, atomic charges) are then computed from the results of the self-consistent molecular calculations.

2.1 Schrödinger Equation

The solution of the Schrödinger equation describes the wave-like characteristics of microscopic particles and gives the spatial range of these particles. The Schrödinger equation for a collection of particles, e.g. such as are present in a molecule, has the following form

$$\hat{H}\Psi = E\Psi \,, \tag{2.1}$$

where $\hat{H}$ is the Hamiltonian, an operator, that represents the total energy of a given system. $\hat{H}$ incorporates the kinetic and potential energy terms of the nuclei and electrons. E is the numerical value for the total energy of a given system determined relative to the state in which the constituent particles (nuclei and electrons) are infinitely separated and at rest. Ψ is the total wavefunction of the system that depends on spatial and spin (nuclear and electronic) coordinates for all constituent particles.

The process of solving the Schrödinger equation involves defining the Hamiltonian and then obtaining the total wavefunction Ψ and the value for the total energy E.

2.1.1 Hamiltonian for a Molecular System

The non-relativistic Hamiltonian for a molecular system is the sum of the kinetic, $\hat{T}$, and the potential, $\hat{V}$, energy terms for all of nuclei and electrons in a given system and can be written as

$$\begin{aligned}\hat{H} &= \hat{T} + \hat{V} \\ &= -\sum_{i=1}^{N} \frac{\hbar^2 \nabla_i^2}{2m_e} - \sum_{A=1}^{M} \frac{\hbar^2 \nabla_A^2}{2M_A} - \sum_{i=1}^{N}\sum_{A=1}^{M} \frac{Z_A e^2}{4\pi\varepsilon_0 r_{iA}} + \sum_{i=1}^{N}\sum_{j>i}^{N} \frac{e^2}{4\pi\varepsilon_0 r_{ij}} + \sum_{A=1}^{M}\sum_{B>A}^{M} \frac{Z_A Z_B e^2}{R_{AB}}\end{aligned} \tag{2.2}$$

where the molecular system consists of N electrons, each of mass m_e and M nuclei of mass M_A. The five terms are: the kinetic energy of the electrons, the kinetic energy of the nuclei, the attractive Coulomb potential energy between electrons and nuclei, the repulsive Coulomb potential energy amongst electrons and the repulsive Coulomb potential energy amongst nuclei.

Considering that the mass of the nucleus, M_A, is much larger than the mass of an electron m_e, i.e., $M_A >> m_e$, we can neglect the nuclear kinetic energy term in Eq. (2.2). Also, because of the difference in their masses, we can assume that electrons in a molecule are moving in a field of fixed nuclei and thus treat the repulsion between nuclei as constant. The above assumptions constitute the well known Born-Oppenheimer approximation that is often employed in quantum mechanical calculations. The main consequence of applying this approximation is the separation of nuclear and electronic motions which leads to a great simplification in computations. For example the total wavefunction can now be approximated by a product of the nuclear and electronic parts, i.e.,

$$\Psi = \Psi_{electronic} \times \Psi_{nuclear} \,. \tag{2.3}$$

The implementation of the above approximations in Eq. (2.2) means that the Hamiltonian due to electrons can be written as

$$\hat{H} = -\sum_{i=1}^{N} \frac{\hbar^2 \nabla_i^2}{2m_e} - \sum_{i=1}^{N} \sum_{A=1}^{M} \frac{Z_A e^2}{4\pi\varepsilon_0 r_{iA}} + \sum_{i=1}^{N} \sum_{j>i}^{N} \frac{e^2}{4\pi\varepsilon_0 r_{ij}} \,. \tag{2.4}$$

In order to eliminate physical constants from $\hat{H}$ atomic units are introduced as follows: the atomic unit of length (the bohr) is expressed in terms of Bohr radius a_0,

$$a_0 = \frac{h^2}{4\pi^2 m_e e^2} \tag{2.5}$$

and consequently the new coordinates, (x', y', z'), are

$$x' = \frac{x}{a_0}, y' = \frac{y}{a_0}, z' = \frac{z}{a_0} \tag{2.6}$$

and the atomic unit of energy (the hartree), E_H, is expressed in terms of the Coulomb repulsion energy between two electrons separated by 1 bohr

$$E_H = \frac{e^2}{a_0}, \tag{2.7}$$

and consequently new energies (E') are

$$E' = \frac{E}{E_H}. \tag{2.8}$$

The Schrödinger equation becomes

$$\hat{H}'\Psi' = E'\Psi' \tag{2.9}$$

where

$$\hat{H}' = -\sum_{i=1}^{N} \frac{\nabla_i'^2}{2} - \sum_{i=1}^{N}\sum_{A=1}^{M} \frac{Z_A}{r'_{iA}} + \sum_{i=1}^{N}\sum_{j>i}^{N} \frac{1}{r'_{ij}}\,. \tag{2.10}$$

Or dropping the primes in the above equation, the Hamiltonian can be written as:

$$\hat{H} = -\sum_{i=1}^{N} \frac{\nabla_i^2}{2} - \sum_{i=1}^{N}\sum_{A=1}^{M} \frac{Z_A}{r_{iA}} + \sum_{i=1}^{N}\sum_{j>i}^{N} \frac{1}{r_{ij}}\,. \tag{2.11}$$

2.1.2 Many–Electron Wavefunction

For a molecular system, $\Psi_{electronic}$, is a function of the N-electron coordinates (henceforth $\Psi_{electronic}$ will simply be referred to as Ψ since most of the discussion in chapter 2 focuses on the quantum mechanical description of electrons). The nuclear coordinates are thought of as being frozen under the Born-Oppenheimer approximation. For a single electron system, the wavefunction Ψ can be constructed from a linear combination of orthonormal functions (spin orbitals), $\chi(\mathbf{r}, \xi)$,

$$\chi(\mathbf{r}, \xi) = \psi(\mathbf{r}) \cdot \gamma(\xi)\,. \tag{2.12}$$

where $\psi(\mathbf{r})$ is the spatial orbital and $\gamma(\xi)$, since electrons are fermions, is the spin function. Since the spin of an electron can take on only two possible values ($\xi = \pm\frac{1}{2}$)

there are two possible spin functions for $\gamma(\xi)$: $\alpha(\xi)$ and $\beta(\xi)$ defined as follows,

$$\alpha(+\tfrac{1}{2}) = 1\,, \qquad \alpha(-\tfrac{1}{2}) = 0\,, \tag{2.13}$$

$$\beta(+\tfrac{1}{2}) = 0\,, \qquad \beta(-\tfrac{1}{2}) = 1\,. \tag{2.14}$$

Thus the one-electron spin orbitals corresponding to the spin up and down electrons are

$$\chi(\mathbf{r},\xi) = \psi(\mathbf{r}) \cdot \alpha(\xi) \tag{2.15}$$

$$\chi(\mathbf{r},\xi) = \psi(\mathbf{r}) \cdot \beta(\xi)\,. \tag{2.16}$$

For an N-electron system, the simplest wavefunction that can be constructed is a product of single electron spin orbitals, i.e.,

$$\Psi(1,2,\cdots N) = \chi_i(1)\chi_j(2)\cdots\chi_k(N) \tag{2.17}$$

where $\chi_j(i)$ stands for the spin orbital for the i^{th} electron, $\chi_j(\mathbf{r}_i,\xi_i)$.

According to the Pauli exclusion principle, no two electrons can occupy the same quantum state (for example two electrons that have the same spin cannot have the same spatial orbital associated with them). A direct consequence of Pauli exclusion principle is that the total electronic wavefunction must be antisymmetric with respect to the interchange of coordinates for any two electrons. The simplest way to satisfy the antisymmetry principle is to express the electronic wavefunction as a single Slater determinant (or as a sum of Slater determinants):

$$\Psi \propto \begin{vmatrix} \chi_i(1) & \chi_j(1) & \cdots & \chi_k(1) \\ \chi_i(2) & \chi_j(2) & \cdots & \chi_k(2) \\ & & \vdots & \\ \chi_i(N) & \chi_j(N) & \cdots & \chi_k(N) \end{vmatrix} \tag{2.18}$$

where $\chi_j(i)$ denotes molecular spin orbital which accommodates a single electron. Or using the notation from Eqs. (2.15) and (2.16), a full multi-electron molecular wavefunction (within the restricted Hartree-Fock approximation) for a closed-shell ground state for a molecule with N(even) electrons occupying doubly filled $\frac{N}{2}$ spatial orbitals can be written as

$$\Psi = \frac{1}{\sqrt{N!}} \begin{vmatrix} \psi_1(\mathbf{r}_1)\alpha(\xi_1) & \psi_1(\mathbf{r}_1)\beta(\xi_1) & \cdots & \psi_{\frac{N}{2}}(\mathbf{r}_1)\beta(\xi_1) \\ \psi_1(\mathbf{r}_2)\alpha(\xi_2) & \psi_1(\mathbf{r}_2)\beta(\xi_2) & \cdots & \psi_{\frac{N}{2}}(\mathbf{r}_2)\beta(\xi_2) \\ & & \vdots & \\ \psi_1(\mathbf{r}_N)\alpha(\mathbf{r}_N) & \psi_1(\mathbf{r}_N)\beta(\xi_N) & \cdots & \psi_{\frac{N}{2}}(\mathbf{r}_N)\beta(\xi_N) \end{vmatrix} \tag{2.19}$$

where, $\frac{1}{\sqrt{N!}}$ is the normalization factor.

2.1.3 Hartree–Fock Equations

Once the Schrödinger equation for a many-electron system is set up, we must solve it. The inclusion of electron-electron interactions in Eq. (2.11) complicates this solution. In general, to obtain the solution the variational principle and the iterative self-consistent field (SCF) method are used.

Variational Principle

In Eq.(2.19), the spatial part of the unknown molecular orbitals which are used to construct the electronic wavefunction can be expanded in terms of a set of known K basis functions ϕ_μ as

$$\psi_i = \sum_{\mu=1}^{K} C_{\mu i}\phi_\mu \tag{2.20}$$

where $C_{\mu i}$ are the molecular orbital expansion coefficients. This type of expansion is referred to as linear combination of atomic orbitals (LCAO) since initially basis

functions were often taken from atomic calculations (this no longer is the case in more recent calculations). Two types of basis functions, ϕ_μ are commonly used. They may be Slater-type or Gaussian-type orbitals. In molecular calculations, a third possibility for ϕ_μ is often employed. Linear combinations of Gaussian functions are used as basis functions. For example, an s-type basis function may be expanded in terms of s-type Gaussians,

$$\phi_\mu = \sum_s d_{\mu s} g_s. \tag{2.21}$$

where $d_{\mu s}$ are fixed coefficients and ϕ_μ are referred to as contracted Gaussians with g_s (see Eg. (2.56)) being termed primitive Gaussians.

Given the form of the molecular orbital as a linear combination of basis functions, solution of the Schrödinger equation requires that we determine the expansion coefficients, $C_{\mu i}$. The variational method is employed to determine them. The variational principle states that the value for the total energy, $E(\Psi)$, which corresponds to any antisymmetric normalized function of the electronic coordinates, Ψ, is greater than $E(\Psi_0)$ which corresponds to the lowest energy function, Ψ_0, i.e.

$$E(\Psi) > E(\Psi_0). \tag{2.22}$$

The above equation implies that the coefficients $C_{\mu i}$ should take values which correspond to the wavefunction which minimizes the energy. This leads to the variational equations

$$\frac{\delta E}{\delta C_{\mu i}} = 0 \qquad (\text{ for all } \mu \text{ and i}) \tag{2.23}$$

where E is the expectation value of the Hamiltonian (see Eq. (2.11)) with respect to Ψ (the form of which is discussed above). Thus with the use of Eq. (2.23), a set of equations is obtained. They are called the Hartree-Fock (HF) integro-differential

equations

$$h(1)\chi_a(1) + \sum_b^N [\int d\mathbf{x}_2 |\chi_b(2)|^2 r_{12}^{-1}]\chi_a(1) - \sum_b^N [\int d\mathbf{x}_2 \chi_b^*(2)\chi_a(2) r_{12}^{-1}]\chi_b(1) = \varepsilon_a \chi_a(1) \tag{2.24}$$

where $\mathbf{x}_2$ stands for $(\mathbf{r}_2, \xi_2)$ and

$$h(1) = -\frac{1}{2}\nabla_1^2 - \sum_{j=1}^N \frac{Z_j}{r_{1j}} \tag{2.25}$$

is a single particle operator. Eq.(2.24) can be written as

$$[h(1) + \sum_b^N \{\mathcal{G}_b(1) - \mathcal{K}_b(1)\}]\chi_a(1) = \varepsilon_a \chi_a(1) \tag{2.26}$$

where $\mathcal{G}_b(1)$, a direct or a Coulomb operator, is given by

$$\mathcal{G}_b(1) = \int d\mathbf{x}_2 |\chi_b(2)|^2 r_{12}^{-1} \tag{2.27}$$

and $\mathcal{K}_b(1)$, an indirect or an exchange operator, is given by

$$\mathcal{K}_b(1)\chi_a(1) = [\int d\mathbf{x}_2 \chi_b^*(2) r_{12}^{-1} \chi_a(2)]\chi_b(1). \tag{2.28}$$

Next we introduce an *effective* one-electron operator, the so called Fock operator,

$$\begin{aligned} f(i) &= -\frac{1}{2}\nabla_i^2 - \sum_{j=1}^N \frac{Z_j}{r_{ij}} + v^{HF}(i) \\ &= h(i) + v^{HF}(i) \end{aligned} \tag{2.29}$$

where $v^{HF}(i)$ is the average potential experienced by the i^{th} electron due to the presence of the other electrons. For example the Fock operator for one electron is:

$$\begin{aligned} f(1) &= h(1) + v^{HF}(1) \\ &= h(1) + \sum_b^N [\mathcal{G}_b(1) - \mathcal{K}_b(1)] \\ &= h(1) + \sum_b^N \int d\mathbf{x}_2 \chi_b^*(2) r_{12}^{-1}(1 - \mathcal{P}_{12})\chi_b(2) \end{aligned} \tag{2.30}$$

where

$$v^{HF}(1) = \sum_{b}^{N} [\mathcal{G}_b(1) - \mathcal{K}_b(1)]. \tag{2.31}$$

The HF equation for the i^{th} electron can now be simply expressed as

$$f(i)\chi(i) = \varepsilon_i \chi(i). \tag{2.32}$$

For closed-shell systems restricted HF equations can be simplified further by integrating out the spin functional dependence in the Fock operator. That is in this case the Fock operator becomes

$$f(\mathbf{r}_1) = h(\mathbf{r}_1) + \sum_{b}^{\frac{N}{2}} [\mathcal{G}_b(\mathbf{r}_1) - \mathcal{K}_b(\mathbf{r}_1)] \tag{2.33}$$

where

$$\mathcal{G}_b(\mathbf{r}_1) = \int d\mathbf{r}_2 |\psi_b(\mathbf{r}_2)|^2 r_{12}^{-1} \tag{2.34}$$

and

$$\mathcal{K}_b(\mathbf{r}_1)\psi_a(\mathbf{r}_1) = [\int d\mathbf{r}_2 \psi_b^*(\mathbf{r}_2) r_{12}^{-1} \psi_a(\mathbf{r}_2)]\psi_b(\mathbf{r}_1)\,. \tag{2.35}$$

Then the closed-shell spatial $\frac{N}{2}$ HF equations are given by spatial integro-differential equations such as

$$f(\mathbf{r})\psi_i(\mathbf{r}) = \varepsilon_i \psi_i(\mathbf{r}) \tag{2.36}$$

where $f(\mathbf{r})$ is defined as in Eq. (2.33).

Roothaan Equations

The HF integro-differential equations, Eq. (2.36), can be transformed into a set of algebraic equations and then solved using standard matrix method. As stated above, with the use of a linear expansion for the spatial part of molecular orbitals (see Eq. (2.20)) the problem of determining the total electronic wavefunction is converted to finding a set of expansion coefficients for each molecular orbital. Inserting

Eq. (2.20) into Eq. (2.36), multiplying the left hand side by ϕ_μ^* and integrating we obtain

$$\sum_{\nu=1}^{K} C_{\nu i} \int d\mathbf{r}_1 \phi_\mu(\mathbf{r}_1)^* f(\mathbf{r}_1) \phi_\nu(\mathbf{r}_1) = \varepsilon_i \sum_{\nu=1}^{K} C_{\nu i} \int d\mathbf{r}_1 \phi_\mu(\mathbf{r}_1)^* \phi_\nu(\mathbf{r}_1) \,. \tag{2.37}$$

Based on this equation two matrices are defined, the overlap matrix **S** and the Fock matrix **F**. The elements of overlap matrix **S** are

$$S_{\mu\nu} = \int d\mathbf{r}_1 \phi_\mu^*(\mathbf{r}_1) \phi_\nu(\mathbf{r}_1) \tag{2.38}$$

and the elements of the Fock matrix **F** are

$$F_{\mu\nu} = \int d\mathbf{r}_1 \phi_\mu^*(\mathbf{r}_1) f(\mathbf{r}_1) \phi_\nu(\mathbf{r}_1). \tag{2.39}$$

Using these matrices, Eq. (2.37) can be written as

$$\sum_\nu F_{\mu\nu} C_{\nu i} = \varepsilon_i \sum_\nu S_{\mu\nu} C_{\nu i} \qquad i = 1, 2, ...N. \tag{2.40}$$

This set of integrated HF equations is often referred as the Roothaan equations. In matrix form, it can be expressed as

$$\mathbf{FC} = \mathbf{SC}\varepsilon \tag{2.41}$$

where **C** is the $K \times K$ expansion coefficients matrix

$$C = \begin{bmatrix} C_{11} & C_{12} & . & . & . & C_{1K} \\ C_{21} & C_{22} & . & . & . & C_{2K} \\ . & . & & & & . \\ . & . & & & & . \\ . & . & & & & . \\ C_{k1} & C_{K2} & . & . & . & C_{KK} \end{bmatrix} \tag{2.42}$$

and ε is a diagonal matrix of one-electron molecular orbital eigenvalues, ε_i, corresponding to spatial part of molecular orbitals, ψ_i, i.e.,

$$\varepsilon = \begin{bmatrix} \varepsilon_1 & & & \\ & \varepsilon_2 & & \\ 0 & & \ddots & 0 \\ & & & \varepsilon_K \end{bmatrix}. \tag{2.43}$$

The next step in solving the Roothaan equations will involve finding an explicit expression for the Fock matrix.

First the concept of density matrix must be introduced. The density matrix, $\mathbf{P}$, for a closed-shell system is defined as

$$P_{\lambda\sigma} = 2\sum_{i=1}^{\frac{N}{2}} C_{\lambda i}^{*} C_{\sigma i} \tag{2.44}$$

then using Eq. (2.44) in Eq. (2.39) we obtain

$$F_{\mu\nu} = H_{\mu\nu}^{core} + \sum_{\lambda=1}^{\frac{N}{2}} \sum_{\sigma=1}^{\frac{N}{2}} P_{\lambda\sigma}[(\mu\nu|\lambda\sigma) - \frac{1}{2}(\mu\lambda|\sigma\nu)] = H_{\mu\nu}^{core} + G_{\mu\nu} \tag{2.45}$$

where $H_{\mu\nu}^{core}$ is a core-Hamiltonian matrix that involves the one-electron operator $h(1)$ (see Eq. (2.25) i.e.

$$H_{\mu\nu}^{core} = T_{\mu\nu} + V_{\mu\nu}^{nucl} \tag{2.46}$$

and $G_{\mu\nu}$ is the two-electron part of the Fock matrix.

Typical basis set used in molecular calculations is not an orthonormal set. Thus we need to orthogonalize the basis functions ϕ_μ in order to express Roothaan's equations in the usual matrix eigenvalue form. This involves transforming basis functions ϕ_μ to the orthogonalized set ϕ'_μ as follows,

$$\phi'_\mu = \sum_\nu X_{\nu\mu}\phi_\nu \qquad \mu = 1, 2, ...K \tag{2.47}$$

where the transformation matrix $\mathbf{X}$ must satisfy the following relation

$$\mathbf{X}^{+}\mathbf{S}\mathbf{X} = 1 \tag{2.48}$$

($\mathbf{S}$ is overlap matrix defined above). One way of obtaining $\mathbf{X}$ is from the procedure called symmetric orthogonalization which requires that we set

$$\mathbf{X} = \mathbf{S}^{-\frac{1}{2}}. \tag{2.49}$$

Within this scheme the new $\mathbf{C}'$ and the old $\mathbf{C}$ coefficient matrices are related as

$$\mathbf{C}' = \mathbf{X}^{-1}\mathbf{C} \tag{2.50}$$

and substituting Eq. (2.50) into Roothaan equations and defining a new matrix $\mathbf{F}'$

$$\mathbf{F}' = \mathbf{X}^{+}\mathbf{F}\mathbf{X} \tag{2.51}$$

we finally obtain

$$\mathbf{F}'\mathbf{C}' = \mathbf{C}'\varepsilon. \tag{2.52}$$

Eq. (2.52) represents a set of transformed Roothaan equations. The solution of Roothaan equation involves diagonalizing $\mathbf{F}'$, solving for $\mathbf{C}'$ and then obtaining $\mathbf{C}$ and $\mathbf{F}$.

SCF Procedure

Solving Roothaan equation involves a self-consistent field method that is summarized in a flow chart as shown in Figure 2.1.

2.1.4 Basis Functions

As was stated above, another important aspect of an approximate ab initio theory is choice of basis functions (see Eq. (2.20)).

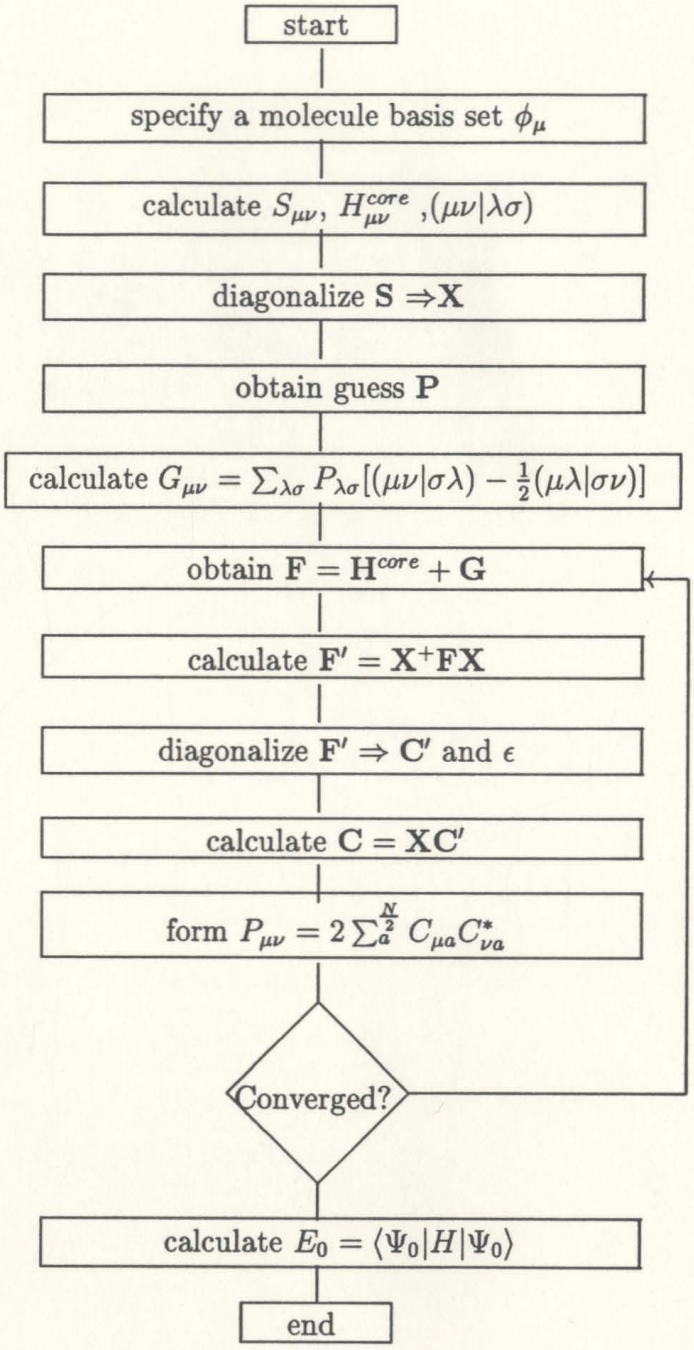

Figure 2.1: SCF flow chart.

Slater And Gaussian Type Orbitals

Two types of basis functions are used to describe the atomic orbitals. One type is Slater-type orbital (STO) functions. These are labeled with atomic quantum numbers 1s, 2s, $2p_x$,...as follows:

$$\phi_{1s} = \sqrt{\frac{\xi_1^3}{96\pi}} e^{-\xi_1 r} \tag{2.53}$$

$$\phi_{2s} = \sqrt{\frac{\xi_2^5}{\pi}} r e^{\frac{-\xi_2 r}{2}} \tag{2.54}$$

$$\phi_{2p_x} = \sqrt{\frac{\xi_2^5}{32\pi}} x e^{\frac{-\xi_2 r}{2}} \quad etc. \tag{2.55}$$

where ξ are constants determining the size of the orbitals. The second type is the Gaussian-type orbital (GTO) functions. They are expressed in the form of

$$g_s(\alpha, \mathbf{r}) = [\frac{2\alpha}{\pi}]^{\frac{3}{2}} e^{-\alpha r^2} \tag{2.56}$$

$$g_x(\alpha, \mathbf{r}) = [\frac{128\alpha^5}{\pi^3}]^{\frac{1}{4}} x e^{-\alpha r^2} \tag{2.57}$$

$$g_y(\alpha, \mathbf{r}) = [\frac{128\alpha^5}{\pi^3}]^{\frac{1}{4}} y e^{-\alpha r^2} \quad etc. \tag{2.58}$$

and so forth, where α is a constant determining the radial extend of the function.

STO's give accurate description of atomic orbitals, but they are not suitable for numerical calculations involving molecules. GTO's do not represent atomic orbitals as well, however they significantly reduce the computational effort, especially, when two-electron integrals are calculated. A linear combination of (primitive) Gaussians can also be used as basis functions (called contracted Gaussians) significantly improving the representation of atomic orbitals.

Basis Sets

A finite set of basis functions is used to form basis sets. The following basis sets (contracted Gaussian functions) are often used in molecular calculations:

1. Minimal Basis Set

In the minimal basis set such as STO-3G each occupied atomic orbital is composed of three Gaussian primitives. The contraction coefficients and exponents are so chosen that the basis functions approximate the orbital shapes of Slater functions. This basis set is most suited for large molecular systems which contain many electrons. It is good for obtaining qualitative results.

2. Split Valence Basis Set

The larger basis set is formed by increasing the number of basis functions per atom. The split valence basis sets employ two types of basis functions for valence electrons. For example, for the basis set, 3-21G three primitive Gaussians are used for core electron basis functions and two primitives are used for the inner valence electrons and only one primitive Gaussian for the outer valence electrons. The procedure is similar for the basis sets such as 4-31G, 6-31G, 6-311G and other split valence basis sets. These basis sets provide a more accurate representation of the real orbitals in comparison to the minimal basis set.

3. Polarized Basis Set

The polarized basis set is constructed by adding orbitals with angular momentum beyond what is required for the ground state of constituent atoms in a given molecule. Its function is to change orbitals' shapes. For example, 3-21G* is based on the basis set 3-21G with d functions added to the second row elements. Higher polarized basis sets include: 6-31G*, 6-31G** basis sets and so on. Diffuse functions are also used in ab initio calculations to improve the description of the long-range behaviour of molecular orbitals with energies close to the ionization limit.

Summarizing, the calculations performed with higher quality basis set often lead to quantitatively better results, however, more accurate basis sets require greater computational effort. Thus, in practice, a balance between these two opposing

factors must be sought.

2.2 Applications of Ab Initio Theory

The solution of HF equations allows us to compute quantities such as net charges on the constituent atoms in a given molecule. This is performed with the Mulliken population analysis.

2.2.1 Mulliken Population Analysis

Mulliken population analysis is one way of describing the electronic distribution in a molecule. The charge density gives the probability of finding an electron in space.

$$\rho(r) = \sum_{\mu}\sum_{\nu} P_{\mu\nu}\phi_{\mu}(\mathbf{r})\phi^{*}_{\nu}(\mathbf{r}). \tag{2.59}$$

The total number of electrons is given by

$$\begin{aligned} N &= 2\sum_{a}^{\frac{N}{2}} \int d\mathbf{r}|\psi_a(\mathbf{r})|^2 \\ &= \sum_{\mu}\sum_{\nu} P_{\mu\nu}S_{\mu\nu} \\ &= \sum_{\mu} (\mathbf{PS})_{\mu\mu} \\ &= tr(\mathbf{PS}). \end{aligned}$$

In the Mulliken population analysis one computes $(\mathbf{PS})_{\mu\mu}$ and treats it as an indication of number of electrons that is to be associated with a given ϕ_{μ} (obtained from the SCF calculations). That is the net charge associated with an atom (with an atomic charge Z_A) within a molecule is taken as

$$q_A = Z_A - \sum_{\mu \in A} (\mathbf{PS})_{\mu\mu}. \tag{2.60}$$

The Mulliken population analysis method is not a unique way of assigning charges. It should only be used in calculations involving the same basis set for different

molecules. It can be used as an aid in assigning electron withdrawing or donating abilities of atoms in molecules.

2.2.2 Gaussian 92 – Brief Description

The Gaussian 92 software package is based on the ab initio molecular orbital theory[35]. It can perform many types of calculations such as single point energy, geometry optimizations, Mulliken population analysis and compute many physical and chemical quantities such as dipole moments.

Input Data

The input file for Gaussian 92 primarily consists of two parts. The first part specifies the task to be performed, the level quantum mechanical approximation and the choice of basis set. The second part specifies the initial molecular geometry and geometrical parameters. They can be in the form of either three dimension Cartesian coordinates or internal coordinates (bond lengths, bond angle and dihedral angles). The input file also specifies the total charge (e.g. 0 for neutral molecules, +1 for single charged cations, and so on) and the multiplicity (1 for singlet, 2 for doublet, 3 for triplet, and so on) for molecules.

Functionalities of Gaussian 92

The procedures performed by Gaussian 92 are summarized in Figure 2.2.

In quantum chemistry, equilibrium structures refer to the arrangement of nuclear positions corresponding to energy minima. The geometry optimization is a procedure for locating extremum points on the potential energy surface (PES). Among the energy minima, there is usually a structure corresponding to the global minimum which is the lowest energy point on the PES. From the starting geometry, the

calculation proceeds along the path on the PES for which energy gradients ($\frac{\partial E}{\partial r}$) are determined. The energy gradient values give the direction along which the energy decreases most rapidly. The point at which

$$F = -\frac{\partial E}{\partial r} = 0 \tag{2.61}$$

corresponds to the extremum on the surface.

That is the points which have zero values associated with the first derivatives of the energy correspond to energy minima or saddle points on the PES. Practical calculations are limited by the accuracy of the software package. Actually, the condition $\frac{\partial E}{\partial r} = 0$ is only satisfied up to a certain convergence criteria which are defined by the threshold values. The convergence criteria used by Gaussian 92 consist of four conditions. The maximum component of the force, $F = -\frac{\partial E}{\partial r}$, (along all directions on the PES), the root-mean-square value of the force, RMS, maximum displacement, i.e., the largest change in any Z-matrix geometrical parameter and the root-mean-square of maximum displacement must all be below certain cutoff values. Typically in our calculations the respective cutoff values are 0.000450, 0.000300, 0.001800, 0.001200.

Output Data

The output file gives results of the iterative SCF procedure after the convergence is achieved. The file lists the final results such as molecular orbital linear combination coefficients $C_{\mu i}$, the SCF energy, the stationary point parameters, net charges, dipole moment, and other quantities

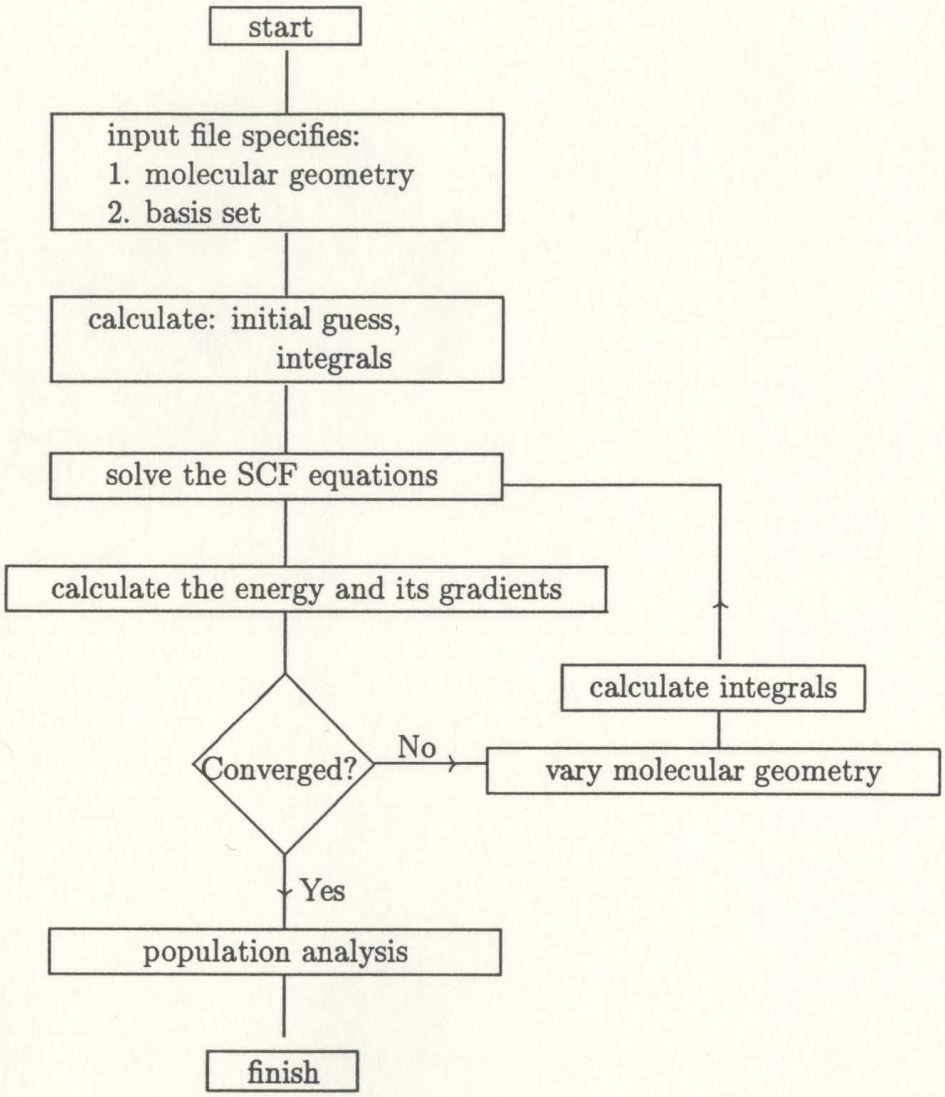

Figure 2.2: Typical sequence of calculations in Gaussian 92 during geometry optimization.

Chapter 3

The Conformational Analysis of Polar Headgroups for Phospholipids

3.1 Introduction

Polar headgroups are characteristic of phospholipid molecules. Their properties, which are mainly a function of the temperature and the hydration level, partially determine the physical state of the phospholipid bilayer membrane. Thus, in order to effectively understand the interaction of lipid molecules with each other, with water, with proteins and with other perturbants in the membrane, the stable (3D) structures of the headgroups should be known. Ab initio molecular orbital theory is a powerful quantum mechanical tool that can be used to perform this type of structural investigation. In principle, this would involve the construction of complete conformational potential energy surfaces (CPESs). However, a complete construction of the CPESs is not computationally feasible even for isolated headgroups. Instead we obtain two dimensional, rigid-rotor scans of the PESs. This procedure, combined with the full geometry optimizations starting from the approximate locations of the minima as identified by the scans is used to determine the global minimum energy structures for the polar headgroups. We also study the relative conformational energies. It should be noted that, in this thesis, we refer to the lowest energy minimum found in this work as the global minimum. It is possible that higher level calculations would disclose even lower energy minima.

As stated above, it is not currently possible to construct a complete CPES as a function of all of the geometrical parameters at an ab initio level for a large

molecular system. However, the CPES generated by single point energy calculations provides valuable input information for the more extensive ab initio calculations of finding the stable conformations that correspond to the minimum (local or global) energies. Since each of the single point calculations for the scan used "rigid-rotor" approximation[12, 13] in which only one torsional angle is varied, the CPES thus obtained does not represent actual CPES exactly. In fact, the one dimensional potential energy curves generated in this way often give energies that may lie far from the exact minimum energy points. For example, in our systems, in addition to the generic computational difficulties involved in generating CPES, very high energies in some scans were produced when certain atoms were forced to approach each other too closely to form a stable conformation (this type of constraint would not be present in the full or partial geometry optimization computations). The "rigid-rotor" scans are useful, however, for identifying the approximate locations of minima (local and global)[12] and in this work this is their primary role. The scans also help us to determine the approximate shape of the minima (i.e. their widths and the slopes of the descent etc.).

In this work five lipid model compounds have been studied extensively. Their chemical structures and their names as used in this thesis are listed below in table 3.1.

Table 3.1: Names and chemical structures of model compounds studied in this thesis.

Name	Chemical structure
compound I	$CH_3PO_4^-CH_3$
compound II	$CH_3CH_2PO_4^-CH_2CH_3$
compound III	$CH_3CH_2PO_4^-CH_2CH_2NH_3$
compound IV (GPC)	$(OH)_2CH_2CHCH_2PO_4^-CH_2CH_2N(CH_3)_3$
(two) compounds IV	GPC (two molecules per unit cell)
compound V (GPE)	$(OH)_2CH_2CHCH_2PO_4^-CH_2CH_2NH_3$

We begin by determining the most stable structures for short model compounds (I, II and III). These compounds are further extended to larger model compounds such as GPC and GPE. The changes in the geometrical parameters as a function of the size of the headgroup model compound will be discussed. Also comparison with experimental data will be made.

All of the calculations were generated using the molecular orbital program, Gaussian 92, which employs the Hartree-Fock approximation and the self-consistent-field methods (see chapter 2 for a more complete discussion).

3.2 Compound I – Dimethyl Phosphate Anion

The dimethyl phosphate anions (compound I in this thesis) are important compounds in biological systems. For example the phosphodiester linkages in nucleic acids are built from dimethyl phosphate anions. They are also the central components of the polar headgroups of the phospholipid molecules. There have been numerous theoretical and experimental studies of this compound. For example, ab initio theoretical studies[14, 9] using the 1970 and 1990 versions of the Gaussian program gave good qualitative agreement with the crystal structures obtained from x-diffraction experiments.[4]. We reexamined the structure and energetics of this system by first performing a complete rigid-rotor scan of the CPES for two torsional angles α_2 (C(1)-O(11)-P-O(12)) and α_3 (O(11)-P-O(12)-C(11)) (see also Figure 1.6) and then, once the stable conformations were identified, by performing full geometry optimization calculations with higher basis sets than were previously employed.

Since the dimethyl phosphate anion is the smallest model compound studied in this work, we will use it to determine the appropriate basis set to be employed in the computations involving the remaining compounds.

3.2.1 Basis Set Determination

A proper basis set should be able to reproduce experimental data adequately and minimize computational time at the same time. For compound I, the calculations using four basis sets have been performed. They are: the minimal basis set, STO-3G, the split valence plus polarization functions on phosphorus only, 3-21G*, the split valence with polarization on all atoms except hydrogen, 6-31G*, and 6-31+G* which is constructed by adding diffuse functions to the 6-31G* basis set for the heavy atoms (see chapter 2 for definitions of minimal, split valence and polarized basis sets, and diffuse functions). Experimentally determined geometrical parameters were used as the initial input data in the STO-3G calculations. The subsequent calculations used the optimized geometries generated in the previous computations with smaller basis sets. In Table 3.2, the comparison of the calculated and experimental results is presented.

Table 3.2: Comparison of theoretical and experimental geometries for the dimethyl phosphate anion. (Bond lengths are in angstroms and angles are in degrees.)

parameters	STO-3G	3-21G*	6-31G*	6-31+G*	experiment [9]
P-O′	1.582	1.473	1.470	1.474	1.490
P-O	1.731	1.634	1.642	1.639	1.536
C-O	1.432	1.435	1.393	1.396	1.425
O(13)-P-O(14)	128.8	124.6	124.9	124.6	117.2
O(11)-P-O(12)	95.9	98.3	99.5	99.8	104.8
P-O-C	120.6	118.2	118.5	119.4	118.3
C-O-P-O	87.0	75.0	75.1	75.3	57.5
energy (hartree)	−710.340393	−715.847778	−719.520867	−719.543525	

We performed the basis set comparison for the lowest energy (gauche-gauche)

conformation for compound I. The experimental data were obtained from the x-ray diffraction investigation of the closely related crystalline structure of dimethylammonium phosphate[9]. Since the structure of compound I is significantly distorted from the perfect C_2 point group symmetry, we present average values for the geometrical parameters in Table 3.2. For example, the bond length P−O′ is equal to the average value of the bond lengths P−O(13) and P−O(14). Similarly, P–O is the average value of the bond lengths P−O(11) and P−O(12). Other parameters are obtained in a similar way.

Table 3.2 clearly shows that geometrical parameters obtained using the minimal basis set, STO-3G, differ considerably from the results obtained using higher basis sets and from the experimental data. Table 3.2 illustrates that bond lengths can differ by as much as 0.1 $\AA$ and are longer than the corresponding bonds in the higher basis set calculations. In the worst case, the difference is nearly 10%. Table 3.2 shows that the difference in bond angles between the minimal basis set and other larger basis sets are in the range of 1.2° for the bond angle C−O−P, 4.2° for unsaturated oxygens and 3.9° for the bond angle O(11)−P−O(12). Especially it should be noted that the important torsional angles α_2 and α_3 (C−O−P−O in Table 3.2) exhibit $\approx 12°$ deviations from the values calculated using other basis sets.

From ab initio molecular orbital theory, the minimum basis set does not adequately represent the orbital shapes of the valence orbitals for the heavier atoms such as phosphorus. Thus, the basis set STO-3G is not a good choice for studying the phospholipid molecules. The geometry predictions using the basis set 3-21G* are very close to those generated by the basis sets 6-31G* and 6-31+G* except that the calculated C−O bond length is about 0.04 $\AA$ longer which is actually closer to the experimental value. The only difference between 6-31G* and 6-31+G* calculations is that some bond lengths and angles differ by at most 0.004 $\AA$ and 0.9°

respectively. This means that the addition of diffuse functions change molecular orbitals shapes without affecting the atomic positions. We conclude that the more complete basis sets (6-31G* and 6-31+G*) do not significantly improve geometrical results. Considering these theoretical results we have chosen the 3-21G* basis set for our studies.

3.2.2 Rigid–Rotor Scans

The rigid-rotor scan has been performed using the 3-21G* basis set. The torsional angles α_2 and α_3 were varied in the range 0–360° in compound I. This covered all of the possible conformations identified by the torsional angles α_2 and α_3. The scan was performed at 30° intervals for both α_2 and α_3 torsional angles in the specified range. The single point energies resulting from the scan are plotted in Figure 3.1(a). Three local minima can be identified in this figure. They are located near the following values for α_2 and α_3 $(75°, 75°)$, $(225°, 75°)$ and $(285°, 285°)$ which is equivalent to $(-75°, -75°)$. We note that the points $(75°, 75°)$ and $(-75°, -75°)$ based on symmetry consideration alone should be equivalent. However they are not equivalent in Figure 3.1 (the reason for this will be given below). Figure 3.1(b) displays the contour plot corresponding to the above scan. It contains the same three minima as presented in the scan plot. It also shows the minimum around the point $(75°, 225°)$ which again can be accounted for by resorting to symmetry considerations. From the scan we also note that there is no minimum located near $(180°, 180°)$ values for α_2 and α_3. This is in disagreement with previous work[9] which predicted a stable conformation near the point $(180°, 180°)$. In our full geometry optimization we found a local minimum energy structure but only with 6-31G* basis set. Thus the reason why this minimum does not occur on our scan could be due to the fact that the scan calculations were performed with 3-21G* basis set.

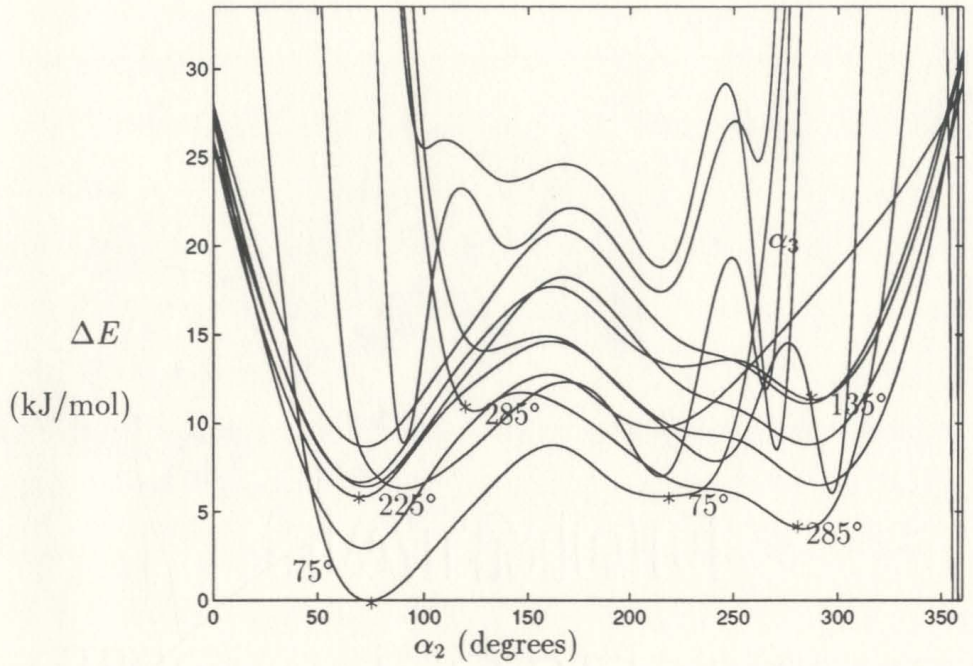

Figure 3.1(a). The plot of scanning results of α_2 and α_3 for compound I. The points labeled by "*" correspond to the minima displayed in Figure 3.1(b). The numbers next to these minima are values for α_3.

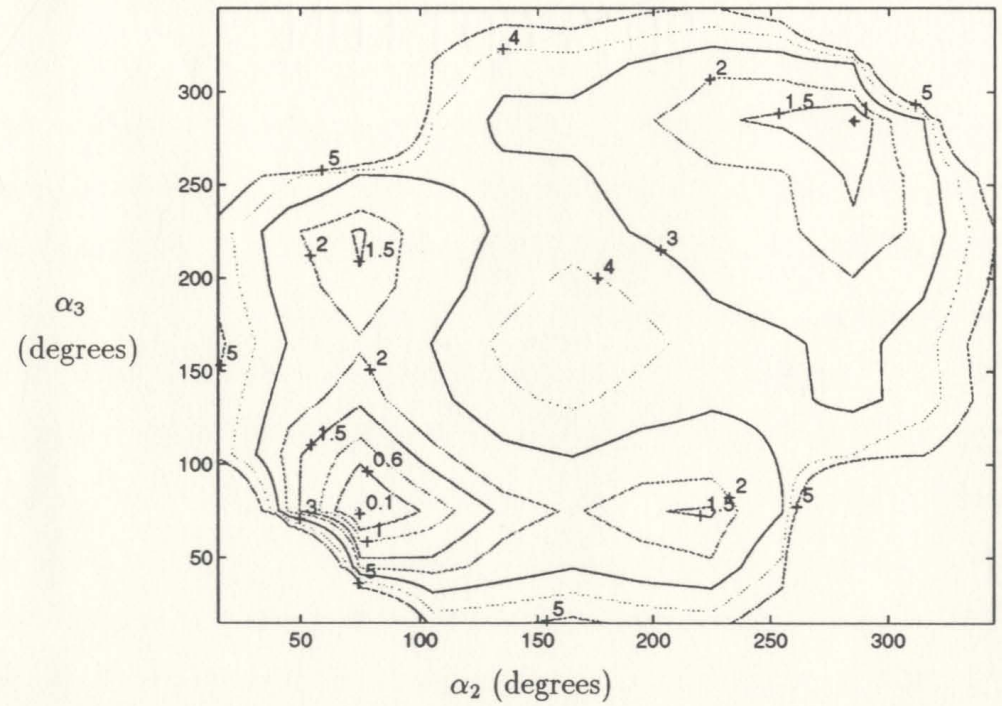

Figure 3.1(b). The contour plot of α_2 and α_3 for compound I.

Figure 3.1(b) illustrates that there is certain symmetry related to the locations of the minima, although the values of the energy are not equivalent. For example, from the scan and contour plot we can see that there is an energy difference between the two conformations: $(75°, 75°)$ and $(-75°, -75°)$. The reason for this is the fact the these calculations were performed with all of the geometrical parameters constrained (with the exception of α_2 and α_3 angles) to the optimized, global minimum values. In the global minimum state $(75°, 75°)$ the perfect C_2 symmetry is destroyed due the interaction between the hydrogens located on the methyl end groups and the oxygens: O(13) and O(14). This asymmetry is manifested in the fact that the (+sc +sc) is not a perfect gauche-gauche conformation. Also the exact three-fold symmetry of the methyl group is not maintained. This is evident from both dihedral angles (see Table 3.4) and non-bonded distances. For example, the distance between O(13) and the closest H on C(1) is 2.894 $\AA$ and the distance between O(12) and its closest H on C(1) is 2.475 $\AA$ in the global minimum conformation. Thus since the global minimum structure exhibits asymmetry when the rigid-rotor calculations are performed the hydrogen atoms on methyl groups are not allowed to relax in the $(-75°, -75°)$ conformation, giving rise to higher energy. To illustrate it even more clearly, we note that for example, in the methyl group around C(1), the distance between the hydrogen atom which is the closest to O(14) and O(13) change from 3.285 $\AA$ in the conformation $(75°, 75°)$ to 2.928 $\AA$ in the conformation $(285°, 285°)$. The situation is the same for the hydrogen around C(11) relative to the positions of O(14) and O(13). Thus the two conformations must give unequal energies even if the main atoms in the backbone have roughly the same relative positions. The same problem with the rigid scan is also present in the second local minimum which is located near $(75°, 225°)$ point. Based on the symmetry arguments alone (i.e. equivalence of both ends), one should obtain four equivalent minima located near

the following points: $(75°, 225°)$, $(225°, 75°)$, $(285°, 135°)$ and $(135°, 285°)$. The first two are clearly visible on the contour plot, the presence of the last two is suggested by the shape of the contour plot lines. Again the fact that these calculations were obtained from rigid-rotor scan explains their higher energies.

3.2.3 Geometry Optimized Results

The systematic rigid-rotor scans revealed the intrinsic stability of two types of conformations for the dimethyl phosphate anion. An additional stable conformation has been found when the 6-31G* basis set was used in our calculations. These conformations and their relative energies are discussed in this section. We summarize our findings for the dihedral angles α_2 and α_3 for compound I in Table 3.3.

The three conformations are shown in Figures 3.2(a)−(c) respectively and the complete set of geometrical parameters given in Tables 3.4−3.6. (In all of the ball-stick figures in this thesis, molecular conformations are displayed as follows: bonds that come out of the page are shown on the top of balls (atoms) and bonds that go into the page end behind balls.) The full geometry optimizations allow us to investigate in detail the interaction between the PO_4^- group and the methyl groups and the relative stability of the global minimum structure.

The calculations illustrate that the conformation with $\alpha_2 = 75°$ and $\alpha_3 = 75°$ (+sc +sc) corresponds to the global minimum energy for compound I. For the second lowest energy conformation, HF/3-21G* and HF/6-31G* basis set optimizations gave somewhat different structural results (see Tables 3.3 and 3.5). For example, α_2's differ by $\approx 20°$ and α_3's differ by 9°. Also, as stated above we were not able to to find the third lowest energy conformation with the 3-21G* basis set. The conformational energy differences (calculated relative to the lowest energy conformation for a given basis set) are in the range 2.89−9.20 kJ/mol (see Table 3.3) which clearly indicates

that compound I is a very flexible system at room temperature (k_BT at $T = 300°$ K is approximately equal to 2.5 kJ/mole).

From Figures 3.2(a)−(c) one notes that the lowest energy conformation, +sc +sc, has the most compact structure. This means that the non-bonded interactions between hydrogens on the methyl groups and oxygens lower the energy of the gauche-gauche system relative to the more extended structures. The nearly trans-trans conformation, "ap ap", gave the highest energy. However, 2.9−9.2 kJ/mol energy differences between conformations illustrate that the molecule will most likely exist in all three conformations at room temperature.

Table 3.3: Magnitudes (in degrees) of dihedral angles, α_2 and α_3, for compound I.

conformation	basis set	angle (deg.)	energy (hartree)	ΔE (kJ/mol)
+sc +sc	STO-3G	$\alpha_2 = 87.3$ $\alpha_3 = 87.0$	−710.340393	
	3-21G*	$\alpha_2 = 74.8$ $\alpha_3 = 75.0$	−715.847778	
	6-31G*	$\alpha_2 = 75.1$ $\alpha_3 = 75.1$	−719.520867	
	6-31+G*	$\alpha_2 = 75.3$ $\alpha_3 = 75.3$	−719.543525	
	MP2/ 3-21G*	$\alpha_2 = 74.8$ $\alpha_3 = 75.0$	−716.592846	
−ac +sc	3-21G*	$\alpha_2 = -146.3$ $\alpha_3 = 65.0$	−715.846728	2.89
	6-31G*	$\alpha_2 = -170.5$ $\alpha_3 = 73.6$	−719.519028	4.98
ap ap	6-31G*	$\alpha_2 = -178.9$ $\alpha_3 = -178.9$	−719.516358	9.20

The results of the 6-31G* basis set calculations will be discussed in more details below. As was alluded to above, the conformation of compound I is determined by the dihedral angles α_2 and α_3. From the values of these two angles, one notes that the lowest and third lowest energy conformations exhibit C_2 symmetry with

Table 3.4: Geometrical parameters for the "sc sc" conformation (corresponding to the global minimum energy) for compound I.

bond length (Å)	STO-3G	3-21G*	6-31G*	6-31+G*
O(13)-P	1.582	1.473	1.470	1.474
O(14)-P	1.582	1.473	1.470	1.474
O(12)-P	1.731	1.634	1.642	1.639
O(11)-P	1.731	1.634	1.642	1.639
C(11)-O(12)	1.423	1.435	1.393	1.396
C(1)-O(11)	1.423	1.435	1.393	1.396
H-C(11)	1.097	1.083	1.086	1.085
H-C(1)	1.097	1.083	1.086	1.085
bond angle (deg.)				
O(14)-P-O(13)	128.8	124.6	124.9	124.6
O(11)-P-O(12)	95.9	98.3	99.5	99.8
C(11)-O(12)-P	120.6	118.2	118.5	119.4
C(1)-O(11)-P	120.6	118.2	118.5	119.4
H-C(11)-O(12)	109.5	109.6	110.2	110.0
H-C(1)-O(11)	109.5	109.6	110.2	110.0
dihedral angle (deg.)				
O(14)-P-O(13)-O(11)	−129.4	−127.4	−127.5	−127.2
O(13)-P-O(14)-O(12)	−129.4	−127.6	−127.5	−127.2
α_3	87.0	75.0	75.1	75.3
α_2	87.4	74.8	75.1	75.3
H(11A)-C(11)-O(12)-P	139.0	168.1	180.0	178.7
H(11B)-C(11)-O(12)-P	18.9	47.4	60.1	58.8
H(11C)-C(11)-O(12)-P	−101.7	−72.4	−61.0	−62.3
H(1A)-C(1)-O(11)-P	138.6	168.3	180.0	178.7
H(1B)-C(1)-O(11)-P	18.5	47.6	60.1	58.8
H(1C)-C(1)-O(11)-P	−102.1	−72.2	−61.0	−62.3

Table 3.5: Geometrical parameters for the "ac ap" conformation for compound I.

bond length ($\AA$)	3-21G*	6-31G*
O(13)-P	1.470	1.469
O(14)-P	1.481	1.477
O(12)-P	1.623	1.627
O(11)-P	1.640	1.648
C(11)-O(12)	1.434	1.394
C(1)-O(11)	1.434	1.392
H-C(11)	1.082	1.085
H-C(1)	1.083	1.086
bond angle (deg.)		
O(14)-P-O(13)	124.6	122.9
O(11)-P-O(12)	98.3	96.7
C(11)-O(12)-P	118.4	119.1
C(1)-O(11)-P	119.0	116.7
H-C(11)-O(12)	109.3	110.9
H-C(1)-O(11)	109.7	110.2
dihedral angle (deg.)		
O(14)-P-O(13)-O(11)	−127.3	−127.9
O(13)-P-O(14)-O(12)	−127.2	−128.8
α_3	65.0	73.6
α_2	−146.3	−170.5
H(11A)-C(11)-O(12)-P	168.2	176.1
H(11B)-C(11)-O(12)-P	48.0	56.3
H(11C)-C(11)-O(12)-P	−72.1	−65.1
H(1A)-C(1)-O(11)-P	159.6	180.5
H(1B)-C(1)-O(11)-P	38.9	60.8
H(1C)-C(1)-O(11)-P	−81.4	−60.5

Table 3.6: Geometrical parameters for the "ap ap" conformation for compound I (obtained with the 6-31G* basis set).

bond length $\AA$		bond angle (deg.)		dihedral angle (deg.)	
O(14)-P	1.477	O(14)-P-O(13)	120.9	O(14)-P-O(13)-O(11)	−128.9
O(13)-P	1.477	O(11)-P-O(12)	94.3	O(13)-P-O(14)-O(12)	−128.9
O(12)-P	1.634	C(11)-O(12)-P	116.5	α_2	−178.9
O(11)-P	1.634	C(1)-O(11)-P	116.5	α_3	−178.9
C(11)-O(12)	1.393	H-C(11)-O(12)	110.1	H(11A)-C(11)-O(12)-P	180.0
C(1)-O(11)	1.393	H-C(1)-O(11)	110.1	H(11B)-C(11)-O(12)-P	60.7
H-C(11)	1.086			H(11C)-C(11)-O(12)-P	−60.7
H-C(1)	1.086			H(1A)-C(1)-O(11)-P	180.0
				H(1B)-C(1)-O(11)-P	60.7
				H(1C)-C(1)-O(11)-P	−60.7

Table 3.7: The summary of Mulliken population analysis (obtained with 6-31G* basis set) for compound I for its three conformations as indicated in the table. The magnitudes of the total and the components of the dipole moments (μ) are also given in this table.

atom	"sc sc"	"ap sc"	"ap ap"
P	1.56	1.53	1.50
O(14)	−0.81	−0.79	−0.82
O(13)	0.81	−0.84	−0.82
O(12)	−0.73	−0.70	−0.70
O(11)	−0.73	−0.73	−0.70
C(11)	0.26	0.27	0.26
C(1)	0.26	0.26	0.26
μ (debye)	5.77	5.03	2.43
μ_X	0.00	0.29	0.00
μ_Y	5.77	5.00	2.43
μ_Z	0.00	0.47	0.00

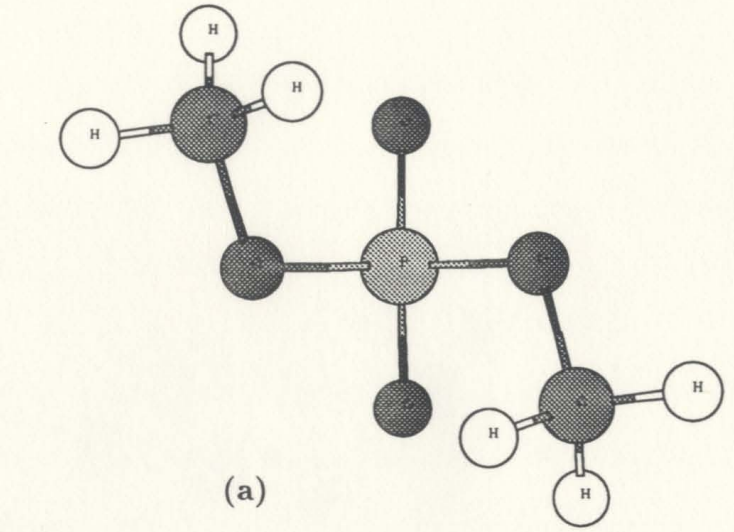

(a)

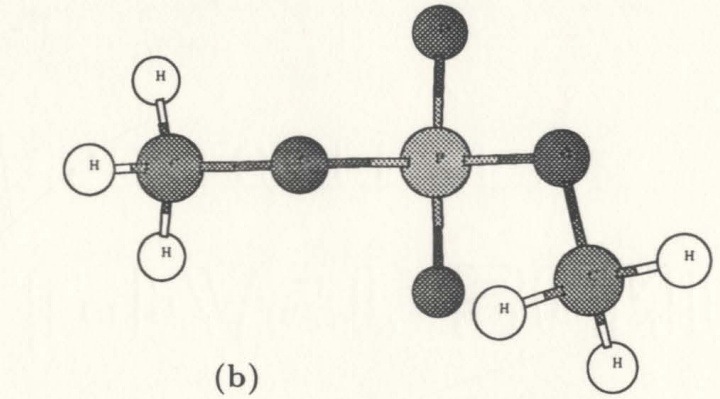

(b)

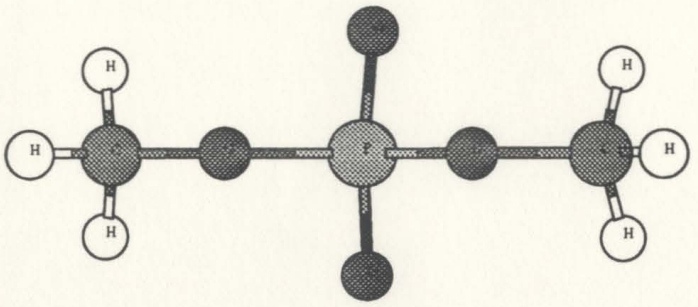

(c)

Figure 3.2 (**a**) The lowest energy conformation for compound I (+sc +sc).

(**b**) The second lowest energy conformation for compound I (+sc ap).

(**c**) The third lowest energy conformation for compound I (ap ap).

The figures correspond to the geometrical parameters obtained in the 6-31G* basis set calculations (see Table 3.3).

the main axis located at the central phosphorus atom (but not the second lowest energy conformation). This result is independent of the basis set used.

The P−O bond lengths also mirror this behavior. The P−O bond lengths along the chain backbone in the lowest energy conformation are slightly longer (1.642 $\AA$) than those in the ap ap conformation (1.634 $\AA$). The lack of C_2 symmetry is displayed in the second lowest energy conformation where two types of (unequal) P−O bonds exist (1.627 $\AA$ and 1.648 $\AA$). This phenomenon may be explained by the anomeric effect.[9] The shorter distance between the hydrogens on the methyl groups and the oxygens strengthens their mutual attractions and consequently lengthens the P−O bond lengths.

The bond angle, the O(11)−P−O(12) decreases (from 99.5° to 94.34°) on going from the lowest to the third lowest energy conformation. It is suspected that the larger distance between the two methyl groups reduces the repulsion between the two methyl groups and thus allows oxygens to approach closer. The bond angle, the O(11)−P−O(12) decreases to 96.7° (from 99.8°) in the second lowest energy conformation. Similarly, the bond angle O(13)−P−O(14) decreases (from 124.9° to 122.9° to 120.9°) as the methyl groups are moved further away from the oxygens.

The HF/6-31G* calculations also show that the +sc +sc (sometimes also referred to as gauche−gauche) conformation corresponds to the global minimum energy. The other two conformations have energies 4.98 and 9.20 kJ/mol higher relative to the +sc +sc conformation. On the other hand, the HF/3-21G* calculations show that there is a 2.89 kJ/mol energy difference between first and second conformations.

In addition, in order to estimate the importance of the beyond HF corrections in the total energy calculations MP2/3-21G* single point energy calculation (using the nuclear geometry as obtained from HF/3-21G* calculation) was performed for

the lowest energy conformation. The total energy difference between the HF/3-21G* and MP2/3-21G* total energy values is 1954.8 kJ/mol. This difference is much smaller (by a factor of five) than the total energy difference obtained from the calculations with 3-21G* and 6-31G* basis sets. This illustrates that the beyond HF corrections do not lower the total energies significantly in comparison to the the lowering obtained when computing with higher basis set. We have not studied the effect of the HF corrections on the conformational energy differences.

The molecular model is an ion, i.e., there is a net charge -1 electron on the molecule. Table 3.7 summarizes the results of Mulliken population analysis for the three conformations of compound I for the 6-31G* basis set calculations. The electron density distributions (net charges) are given. As discussed in chapter 2, their values are a function of molecular orbitals and thus cannot be determined uniquely i.e. the net charges depend on the choice of basis set. The charges of every atom labeled in the Table 3.7 indicate the estimated total net charge on each atom plus its neighboring hydrogen atoms if there are any. For example, the total net charge for the central carbon atom in the methyl end groups is a sum of the net charges of carbon and the three hydrogen atoms. From Table 3.7, it is evident that the lowest energy conformation displays largest charge separation as indicated by the large positive charge on the phosphorus atom. This conformation also has the largest magnitude of the dipole moment. In all three conformations the dipole moment points (in this work, the dipole moment is taken to point from a net negative charge towards a net positive charge) away from the oxygens O(13) and O(14) (with net negative charges) towards phosphorus and methyl end groups (with net positive charges). For example in the both the +sc +sc and ap ap conformations the direction of the dipole moments is along the two-fold axis of symmetry. It is interesting to note that the net positive charge in the total dipole moment in these conformations is

due to two approximately equivalent contributions from the phosphorus and methyl end groups. In the ap ap conformation the contribution from methyl groups is significantly smaller due to the decreased distance between the methyl groups and oxygens O(13) and O(14). Thus in this conformation the dipole moment is primarily due to the charge separation between oxygens and the phosphorus atom.

The significance of compound I is that its global conformation is +sc +sc. We will find that with small modifications α_2 and α_3 will remain close to 70° in all global conformations for compounds II–V.

3.3 Compound II

3.3.1 Rigid–Rotor Scans

Compound II has the molecular structure as shown in Figure 3.4. It is an extension of compound I. Therefore the studies of compound II and compound I are closely related. In section 3.2, we established that the +sc, +sc (as it relates to the two dihedral angles α_2 and α_3) conformation is the most stable conformation for the dimethyl phosphate anion. In this part of the work we focus on determining the values for the two other torsional angles, α_1 (C(2)-C(1)-O(11)-P) and α_4 (P-O(12)-C(11)-C(12)), which in turn determine the positions of the C(2) and C(12) atoms relative to the chain backbone (see Figure 1.6). As before, in order to determine the approximate values for these two angles, we performed a rigid-rotor scans which involved the calculations of single point energies as a function of α_1 and α_4 in the range of 0–360° at 30° intervals (in these scans, the central part of compound II, α_2 and α_3 and the other geometrical parameters were fixed at the global minimum values as was determined for compound I, the additional parameters for the end methyl groups were taken to have tetrahedral geometry with the ideal values for bond lengths and angles).

The results of the scan are shown in Figure 3.3(a). From this figure we can predict that there are three minima at the approximate values of α_1 and α_4: ($\alpha_1 = 90°$, $\alpha_4 = 90°$), ($\alpha_1 = 180°$, $\alpha_4 = 90°$) and ($\alpha_1 = 270°(-90°)$, $\alpha_4 = 90°$) with α_2 and α_3 taking +sc +sc conformation. The results are also shown in the contour (Figure 3.3(b)). In addition, the contour figure displays other minima at points ($\alpha_1 = 270°$, $\alpha_4 = 90°$) and ($\alpha_4 = 270°$, $\alpha_4 = 270°$). The point ($\alpha_1 = 270°$, $\alpha_4 = 90°$) is roughly equivalent to ($\alpha_1 = 270°(-90°)$, $\alpha_4 = 90°$) minimum on the contour plot. Based on symmetry arguments alone we would say that these minima should have identical energies associated with them. The minimum at $\alpha_1 = 180°$, $\alpha_4 = 90°$ is not clearly visible on the contour figure. However, a small plateau is located near this region. We note that there is a similar leveling off at the $\alpha_1 = 90°$, $\alpha_4 = 180°$ point, which again from the symmetry alone should be equivalent to $\alpha_1 = 180°$, $\alpha_4 = 90°$ point. It is interesting to note that the shape of the global minimum ($\alpha_1 = 90°$, $\alpha_4 = 90°$) is shallow and very broad, whereas the ($\alpha_1 = 270°(-90°)$, $\alpha_4 = 90°$) minimum is deep and narrow with large energy barriers due to rotation surrounding it. This feature of the conformational surface will affect the dynamic torsional flexibility of this molecular system. Typically larger barriers indicate longer relaxation times which in turn lengthen the interconversion times between the two conformations.

Finally, we note that the comparison between Figures 3.1 and 3.3 illustrates that the energy differences for compound II are hundreds of kJ/mole instead of tens of kJ/mole. This is due to the fact that in compound II there are large steric interactions when the ethyl groups containing $C(12)H_3$ and/or $C(2)H_3$ are rotated. These steric interactions are significantly decreased when atoms are allowed to relax in the geometry optimizations (all optimized energy differences are less than 9.2 kJ/mole).

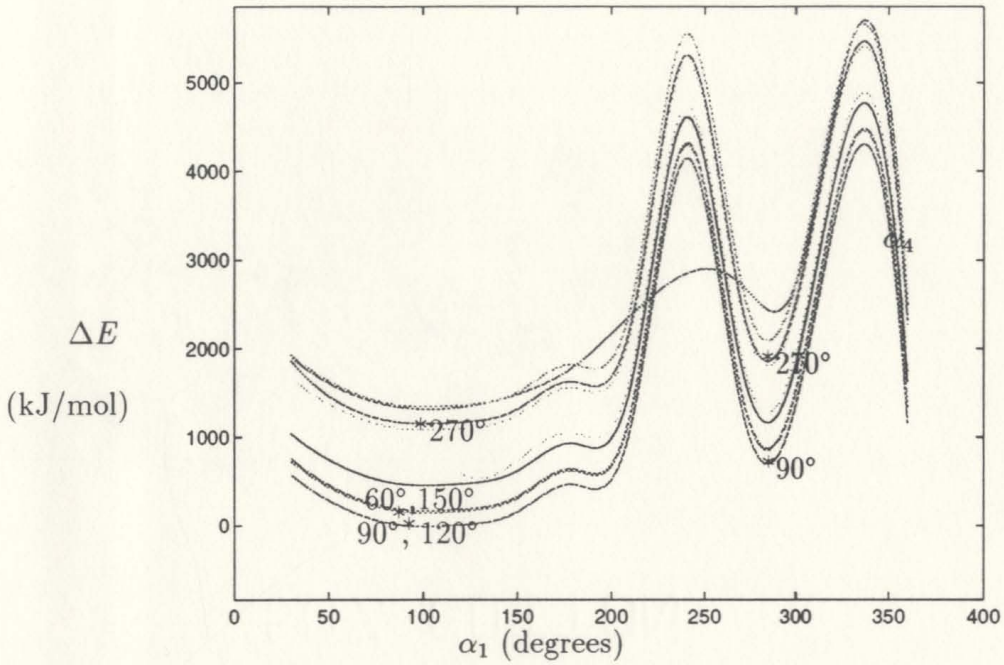

Figure 3.3(a). The plot of scanning results of α_1 and α_4 for compound II. The points labeled by "*" correspond to the minima displayed in Figure 3.3(b). The numbers next to these minima are values for α_4.

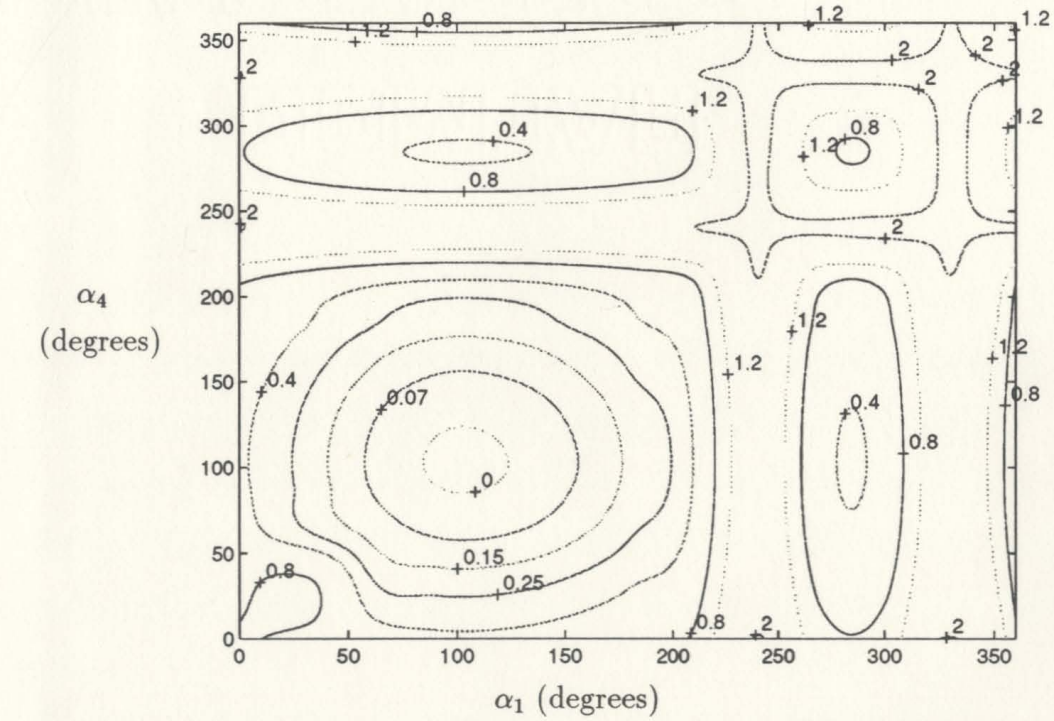

Figure 3.3(b). The contour plot of α_1 and α_4 for compound II.

3.3.2 Geometry Optimized Results

Given these approximate locations for the minima as obtained from the rigid-rotor scans, we have performed complete geometry optimizations around them. Table 3.8 summarizes our findings. All four inequivalent minima described above have the corresponding stable (optimized) structures associated with them with some adjustments for geometrical parameters. For example, α_2 and α_3 are less than 75° in the global minimum conformation and α_1 and α_4 exhibit deviations of order of 10° to 20° from the expected values of 90° as predicted by the rigid-rotor scans. The corresponding conformational energy differences for these local minimum structures are 2.89, 5.52 and 6.02 kJ/mole. Based on the energy difference values it would appear that the system would oscillate between the global minimum (sc sc sc sc conformation) and the first local minimum (sc sc ac −sc conformation) structures (which is only 2.89 kJ/mole higher). However, from the scan (Figure 3.3) we note that the global minimum and the first local minimum are separated by a large rotational energy barrier and the shapes of the minima are as described above. On the other hand the third local minimum (ap sc ac sc conformation) structure (which is 6.02 kJ/mole higher than the global minimum) is separated from the global minimum by a relatively small energy barrier (see Figure 3.3(a)). This combined with the fact that the global minimum energy well is rather shallow would indicate that the system would oscillate between the global minimum and the third local minimum conformations. It should also be noted that geometry optimization is critical in order to obtain reasonable values for the energy differences. The rigid-rotor scan indicates that they are of the order of hundreds of kJ/mole instead of 1 kJ/mole. Similar scaling factors should probably be applied to the rotational energy barriers.

Optimized geometrical parameters for compound II are listed in Tables 3.9–3.12.

Table 3.8: Magnitudes (in degrees) of dihedral angles, α_1 to α_4, for compound II.

conformation	angle (deg.)	energy (hartree)	Δ E (kJ/mol)
	$\alpha_1 = 83.6$		
I	$\alpha_2 = 70.8$		
+sc +sc +sc +sc	$\alpha_3 = 70.8$		
	$\alpha_4 = 83.6$	−793.502923	
	$\alpha_1 = 83.6$		
II	$\alpha_2 = 66.1$		
+sc +sc +ac −sc	$\alpha_3 = 98.7$		
	$\alpha_4 = -70.4$	−793.501792	2.89
	$\alpha_1 = -70.1$		
III	$\alpha_2 = 96.4$		
−sc +ac +ac −sc	$\alpha_3 = 96.5$		
	$\alpha_4 = -70.1$	−793.500795	5.52
	$\alpha_1 = 170.8$		
IV	$\alpha_2 = 73.7$		
ap +sc +sc +sc	$\alpha_3 = 73.5$		
	$\alpha_4 = 83.9$	−793.500627	6.02
	$\alpha_1 = -76$		
V	$\alpha_2 = -106$		
−sc −ac +ac +sc	$\alpha_3 = 105.5$		
	$\alpha_4 = 75.8$	−793.500472	6.32
	$\alpha_1 = 162.6$		
VI	$\alpha_2 = -146.2$		
ap −ac +sc +sc	$\alpha_3 = 65.2$		
	$\alpha_4 = 82$	−793.499878	8.16
	$\alpha_1 = 64.8$		
VII	$\alpha_2 = 130.3$		
+sc +ac −sc +ac	$\alpha_3 = -67.8$		
	$\alpha_4 = 100.9$	−793.499394	9.20

Table 3.9: Geometrical parameters the "sc sc sc sc" and "sc sc ac −sc" conformations for compound II.

bond length ($\AA$)		bond angle (deg.)		dihedral angle (deg.)	
conformation I					
O(13)-P	1.475	O(14)-P-O(13)	124.1	O(14)-P-O(13)-O(11)	−127.9
O(14)-P	1.475	O(12)-P-O(11)	98.1	O(13)-P-O(14)-O(12)	−127.9
O(12)-P	1.633	C(11)-O(12)-P	119.4	α_1	83.6
O(11)-P	1.633	C(1)-O(11)-P	119.4	α_2	70.8
C(11)-O(12)	1.441	C(12)-C(11)-O(12)	110.3	α_3	70.8
C(1)-O(11)	1.441	C(2)-C(1)-O(11)	108.4	α_4	83.6
C(12)-C(11)	1.530	H-C(11)-O(12)	108.4	H(11A)-C(11)-O(12)-P	−155.7
C(2)-C(1)	1.530	H-C(1)-O(11)	108.4	H(11B)-C(11)-O(12)-P	−38.0
H-C(11)	1.083	H-C(12)-C(11)	109.2	H(1A)-C(1)-O(11)-P	−155.7
H-C(1)	1.083	H-C(2)-C(1)	109.4	H(1B)-C(1)-O(11)-P	−38.0
H-C(12)	1.086			H(12A)-C(12)-C(11)-O(12)	180.2
H-C(2)	1.084			H(12B)-C(12)-C(11)-O(12)	59.5
				H(12C)-C(12)-C(11)-O(12)	−59.0
				H(2A)-C(2)-C(1)-O(11)	180.2
				H(2B)-C(2)-C(1)-O(11)	59.6
				H(2C)-C(2)-C(1)-O(11)	−59.0
conformation II					
O(13)-P	1.480	O(14)-P-O(13)	124.2	O(14)-P-O(13)-O(11)	−126.7
O(14)-P	1.474	O(12)-P-O(11)	98.7	O(13)-P-O(14)-O(12)	−128.0
O(12)-P	1.633	C(11)-O(12)-P	119.7	α_1	83.6
O(11)-P	1.630	C(1)-O(11)-P	119.9	α_2	66.1
C(11)-O(12)	1.438	C(12)-C(11)-O(12)	111.4	α_3	98.7
C(1)-O(11)	1.441	C(2)-C(1)-O(11)	110.4	α_4	−70.4
C(12)-C(11)	1.533	H-C(11)-O(12)	107.6	H(11A)-C(11)-O(12)-P	168.9
C(2)-C(1)	1.531	H-C(1)-O(11)	108.4	H(11B)-C(11)-O(12)-P	50.4
H-C(11)	1.081	H-C(12)-C(11)	107.5	H(1A)-C(1)-O(11)-P	−155.8
H-C(1)	1.083	H-C(2)-C(1)	109.2	H(1B)-C(1)-O(11)-P	−38.3
H-C(12)	1.083			H(12A)-C(12)-C(11)-O(12)	−174.7
H-C(2)	1.084			H(12B)-C(12)-C(11)-O(12)	65.2
				H(12C)-C(12)-C(11)-O(12)	−54.0
				H(2A)-C(2)-C(1)-O(11)	−178.9
				H(2B)-C(2)-C(1)-O(11)	60.5
				H(2C)-C(2)-C(1)-O(11)	−58.0

Table 3.10: Geometrical parameters the "−sc ac ac −sc" and "ap sc sc sc" conformations for compound II.

bond length (Å)		bond angle (deg.)		dihedral angle (deg.)	
conformation III					
O(13)-P	1.475	O(14)-P-O(13)	124.5	O(14)-P-O(13)-O(11)	−126.7
O(14)-P	1.475	O(12)-P-O(11)	99.5	O(13)-P-O(14)-O(12)	−126.7
O(12)-P	1.630	C(11)-O(12)-P	120.1	α_1	−70.1
O(11)-P	1.630	C(1)-O(11)-P	120.1	α_2	96.4
C(11)-O(12)	1.438	C(12)-C(11)-O(12)	111.3	α_3	96.5
C(1)-O(11)	1.438	C(2)-C(1)-O(11)	111.3	α_4	−70.1
C(12)-C(11)	1.533	H-C(11)-O(12)	108.1	H(11A)-C(11)-O(12)-P	50.9
C(2)-C(1)	1.533	H-C(1)-O(11)	108.1	H(11B)-C(11)-O(12)-P	169.3
H-C(11)	1.081	H-C(12)-C(11)	109.6	H(1A)-C(1)-O(11)-P	50.8
H-C(1)	1.081	H-C(2)-C(1)	109.6	H(1B)-C(1)-O(11)-P	169.3
H-C(12)	1.083			H(12A)-C(12)-C(11)-O(12)	−174.2
H-C(2)	1.083			H(12B)-C(12)-C(11)-O(12)	65.6
				H(12C)-C(12)-C(11)-O(12)	−53.3
				H(2A)-C(2)-C(1)-O(11)	−174.3
				H(2B)-C(2)-C(1)-O(11)	65.5
				H(2C)-C(2)-C(1)-O(11)	−53.4
conformation IV					
O(13)-P	1.472	O(14)-P-O(13)	124.5	O(14)-P-O(13)-O(11)	−128.0
O(14)-P	1.475	O(12)-P-O(11)	98.2	O(13)-P-O(14)-O(12)	−127.5
O(12)-P	1.633	C(11)-O(12)-P	119.3	α_1	170.8
O(11)-P	1.634	C(1)-O(11)-P	118.5	α_2	73.7
C(11)-O(12)	1.440	C(12)-C(11)-O(12)	110.2	α_3	73.5
C(1)-O(11)	1.438	C(2)-C(1)-O(11)	107.2	α_4	83.9
C(12)-C(11)	1.530	H-C(11)-O(12)	108.5	H(11A)-C(11)-O(12)-P	−155.4
C(2)-C(1)	1.527	H-C(1)-O(11)	109.6	H(11B)-C(11)-O(12)-P	−37.7
H-C(11)	1.083	H-C(12)-C(11)	109.6	H(1A)-C(1)-O(11)-P	49.5
H-C(1)	1.082	H-C(2)-C(1)	109.2	H(1B)-C(1)-O(11)-P	−68.9
H-C(12)	1.083			H(12A)-C(12)-C(11)-O(12)	179.9
H-C(2)	1.084			H(12B)-C(12)-C(11)-O(12)	59.2
				H(12C)-C(12)-C(11)-O(12)	−59.4
				H(2A)-C(2)-C(1)-O(11)	179.6
				H(2B)-C(2)-C(1)-O(11)	58.8
				H(2C)-C(2)-C(1)-O(11)	−59.7

Table 3.11: Geometrical parameters the "−sc −ac ac sc" and "ap −ac sc sc" conformations for compound II.

bond length (Å)		bond angle (deg.)		dihedral angle (deg.)	
conformation V					
O(13)-P	1.468	O(14)-P-O(13)	123.0	O(14)-P-O(13)-O(11)	−126.7
O(14)-P	1.488	O(12)-P-O(11)	100.5	O(13)-P-O(14)-O(12)	−125.5
O(12)-P	1.630	C(11)-O(12)-P	121.1	α_1	−75.5
O(11)-P	1.630	C(1)-O(11)-P	121.1	α_2	−106.0
C(11)-O(12)	1.438	C(12)-C(11)-O(12)	110.6	α_3	105.5
C(1)-O(11)	1.438	C(2)-C(1)-O(11)	110.6	α_4	75.8
C(12)-C(11)	1.531	H-C(11)-O(12)	108.6	H(11A)-C(11)-O(12)-P	−45.1
C(2)-C(1)	1.531	H-C(1)-O(11)	108.6	H(11B)-C(11)-O(12)-P	−163.6
H-C(11)	1.081	H-C(12)-C(11)	108.9	H(1A)-C(1)-O(11)-P	163.8
H-C(1)	1.081	H-C(2)-C(1)	109.3	H(1B)-C(1)-O(11)-P	45.0
H-C(12)	1.083			H(12A)-C(12)-C(11)-O(12)	176.4
H-C(2)	1.083			H(12B)-C(12)-C(11)-O(12)	55.5
				H(12C)-C(12)-C(11)-O(12)	−63.5
				H(2A)-C(2)-C(1)-O(11)	−176.4
				H(2B)-C(2)-C(1)-O(11)	63.5
				H(2C)-C(2)-C(1)-O(11)	−55.5
conformation VI					
O(13)-P	1.469	O(14)-P-O(13)	122.5	O(14)-P-O(13)-O(11)	−128.7
O(14)-P	1.484	O(12)-P-O(11)	97.3	O(13)-P-O(14)-O(12)	−127.9
O(12)-P	1.621	C(11)-O(12)-P	120.3	α_1	162.6
O(11)-P	1.640	C(1)-O(11)-P	119.4	α_2	−136.2
C(11)-O(12)	1.439	C(12)-C(11)-O(12)	110.3	α_3	65.2
C(1)-O(11)	1.438	C(2)-C(1)-O(11)	107.3	α_4	82.3
C(12)-C(11)	1.531	H-C(11)-O(12)	108.8	H(11A)-C(11)-O(12)-P	−156.9
C(2)-C(1)	1.527	H-C(1)-O(11)	108.1	H(11B)-C(11)-O(12)-P	−39.5
H-C(11)	1.082	H-C(12)-C(11)	109.0	H(1A)-C(1)-O(11)-P	41.1
H-C(1)	1.081	H-C(2)-C(1)	109.7	H(1B)-C(1)-O(11)-P	−77.6
H-C(12)	1.083			H(12A)-C(12)-C(11)-O(12)	−178.5
H-C(2)	1.084			H(12B)-C(12)-C(11)-O(12)	60.9
				H(12C)-C(12)-C(11)-O(12)	−57.5
				H(2A)-C(2)-C(1)-O(11)	178.8
				H(2B)-C(2)-C(1)-O(11)	58.1
				H(2C)-C(2)-C(1)-O(11)	−60.5

In addition to performing our conformational analysis for compound II with α_2 and α_3 near 75°, we could also begin geometry optimizations with α_2 and α_3 close to the $-146°$ and 65° respective values corresponding to the −ac +sc conformation which is the first local minimum structure for compound I. In this case, we find that α_1 and α_4 take on values close to $-90°$ and 90° (actual values are $-76°$ and 76°) and 180° and 90° (actual values are 163° and 82°) for the next two lowest conformations corresponding to

Table 3.12: Geometrical parameters the "sc ac −sc ac" conformation for compound II.

bond length (Å)		bond angle (deg.)		dihedral angle (deg.)	
conformation VII					
O(13)-P	1.483	O(14)-P-O(13)	123.2	O(14)-P-O(13)-O(11)	−127.9
O(14)-P	1.468	O(12)-P-O(11)	99.0	O(13)-P-O(14)-O(12)	−124.8
O(12)-P	1.624	C(11)-O(12)-P	120.2	α_1	64.8
O(11)-P	1.642	C(1)-O(11)-P	119.9	α_2	130.3
C(11)-O(12)	1.438	C(12)-C(11)-O(12)	109.2	α_3	−67.8
C(1)-O(11)	1.440	C(2)-C(1)-O(11)	111.8	α_4	100.9
C(12)-C(11)	1.531	H-C(11)-O(12)	108.6	H(11A)-C(11)-O(12)-P	−139.1
C(2)-C(1)	1.532	H-C(1)-O(11)	108.4	H(11B)-C(11)-O(12)-P	−21.2
H-C(11)	1.082	H-C(12)-C(11)	107.5	H(1A)-C(1)-O(11)-P	174.5
H-C(1)	1.081	H-C(2)-C(1)	109.4	H(1B)-C(1)-O(11)-P	−56.2
H-C(12)	1.083			H(12A)-C(12)-C(11)-O(12)	177.5
H-C(2)	1.084			H(12B)-C(12)-C(11)-O(12)	61.7
				H(12C)-C(12)-C(11)-O(12)	−56.3
				H(2A)-C(2)-C(1)-O(11)	173.6
				H(2B)-C(2)-C(1)-O(11)	52.6
				H(2C)-C(2)-C(1)-O(11)	−66.6

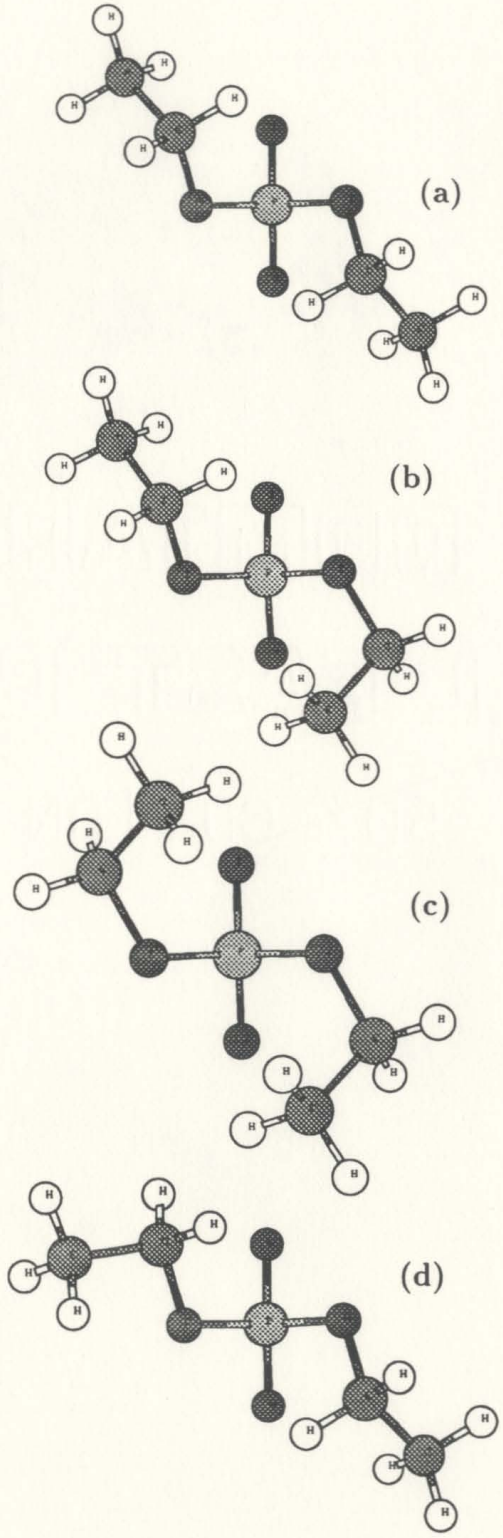

Figure 3.4 The conformations for compound II
shown in order of increasing energies as listed in Table 3.8.

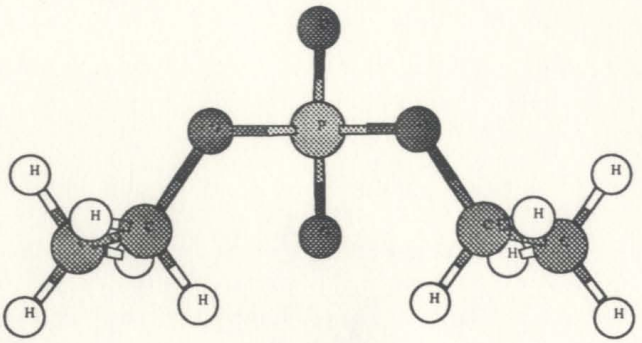

(e)

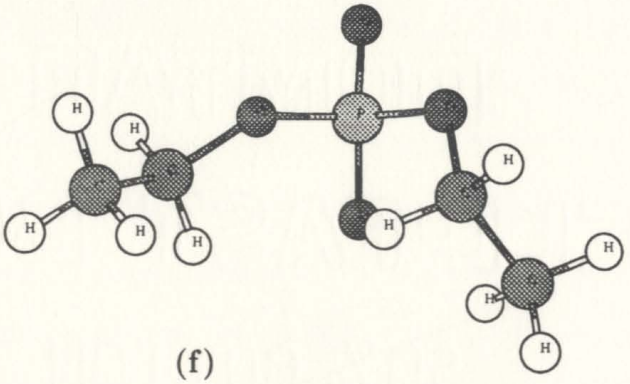

(f)

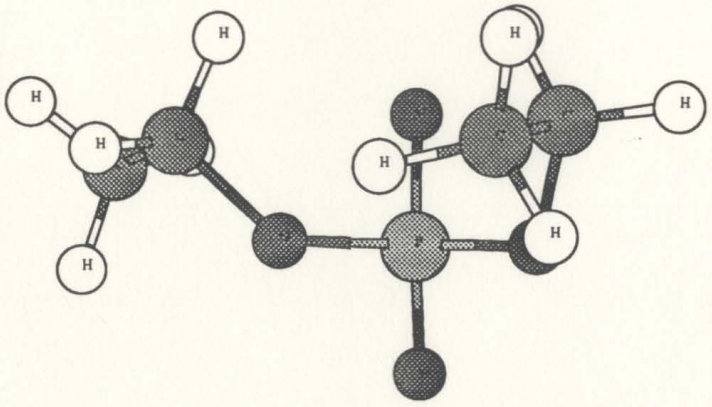

(g)

Figure 3.4 The conformations for compound II
shown in order of increasing energies as listed in Table 3.8.

the energies 6.32 and 8.16 kcal/mole above the global minimum. The highest energy local minimum structure has energy difference of 9.20 kJ/mole and has its α_1 and α_4 angles close to 65° and 101° (which would correspond roughly to the 90° and 90° values on the scan which in turn are close to the global minimum values). It should be noted that compound II has a near C_2 symmetry in its global minimum conformation, thus α_1 and α_4 are interchangeable and cannot be uniquely defined. This is important in our conformational analysis since it decreases our conformational search.

As stated above we have found seven possible stable conformations for compound II. The three lowest energy structures have approximate "sc sc" conformation about the phosphate. Their bond lengths and bond angles are very similar to those in the "sc sc" conformation for the dimethyl phosphate. The lowest energy conformations for compound I and II both exhibit similar values for the torsional angles α_2, α_3 (see Tables 3.4 and 3.9). In compound II, the values of α_1, α_4 dihedral angles are similar to those of α_2, α_3. This means that the carbon atoms C(1), C(11) and C(2), C(12) are symmetric relative to the central phosphorus atom. Comparing the global minimum conformations for compounds I and II we observe that their O(13)−P (=O(14)−P) bonds differ by 0.002 $\AA$ and bond angles O(14)−P−O(13) and C(11)−O(12)−P differ by 0.5° and 1° respectively. The torsional angles α_2 and α_3 decrease from 75.0° to 70.8°. That is in compound II (relative to compound I) there are small decreases in the torsional angles α_2 and α_3 that are accompanied by small increases in bond lengths and bond angles due to the presence of the additional carbon atoms, C(2) and C(12).

For most geometrical parameters, there are only small differences between bond lengths and bond angles between the lowest and the second lowest energy conformations for compound II. On the other hand, the dihedral angle α_3 significantly

deviates (by 28°) from the 71° value in order to accommodate the steric interactions that accompanies the rotation around O(12)−C(11) bond. The energy difference between these conformations is 2.89 kJ/mol.

It is significant to point out that x-ray diffraction studies that are used to determine geometry of many phospholipid molecules[4] give α_1 close to 180°. In our conformational analysis, this corresponds to the fourth lowest energy conformation which, from the rigid-rotor scan, is the most accessible local minimum from the global minimum state for compound II. It would thus appear that the atoms beyond compound II play a very important role in determining the geometrical structure and energetics of phospholipids.

Table 3.13 summarizes the results of Mulliken population analysis for the seven conformations of compound II for the 3-21G* basis set calculations. Similarly to the Table 3.7, only the net charges of "heavy" atoms are listed in this table (the charges of neighboring, covalently bonded hydrogens are included in the net charge of the "heavy" atoms). The magnitudes of the dipole moments for all conformations ranges from approximately 6 to 7 debye as shown in Table 3.13. In all of the seven conformations the net charges on O(11), O(12), O(13) and O(14) remain relatively unchanged. This is also true for the phosphorus atoms and the hydrocarbon groups belonging to C(1) and C(11), and C(2) and C(12) atoms respectively (with the net charge on C(2) and C(12) considerably less, by a factor of $\approx$ ten, than on C(1) and C(11)). Yet the dipole moments for the seven conformations tend to increase as the conformation changes from the lowest to the highest conformational energy difference. Since the positions of the oxygens do not change, the increase in the magnitudes of the dipole moment must be attributed to the positions of the ethyl groups. A similar conclusion has been reached for compound I (see discussion above). In all conformations (again similar to compound I) a single component of

the dipole moment contributes all or almost all value to its total magnitude. This property is a reflection of the underlying near C_2 symmetry of this molecule. That is, the more symmetric the particular conformation is, the less contribution from the other components to the total dipole moment. As in the case of compound I this component (and thus the dipole moment) points away from the O(13) and O(14) toward the phosphorus atoms and the alkane side groups roughly along the axis centered on the phosphorus atom and perpendicular to the plane bisecting the four oxygen atoms. In general the magnitudes of dipole moments for compound II are somewhat larger than for compound I (in the +sc +sc and +sc ap conformations). This could be attributed to the presence of the additional small charge separations in the end methyl groups centered on C(12) and C(2).

Table 3.13: The summary of Mulliken population analysis (obtained with 3-21G* basis set) for compound II for its seven conformations as indicated in the table. The magnitudes of the total and the components of the dipole moments (μ) are also given in this table.

atom group	I	II	III	IV	V	VI	VII
P	1.53	1.54	1.55	1.52	1.52	1.51	1.52
O(14)	−0.76	−0.76	−0.77	−0.76	−0.72	−0.72	−0.80
O(13)	−0.76	−0.77	−0.77	−0.76	−0.81	−0.79	−0.72
O(12)	−0.75	−0.76	−0.76	−0.75	−0.74	−0.74	−0.73
O(11)	−0.75	−0.74	−0.76	−0.75	−0.74	−0.76	−0.76
C(11)	0.28	0.30	0.30	0.28	0.29	0.28	0.29
C(1)	0.28	0.28	0.30	0.31	0.29	0.32	0.29
C(12)	−0.03	−0.04	−0.04	−0.03	−0.04	−0.04	−0.04
C(2)	−0.03	−0.03	−0.04	−0.05	−0.04	−0.05	−0.04
μ (debye)	5.99	6.02	5.81	6.62	6.02	7.04	6.81
μ_X	0.00	0.80	0.00	−1.70	0.00	−1.94	−1.48
μ_Y	5.99	5.79	5.82	6.33	5.93	6.76	6.60
μ_Z	0.00	−1.32	0.00	0.85	1.00	0.19	0.85

We summarize this section by noting that the rotation of the ethyl groups (about

O(12)−C(11) bond and O(11)−C(1) bond respectively) at the two ends of the compound II plays an important role in determining the system energy and its stability. However, Table 3.8 shows that there are small energy differences between the six conformations indicating once again that these compounds are quite flexible.

3.4 Compound III – PE Plus Methyl End Group

3.4.1 Rigid−Rotor Scans

Compound III is constructed by attaching NH_3^+ group to the terminal carbon atom, C(12), of compound II. That is, compound III has a molecular structure of PE with an additional methyl end group $C(2)H_3$. This compound contains most of the atoms present in a typical headgroup of a phospholipid molecule. Therefore, the studies on compound III might reveal a number of interesting properties of the headgroup of phospholipid molecule. However, since compound III is a single model molecule, we will find that it is rather a poor model of phospholipid headgroup. In fact, this model compound dramatically illustrates the important role of hydration forces due to water molecules in stabilizing the structures of the phospholipid headgroups (see chapter 4). We performed similar conformational analysis for compound III as was done for compounds I and II. However, because the primary role of this compound is to illustrate the role of water molecules in determining the structure of polar headgroups, we will not discuss it as extensively.

We have used the structural results from compounds I and II to determine the beginning structure for the rigid-rotor scans for compound III. The addition of the NH_3^+ group means that the critical parameters determining the system energy must now include five dihedral angles: α_1, α_2, α_3, α_4 (as in compound I) and the new angle α_5 (O(12)-C(11)-C(12)-N) (see Figure 1.6). We performed two types of two-dimensional CPES scans by varying the following sets of the torsional angles (α_1,

α_5) and (α_4, α_5). The scanning results are displayed in Figure 3.5 and 3.6. In the scans, the three torsional angles α_1, α_4 and α_5 are varied from 30° to 360° in intervals of 30°. As can be seen from Figures 3.5 and 3.6 the energy scans are accompanied by large energy changes. The largest energy difference is close to 1.2×10^4 kJ/mol. The scans do not allow for relaxation of geometrical parameters other than one of the torsional angles as listed above. As a consequence some atoms approach each other too closely and give rise to large variations in energy.

From Figure 3.5(a) and 3.6(a) we can observe four minimum energy structures. They are located near the following torsional angles:

1. $\alpha_1 = 83°$, $\alpha_2 = 71°$, $\alpha_3 = 71°$, $\alpha_4 = 90°$, $\alpha_5 = 180°$,
2. $\alpha_1 = 83°$, $\alpha_2 = 71°$, $\alpha_3 = 71°$, $\alpha_4 = 270°$, $\alpha_5 = 180°$,
3. $\alpha_1 = 90°$, $\alpha_2 = 71°$, $\alpha_3 = 71°$, $\alpha_4 = 83°$, $\alpha_5 = 180°$,
4. $\alpha_1 = 270°$, $\alpha_2 = 71°$, $\alpha_3 = 71°$, $\alpha_4 = 83°$, $\alpha_5 = 180°$

From the contour plots (Figure 3.5(b) and 3.6(b)) we identify additional minima close to the following torsional angles (of course at higher energies than above):

5. $\alpha_1 = 83°$, $\alpha_2 = 71°$, $\alpha_3 = 71°$, $\alpha_4 = 90°$, $\alpha_5 = 330°$,
6. $\alpha_1 = 83°$, $\alpha_2 = 71°$, $\alpha_3 = 71°$, $\alpha_4 = 270°$, $\alpha_5 = 330°$,
7. $\alpha_1 = 90°$, $\alpha_2 = 71°$, $\alpha_3 = 71°$, $\alpha_4 = 83°$, $\alpha_5 = 330°$,
8. $\alpha_1 = 270°$, $\alpha_2 = 71°$, $\alpha_3 = 71°$, $\alpha_4 = 83°$, $\alpha_5 = 330°$

In compound II, α_1 and α_4 are equivalent. Thus minima corresponding to the first and the third or to the fifth and the seventh set of angles (see above) are also equivalent. Due to the presence of NH_3^+, this is not exactly the case in this compound, however it is expected that the structures in these minima for similar values of α_5 would exhibit small energy differences. It is important to note that in our scans we have fixed the values of the dihedral angles α_2 and α_3 to 71° as has been obtained in compound II. The sc sc conformation for α_1 and α_4 is also consistent

with the experimental findings[4] for most of the biological membrane lipids. Our scans also indicate that the torsional angle, α_5, remains close to the value of 180° in the most stable conformation. This result disagrees with x-ray observations which find "±sc" conformation for this dihedral angle. In the higher energy conformations the torsional angle, α_5, takes on a value close to 330° or −30° which is closer to the experimentally determined value. The dihedral angles, α_1 and α_4, are close to the ±sc conformation instead of the ap found in experiment. We suspect that all of these inadequacies are due to the fact that scans were of the "rigid-rotor" type. Finally we note that minima of the type 1 and 3 (see above) are rather broad and shallow and the contour plots (Figures 3.5(b) and 3.6(b)) display near symmetry in the locations of the minima.

3.4.2 Geometry Optimized Results

As in sections 3.2 and 3.3 we have used the results of the rigid-rotor scans to find the most stable (fully geometry optimized) structure for compound III. The results from the complete geometry optimizations are summarized in Table 3.13 and the complete set of geometrical parameters is given in Tables 3.14–3.16. Their respective three-dimensional conformations are displayed in Figure 3.7. The geometry optimized conformations for compound III differ significantly from the expected experimental findings for GPE for the corresponding parts. The lowest energy conformation (+ac +sc +ap +sc −sc) give the unexpected result of NH_3^+ group losing one of its hydrogens to the oxygen attached to the phosphorus. That is, an intramolecular hydration bond, N...O−H, was formed. The same phenomena occurs in second and fourth lowest energy conformations (see Table 3.14). In all of the stable conformations for compound III, the dihedral angles, α_2 and α_3 are far from

the expected +sc +sc conformation. As well, α_1 and α_4 angles are far from the expected 180° values. Only α_5 takes on the value close to $-60°$ which is in agreement with the experimental (crystallographic) findings. Compound III clearly illustrates the importance of hydrogen bonds in stabilizing the structure of the phospholipid headgroups. This will be farther discussed in chapter 4.

The results from the Mulliken population analysis for compound III are given in Table 3.18. Compound III has the net charge of zero (in contrast to compounds I and II which had the net charge of -1). The presence of both ionic groups PO_4^- and NH_3^+ results in the redistribution of the charges among the atoms. As before, the larger amount of positive charge accumulates on the phosphorus. There is net negative charge on the PO_4^- group and net positive charge on the two ends of compound III with slightly larger positive charge on the end containing the NH_3^+ group. In compound III, the direction of the total dipole moment is not determined by a single component but by two components in its most stable conformation. The resultant dipole points away from the phosphorus towards O(12) and C(11) (see Figure 3.8).

As stated above, detailed analysis for compound III is not given in this section since the unexpected hydration bond leads to us to conclude that compound III is not a good model for phospholipid headgroups. However, the inclusion of this compound in this chapter will result in greater understanding of the hydration phenomena of phospholipid molecules in biological membranes.

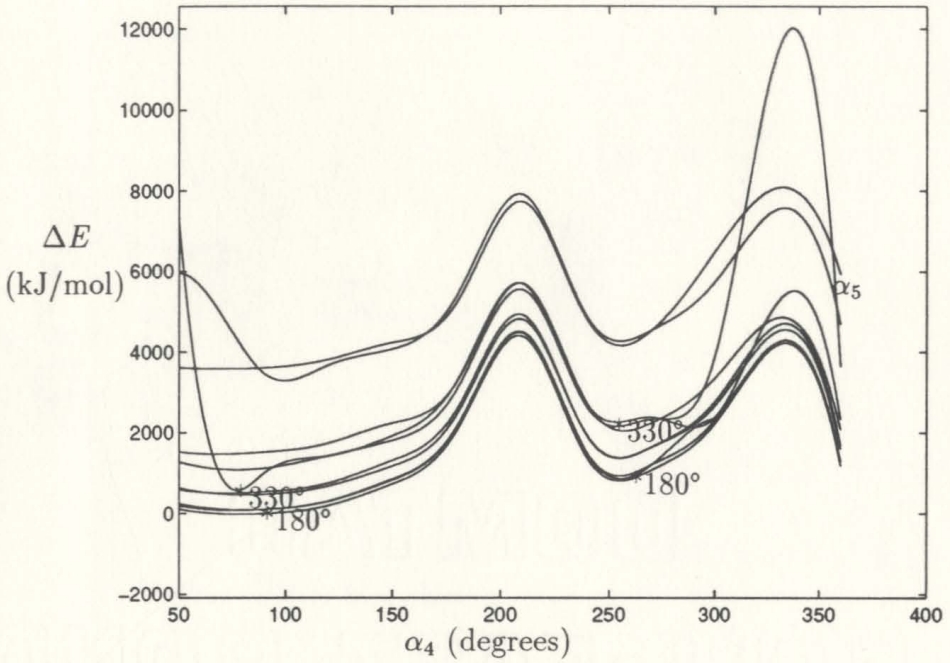

Figure 3.5(a) The plot of scanning results of α_4 and α_5 for compound III. The points labeled by "*" correspond to the minima displayed in Figure 3.5(b). The numbers next to these minima are values for α_5.

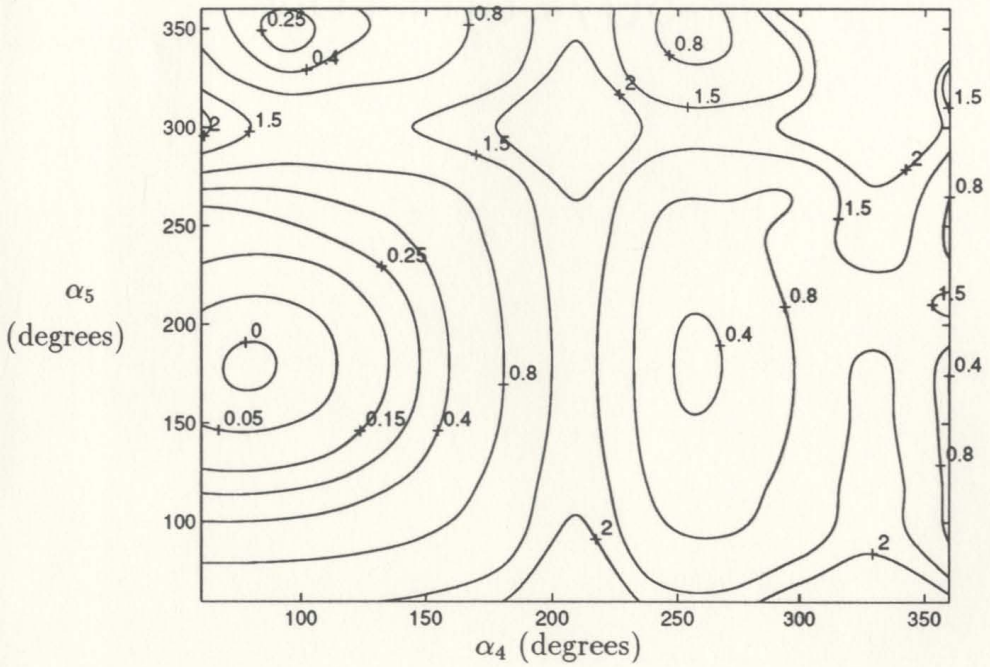

Figure 3.5(b) The contour plot of α_4 and α_5 for compound III.

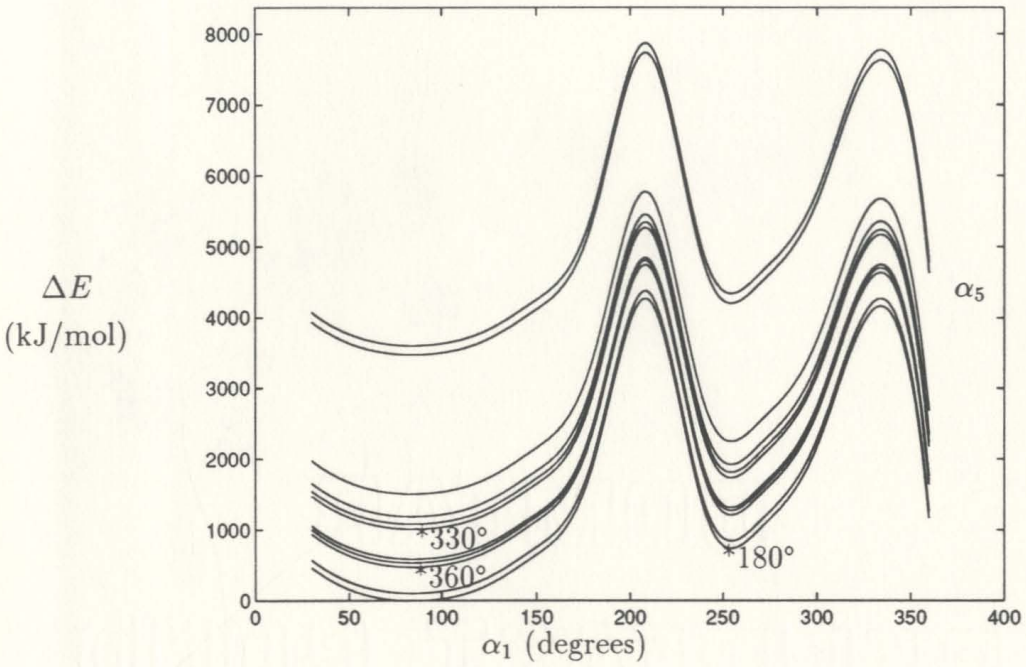

Figure 3.6(a) The plot of scanning results of α_1 and α_5 for compound III. The points labeled by "*" correspond to the minima displayed in Figure 3.6(b). The numbers next to these minima are values for α_5.

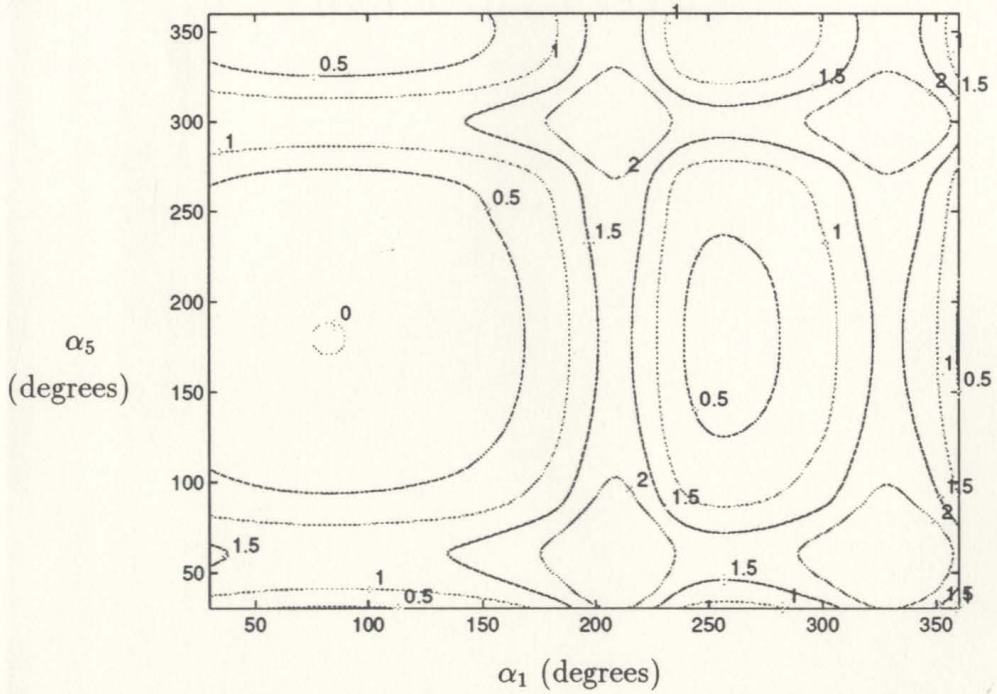

Figure 3.6(b) The contour plot of α_1 and α_5 for compound III.

Table 3.14: Magnitudes (in degrees) of dihedral angles, α_1 to α_5, for compound III.

conformation	angle (deg.)	energy (hartree)	Δ E (kJ/mol)
I +ac +sc +ap +sc −sc	$\alpha_1 = 91.3$ $\alpha_2 = 52.7$ $\alpha_3 = 151.8$ $\alpha_4 = 81.2$ $\alpha_5 = -59.1$	−848.793503	
II sc +ac +sc +ac −sc	$\alpha_1 = 74.0$ $\alpha_2 = 121.4$ $\alpha_3 = 40.6$ $\alpha_4 = 95.9$ $\alpha_5 = -70.5$	−848.791734	4.64
III −sc +ac +sc +ac −sc	$\alpha_1 = -76.8$ $\alpha_2 = 134.7$ $\alpha_3 = 39.0$ $\alpha_4 = 95.1$ $\alpha_5 = -70.1$	−848.791722	4.69
IV +sc +ac +sc +sc +sc	$\alpha_1 = 72.7$ $\alpha_2 = 128.6$ $\alpha_3 = 31.1$ $\alpha_4 = 51.2$ $\alpha_5 = 46.4$	−848.790558	7.70
V +sc −ac −ac +sc +sc	$\alpha_1 = 83.0$ $\alpha_2 = -132.3$ $\alpha_3 = -99.0$ $\alpha_4 = 62.2$ $\alpha_5 = 39.4$	−848.757111	95.56

Table 3.15: Geometrical parameters for the "ac sc ap sc −sc" and "sc ac sc ac −sc" conformations for compound III.

bond length ($\AA$)		bond angle (deg.)		dihedral angle (deg.)	
conformation I					
O(13)-P	1.572	O(13)-P-O(14)	115.8	O(14)-P-O(14)-O(11)	−123.4
O(14)-P	1.457	O(12)-P-O(11)	103.7	O(13)-P-O(13)-O(12)	−122.3
O(12)-P	1.592	C(11)-O(12)-P	120.9	α_1	91.3
O(11)-P	1.557	C(1)-O(11)-P	125.8	α_2	52.7
C(11)-O(12)	1.453	C(12)-C(11)-O(12)	110.5	α_3	151.8
C(1)-O(11)	1.468	C(2)-C(1)-O(11)	109.5	α_4	81.2
C(12)-C(11)	1.529	H-C(11)-O(12)	107.6	α_5	−59.1
C(2)-C(1)	1.524	H-C(1)-O(11)	106.9	H(11A)-C(11)-O(12)-P	−106.2
H-C(11)	1.078	N-C(12)-C(11)	110.6	H(11B)-C(11)-O(12)-P	−41.5
H-C(1)	1.078	H-C(12)-C(11)	108.5	H(1A)-C(1)-O(11)-P	−31.3
N-C(12)	1.486	H-C(2)-C(1)	109.8	H(1B)-C(1)-O(11)-P	−148.5
H-C(12)	1.083	H-N-C(12)	112.3	H(12A)-C(12)-C(11)-O(12)	−59.0
H-C(2)	1.082			H(12B)-C(12)-C(11)-O(12)	177.4
H(NA)-N	1.006			H(2A)-C(2)-C(1)-O(11)	178.9
H(NB)-N	1.914			H(2B)-C(2)-C(1)-O(11)	59.0
H(NC)-N	1.009			H(2C)-C(2)-C(1)-O(11)	−60.6
				H(NA)-N-C(12)-C(11)	−175.0
				H(NB)-N-C(12)-C(11)	61.7
				H(NC)-N-C(12)-C(11)	−49.1
conformation II					
O(13)-P	1.452	O(13)-P-O(14)	117.4	O(14)-P-O(14)-O(11)	−126.8
O(14)-P	1.553	O(12)-P-O(11)	102.1	O(13)-P-O(13)-O(12)	−121.2
O(12)-P	1.591	C(11)-O(12)-P	125.9	α_1	74.1
O(11)-P	1.584	C(1)-O(11)-P	122.8	α_2	121.3
C(11)-O(12)	1.448	C(12)-C(11)-O(12)	110.0	α_3	40.7
C(1)-O(11)	1.467	C(2)-C(1)-O(11)	110.3	α_4	95.9
C(12)-C(11)	1.527	H-C(11)-O(12)	108.2	α_5	−70.6
C(2)-C(1)	1.525	H-C(1)-O(11)	107.0	H(11A)-C(11)-O(12)-P	−135.6
H-C(11)	1.079	N-C(12)-C(11)	111.2	H(11B)-C(11)-O(12)-P	−27.7
H-C(1)	1.078	H-C(12)-C(11)	108.6	H(1A)-C(1)-O(11)-P	−165.2
N-C(12)	1.491	H-C(2)-C(1)	109.8	H(1B)-C(1)-O(11)-P	−47.4
H-C(12)	1.082	H-N-C(12)	111.2	H(12A)-C(12)-C(11)-O(12)	165.7
H-C(2)	1.082			H(12B)-C(12)-C(11)-O(12)	47.6
H(NA)-N	1.008			H(1A)-C(2)-C(1)-O(11)	175.7
H(NB)-N	1.700			H(2B)-C(2)-C(1)-O(11)	55.5
H(NC)-N	1.009			H(2C)-C(2)-C(1)-O(11)	−64.6
				H(12A)-N-C(12)-C(11)	162.4
				H(12B)-N-C(12)-C(11)	41.9
				H(12C)-N-C(12)-C(11)	−73.6

Table 3.16: Geometrical parameters for the "−sc ac sc ac −sc" and "sc ac sc sc sc" conformations for compound III.

bond length (Å)		bond angle (deg.)		dihedral angle (deg.)	
conformation III					
O(13)-P	1.452	O(13)-P-O(14)	116.8	O(14)-P-O(14)-O(11)	−126.9
O(14)-P	1.556	O(12)-P-O(11)	119.2	O(13)-P-O(13)-O(12)	−121.3
O(12)-P	1.589	C(11)-O(12)-P	126.1	α_1	−76.8
O(11)-P	1.584	C(1)-O(11)-P	122.9	α_2	134.7
C(11)-O(12)	1.448	C(12)-C(11)-O(12)	110.0	α_3	39.0
C(1)-O(11)	1.467	C(2)-C(1)-O(11)	110.2	α_4	95.1
C(12)-C(11)	1.527	H-C(11)-O(12)	108.1	α_5	−70.6
C(2)-C(1)	1.525	H-C(1)-O(11)	107.0	H(11A)-C(11)-O(12)-P	−146.4
H-C(11)	1.080	N-C(12)-C(11)	111.2	H(11B)-C(11)-O(12)-P	−28.1
H-C(1)	1.078	H-C(12)-C(11)	108.6	H(1A)-C(1)-O(11)-P	162.3
N-C(12)	1.491	H-C(2)-C(1)	109.7	H(1B)-C(1)-O(11)-P	44.7
H-C(12)	1.088	H-N-C(12)	111.2	H(12A)-C(12)-C(11)-O(12)	166.2
H-C(2)	1.082			H(12B)-C(12)-C(11)-O(12)	48.0
H(NA)-N	1.0075			H(2A)-C(2)-C(1)-O(11)	−176.5
H(NB)-N	1.7111			H(2B)-C(2)-C(1)-O(11)	63.7
H(NC)-N	1.0087			H(2C)-C(2)-C(1)-O(11)	−56.4
				H(NA)-N-C(12)-C(11)	163.8
				H(NB)-N-C(12)-C(11)	43.5
				H(NC)-N-C(12)-C(11)	−72.3
conformation IV					
O(13)-P	1.452	O(13)-P-O(14)	117.4	O(14)-P-O(14)-O(11)	−126.9
O(14)-P	1.554	O(12)-P-O(11)	101.7	O(13)-P-O(13)-O(12)	−120.9
O(12)-P	1.590	C(11)-O(12)-P	126.1	α_1	72.65
O(11)-P	1.585	C(1)-O(11)-P	122.7	α_2	128.6
C(11)-O(12)	1.446	C(12)-C(11)-O(12)	112.8	α_3	31.1
C(1)-O(11)	1.467	C(2)-C(1)-O(11)	110.4	α_4	51.2
C(12)-C(11)	1.534	H-C(11)-O(12)	107.4	α_5	−70.6
C(2)-C(1)	1.525	H-C(1)-O(11)	106.9	H(11A)-C(11)-O(12)-P	171.8
H-C(11)	1.079	N-C(12)-C(11)	110.4	H(11B)-C(11)-O(12)-P	−70.5
H-C(1)	1.078	H-C(12)-C(11)	108.7	H(1A)-C(1)-O(11)-P	−48.8
N-C(12)	1.488	H-C(2)-C(1)	109.8	H(1B)-C(1)-O(11)-P	−166.6
H-C(12)	1.082	H-N-C(12)	108.2	H(12A)-C(12)-C(11)-O(12)	169.9
H-C(2)	1.083			H(12B)-C(12)-C(11)-O(12)	−71.9
H(NA)-N	1.007			H(2A)-C(2)-C(1)-O(11)	175.1
H(NB)-N	1.702			H(2B)-C(2)-C(1)-O(11)	54.9
H(NC)-N	1.007			H(2C)-C(2)-C(1)-O(11)	−65.3
				H(NA)-N-C(12)-C(11)	173.0
				H(NB)-N-C(12)-C(11)	47.1
				H(NC)-N-C(12)-C(11)	−71.3

Table 3.17: Geometrical parameters for the "sc −ac −ac sc sc" conformation for compound III.

bond length ($\AA$)		bond angle (deg.)		dihedral angle (deg.)	
conformation V					
O(13)-P	1.455	O(13)-P-O(14)	127.0	O(14)-P-O(14)-O(11)	−127.7
O(14)-P	1.459	O(12)-P-O(11)	93.9	O(13)-P-O(13)-O(12)	−133.2
O(12)-P	1.844	C(11)-O(12)-P	120.1	α_1	83.0
O(11)-P	1.571	C(1)-O(11)-P	120.5	α_2	−132.2
C(11)-O(12)	1.244	C(12)-C(11)-O(12)	109.4	α_3	-99.0
C(1)-O(11)	1.465	C(2)-C(1)-O(11)	110.2	α_4	62.3
C(12)-C(11)	1.475	H(1)-C(11)-O(12)	111.6	α_5	39.4
C(2)-C(1)	1.525	H(2)-C(11)-O(12)	106.7	H(11A)-C(11)-O(12)-P	−57.1
H-C(11)	1.077	H-C(1)-O(11)	107.1	H(11B)-C(11)-O(12)-P	−177.5
H-C(1)	1.087	N-C(12)-C(11)	107.6	H(1A)-C(1)-O(11)-P	−155.4
N-C(12)	3.260	H-C(12)-C(11)	110.5	H(1B)-C(1)-O(11)-P	−37.7
H-C(12)	1.088	H-C(2)-C(1)	110.0	H(12A)-C(12)-C(11)-O(12)	39.4
H-C(2)	1.082	H(NA)-N-C(12)	106.2	H(12B)-C(12)-C(11)-O(12)	−75.3
H(NA)-N	1.0059	H(NB)-N-C(12)	111.6	H(12C)-C(12)-C(11)-O(12)	159.6
H(NB)-N	1.0052	H(NC)-N-C(12)	110.9	H(2A)-C(2)-C(1)-O(11)	178.4
H(BC)-N	1.0056			H(2B)-C(2)-C(1)-O(11)	58.2
				H(2C)-C(2)-C(1)-O(11)	−62.0
				H(NA)-N-C(12)-C(11)	−67.6
				H(NB)-N-C(12)-C(11)	172.6
				H(NC)-N-C(12)-C(11)	49.8

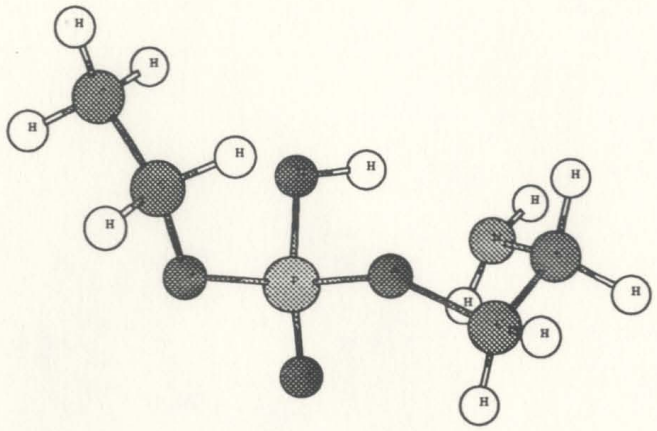

(a)

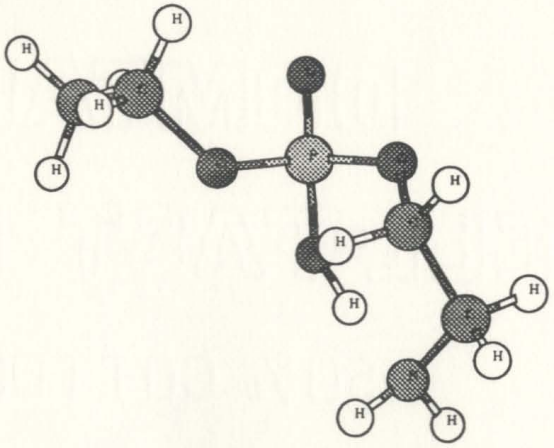

b)

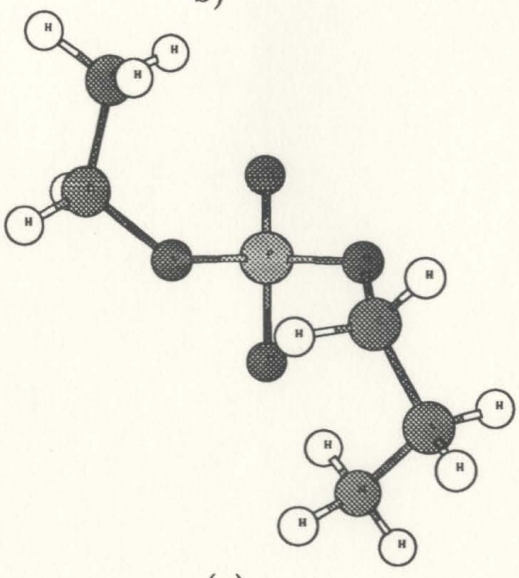

(c)

Figure 3.7 The conformations for compound III
shown in order of increasing energies as listed in Table 3.14.

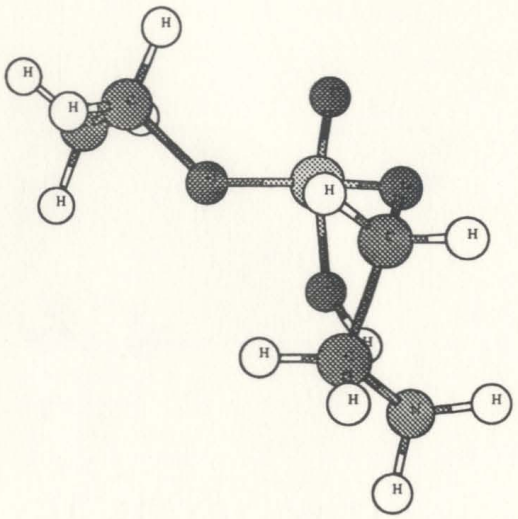

(d)

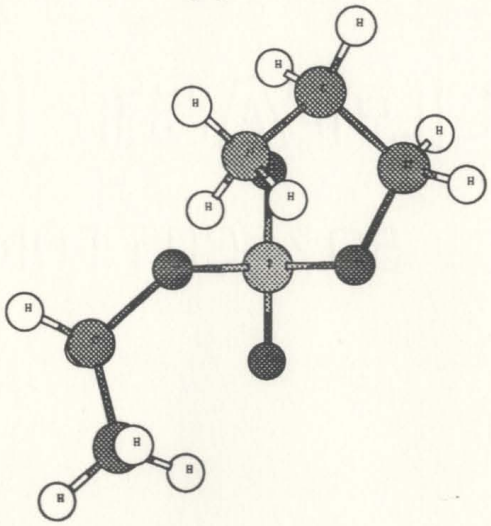

(e)

Figure 3.7 The conformations for compound III
shown in order of increasing energies as listed in Table 3.14.

Table 3.18: The summary of Mulliken population analysis (obtained with 3-21G* basis set) of compound III for its five conformations as indicated in the table. The magnitudes of the total and the components of the dipole moments (μ) are also given in this table.

atoms/ groups	conformation I	conformation II	conformation III	conformation IV	conformation V
P	1.67	1.65	1.65	1.67	1.55
O(14)	−0.33	−0.66	−0.66	−0.66	−0.74
O(13)	−0.68	−0.32	−0.80	−0.32	−0.69
O(12)	−0.74	−0.73	−0.73	−0.74	−0.76
O(11)	−0.71	−0.76	−0.76	−0.76	−0.82
$C(11)H_2$	0.37	0.38	−0.09	0.40	0.41
$C(1)H_2$	0.35	0.36	−0.09	0.36	0.36
$C(12)H_2$	0.20	0.22	−0.25	0.18	0.24
C(2)3H	0.04	0.03	−0.64	0.03	0.02
NH_3	−0.18	−0.17	−0.83	−0.16	0.43
μ (debye)	5.58	8.12	8.15	7.78	12.32
μ_X	−3.26	5.53	−5.26	5.17	5.51
μ_Y	−0.58	4.90	−5.02	5.75	11.02
μ_Z	−4.49	3.36	3.68	0.85	0.12

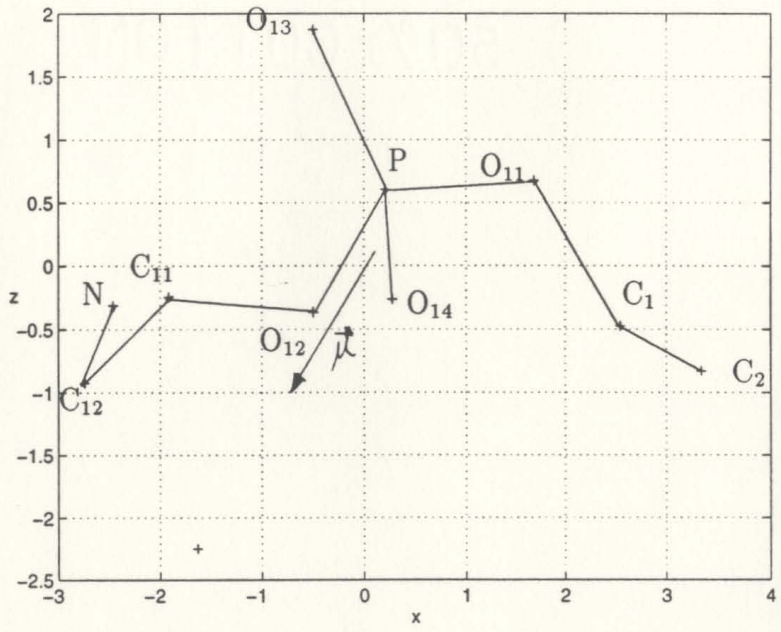

Figure 3.8 The dipole moment projected on xz plane for compound III.

3.5 Compound IV (GPC) and Compound V (GPE)

GPE and GPC are headgroups made by expanding PE and PC. They can exist in two steric forms that are mirror isomers of each other[4]. Thus in some crystalline structures (depending on packing symmetries of the crystals) of GPC and GPE, there could be two independent molecules in a given unit cell. On the other hand, the phosphate groups are closely linked forming rows or zig-zag ribbons. In this case the intermolecular interactions that include hydrogen bonds, ionic ($NH_3^+ - PO_4^-$) contacts are very important. Together they determine the conformation of each phospholipid molecule. From x-ray experimental studies[4], the polar constituents of GPC and GPE have preferred conformations similar to those of their parent compounds. That is their respective torsional angles are almost the same. The torsional angles, α_1, α_2, α_3 and α_5, remain in roughly the same range for all phospholipid molecules. The typical values for these angles are:

α_1=ap;

α_2/α_3=+sc/+sc as θ_1=$\pm$ sc, α_2/α_3=$-$sc/$-$sc as θ_1=ap;

α_4 is flexible varying between +ac to $-$ac. It adjusts the position of the nitrogen atom at the layer surface. Obviously, this position is very much affected by its environment.;

$\alpha_5 = \pm$ sc is determined by the intra-molecular attraction between the ammonium nitrogen and the phosphate group.

Our theoretical calculations have begun with the experimentally determined conformations of GPC and GPE. Starting geometrical parameters were taken from the x-ray experimental finding. We performed full geometry optimizations for single GPC and GPE molecules and for two GPC molecules. Due to their large size, no rigid-rotor scans have been performed for these systems.

3.5.1 GPC – Single Isolated Molecule

As stated above, we took the x-ray experimental data as the starting geometry for GPC: $\alpha_1 = -172°$, $\alpha_2 = 64°$, $\alpha_3 = 65°$, $\alpha_4 = 140°$, $\alpha_5 = -75°$, $\alpha_6 = -176°$, $\theta_1 = -63°$, $\theta_2 = 61°$, $\theta_3 = -69°$, $\theta_4 = 169°$ (recall α_6 =C(11)-C(12)-N-C(13), θ_1 =O(11)-C(1)-C(2)-C(3), θ_2 =O(11)-C(1)-C(2)-O(21), θ_3 =C(1)-C(2)-C(3)-O(31), θ_4=O(21)-C(2)-C(3)-O(31) and the remaining dihedral angles are defined as indicated above, see also Figure 1.6). A full optimization for all of the geometry parameters was performed. A comparison between this work and x-ray experimental results for the major torsional angles $\alpha_1 - \alpha_6$, $\theta_1 - \theta_4$ is made in Table 3.19. The last column of Table 3.19 gives differences between theoretical and experiment results. The structure of GPC is displayed in Figure 3.9. The complete set of geometrical parameters is given in Table 3.20.

From Table 3.19 we see that predicted GPC structure agrees closely with the experimental finding. The torsional angles $\alpha_1 - \alpha_6$ take the values in the range −ac +sc +sc +ac −sc. Particularly for dihedral angles α_2, α_3, α_5 and α_6, very close agreement with experimental data has been obtained. One of the bigger differences has been obtained for α_1 (27°). The value of α_1 determines the extent of bending of the bond C(1)−C(2). Previous work[34] found no preferred value for α_1 to minimize the energy. X-ray diffraction studies also assign a convenient reference value for this angle. The torsional angles $\alpha_2 - \alpha_6$ have shown a much closer agreement with experimental data than $\theta_2 - \theta_4$. This means that atoms O(21) and O(31) are more affected by the molecular packing than the remaining part of the headgroup. Oxygens are highly electronegative atoms. Their bonding conditions and stability are determined by both the chemical composition of the molecules and their packing conditions. Figure 3.9 shows a stable ammonium group. Unlike conformation I of

Table 3.19: Magnitudes (in degrees) of dihedral angles, α_1 to α_6, θ_1 to θ_4, for compound IV (GPC).

conformation	angle (deg.)	angle (deg.)[4]	difference (deg.) [2]
	$\alpha_1 = -146$	$\alpha_1 = -172$	26
	$\alpha_2 = 67$	$\alpha_2 = 64$	3
	$\alpha_3 = 55$	$\alpha_3 = 65$	-10
$\alpha_1 - \alpha_5$	$\alpha_4 = 127$	$\alpha_4 = 140$	-13
$-$ac $+$sc $+$sc $+$ac $-$sc	$\alpha_5 = -68$	$\alpha_5 = -75$	7
	$\alpha_6 = -173$	$\alpha_6 = -176$	3
	$\theta_1 = -36$	$\theta_1 = -63.$	27
	$\theta_2 = 83$	$\theta_2 = 61$	22
	$\theta_3 = -44$	$\theta_3 = -69$	25
	$\theta_4 = -162$	$\theta_4 = 169$	29

[1]Dihedral angles as calculated in this work. [2]Differences obtained by subtracting numbers in column 2 from column 3.

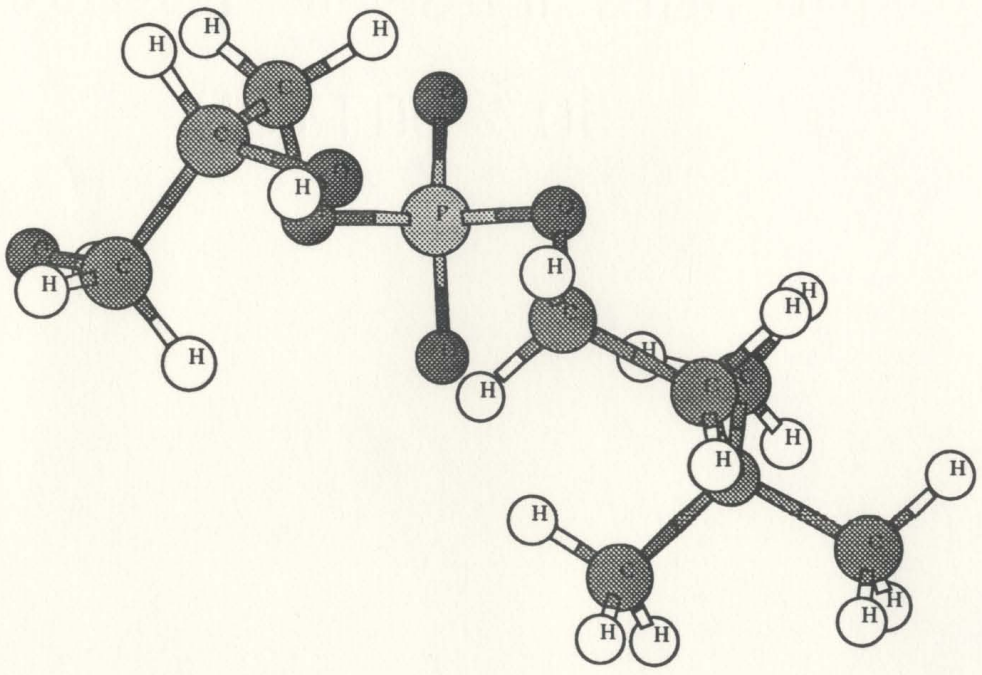

Figure 3.9 The structure of a single GPC molecule.

Table 3.20: Geometrical parameters for compound IV (GPC).

bond length ($\AA$)		bond angle (deg.)		dihedral angle (deg.)	
O(13)-P	1.460	O(14)-P-O(13)	124.6	O(14)-P-O(13)-O(11)	−131.7
O(14)-P	1.488	O(12)-P-O(11)	97.8	O(13)-P-O(14)-O(11)	−123.7
O(12)-P	1.640	C(11)-O(12)-P	117.5	α_1	−146.4
O(11)-P	1.622	C(1)-O(11)-P	120.2	α_2	66.5
C(11)-O(12)	1.434	C(12)-C(11)-O(12)	109.3	α_3	55.3
C(1)-O(11)	1.452	C(2)-C(1)-O(11)	108.4	α_4	126.5
C(12)-C(11)	1.519	H-C(11)-O(12)	110.2	α_5	−68.3
C(2)-C(1)	1.519	H-C(1)-O(11)	109.6	H(11A)-C(11)-O(12)-P	3.4
H-C(11)	1.077	N-C(12)-C(11)	116.0	H(11B)-C(11)-O(12)-P	−114.9
H-C(1)	1.078	H-C(12)-C(11)	109.6	H(1A)-C(1)-O(11)-P	94.1
H-C(12)	1.080	H-C(2)-C(1)	108.1	H(1B)-C(1)-O(11)-P	−26.4
H-C(2)	1.084	C(3)-C(2)-C(1)	110.6	H(12A)-C(12)-C(11)-O(12)	51.6
N-C(12)	1.531	O(21)-C(2)-C(1)	107.9	H(12B)-C(12)-C(11)-O(12)	172.1
H-C(3)	1.080	C(13)-N-C(12)	107.3	H(2A)-C(2)-C(1)-O(11)	−157.6
H-O(21)	0.967	C(14)-N-C(12)	111.9	C(3)-C(2)-C(1)-O(11)	−36.0
C(2)-O(21)	1.454	C(15)-N-C(12)	111.2	O(21)-C(2)-C(1)-O(11)	83.3
H-C(13)	1.505	H-C(13)-N	108.9	C(13)-N-C(12)-C(11)	−173.0
H-C(14)	1.529	H-C(14)-N	107.7	C(14)-N-C(12)-C(11)	67.4
H-C(15)	1.522	H-C(15)-N	107.8	C(15)-N-C(12)-C(11)	−52.8
H-O(31)	0.970	H-O(21)-C(2)	110.4	H(13A)-C(13)-N-C(12)	180.5
C(3)-O(31)	1.431	O(31)-C(3)-C(2)	111.2	H(13B)-C(13)-N-C(12)	60.5
N-C(13)	1.505	H-O(31)-C(3)	107.3	H(13C)-C(13)-N-C(12)	−59.8
N-C(14)	1.529	H-C(3)-C(2)	106.7	H(14A)-C(14)-N-C(12)	163.7
N-C(15)	1.522	H-C(3)-C(2)	110.8	H(14B)-C(14)-N-C(12)	43.6
				H(14C)-C(14)-N-C(12)	−77.3
				H(15A)-C(15)-N-C(12)	−169.7
				H(15B)-C(15)-N-C(12)	71.9
				H(15C)-C(15)-N-C(12)	−50.6
				O(31)-C(3)-C(2)-C(1)	−43.6
				H-O(31)-C(3)-C(2)	73.1
				H(3A)-C(3)-C(2)-C(1)	78.9
				H(3B)-C(3)-C(2)-C(1)	−162.5

E (RHF) = −1152.886762 hartree

Table 3.21: The summary of Mulliken population analysis (obtained with 3-21G* basis set) for GPC, two GPC's and GPE. The magnitudes of the total and the components of the dipole moments (μ) are also given in this table.

atom group	GPC	GPC_A	GPC_B	GPE
P	1.55	1.55	1.57	1.63
O(14)	−0.68	−0.69	−0.78	−0.32
O(13)	−0.76	−0.76	−0.66	−0.64
O(12)	−0.75	−0.76	−0.75	−0.73
O(11)	−0.77	−0.77	−0.79	−0.76
C(11)	0.38	0.37	0.39	0.37
C(1)	0.40	0.40	0.40	0.40
C(12)	0.28	0.28	0.30	0.23
C(2)	0.19	0.19	0.21	0.26
N	−0.74	−0.76	−0.75	−0.16
C(3)	0.33	0.33	0.35	0.33
O(21)	−0.31	−0.31	−0.30	−0.30
O(31)	−0.28	−0.29	−0.27	−0.30
C(13)	0.37	0.38	0.39	
C(14)	0.39	0.37	0.40	
C(15)	0.38	0.38	0.38	
μ (debye)	15.24	29.07		7.80
μ_X	−10.41	26.19		−4.40
μ_Y	−11.12	3.68		−5.73
μ_Z	−0.55	−12.07		3.01

Page 82 & 83

missing from the original book

Table 3.22: Summary of major dihedral angles for two compounds IV (GPC).

conformation	angle (deg.)	angle (deg.)	difference (deg.) [2]
	$\alpha_1 = -146$	$\alpha_1 = -172$	26
	$\alpha_2 = -48$	$\alpha_2 = 64$	-112
	$\alpha_3 = 172$	$\alpha_3 = 65$	107
GPC_A	$\alpha_4 = 127$	$\alpha_4 = 140$	-13
$\alpha_1 - \alpha_5$	$\alpha_5 = -68$	$\alpha_5 = -75$	7
$-ac\ -sc\ ap\ +ac\ -sc$	$\alpha_6 = -175$	$\alpha_6 = -176$	1
	$\theta_1 = -34$	$\theta_1 = -63$	29
	$\theta_2 = 86$	$\theta_2 = 61$	25
	$\theta_3 = -45$	$\theta_3 = -69$	24
	$\theta_4 = -163$	$\theta_4 = 169$	-6
	$\alpha_1 = 145$	$\alpha_1 = 165$	-20
	$\alpha_2 = -168$	$\alpha_2 = -71$	-87
	$\alpha_3 = 49$	$\alpha_3 = -59$	108
GPC_B	$\alpha_4 = -127$	$\alpha_4 = -138$	11
$\alpha_1 - \alpha_5$	$\alpha_5 = 69$	$\alpha_5 = 73$	-4
$+ac\ ap\ +sc\ -ac\ +sc$	$\alpha_6 = 174$	$\alpha_6 = 174$	0
	$\theta_1 = 31$	$\theta_1 = 172$	-141
	$\theta_2 = -88$	$\theta_2 = -71$	-17
	$\theta_3 = 44$	$\theta_3 = 63$	-19
	$\theta_4 = 161$	$\theta_4 = 180$	-21

[1]Dihedral angles as calculated in this work. [2]Differences obtained by subtracting numbers in column 2 from column 3.

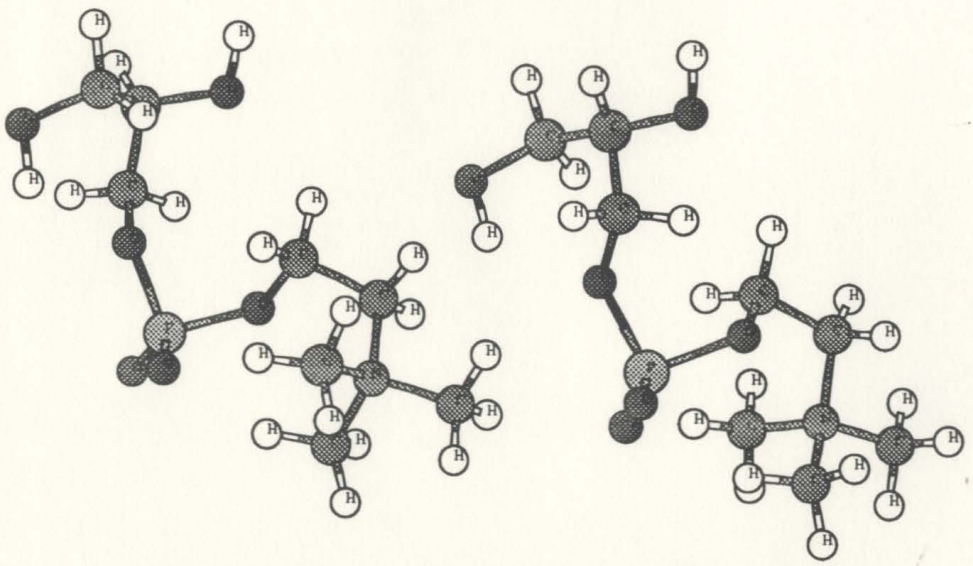

Figure 3.10 The conformation for two GPC molecules.

Table 3.23: Geometrical parameters for GPC_A.

bond length ($\AA$)		bond angle (deg.)		dihedral angle (deg.)	
O(13)-P	1.462	O(14)-P-O(13)	124.6	O(14)-P-O(13)-O(11)	−130.3
O(14)-P	1.486	O(12)-P-O(11)	97.8	O(13)-P-O(14)-O(12)	−124.7
O(12)-P	1.635	C(11)-O(12)-P	117.7	α_1	−146.4
O(11)-P	1.626	C(1)-O(11)-P	120.1	α_2	−47.6
C(11)-O(12)	1.438	C(12)-C(11)-O(12)	109.9	α_3	171.6
C(1)-O(11)	1.450	C(2)-C(1)-O(11)	108.5	α_4	127.2
C(12)-C(11)	1.517	H-C(11)-O(12)	109.9	α_5	−68.4
C(2)-C(1)	1.520	H-C(1)-O(11)	109.6	H(11A)-C(11)-O(12)-P	3.9
H-C(11)	1.077	N-C(12)-C(11)	115.8	H(11B)-C(11)-O(12)-P	−114.0
H-C(1)	1.078	H-C(12)-C(11)	109.5	H(1A)-C(1)-O(11)-P	94.1
H-C(12)	1.077	H-C(2)-C(1)	108.2	H(1B)-C(1)-O(11)-P	−27.4
H-C(2)	1.078	C(3)-C(2)-C(1)	110.6	H(12A)-C(12)-C(11)-O(12)	−68.4
N-C(12)	1.530	O(21)-C(2)-C(1)	107.8	H(12B)-C(12)-C(11)-O(12)	172.2
H-C(3)	1.080	C(13)-N-C(12)	107.2	H(2A)-C(2)-C(1)-O(11)	−155.4
H-O(21)	1.080	C(14)-N-C(12)	112.4	C(3)-C(2)-C(1)-O(11)	−33.8
C(2)-O(21)	1.531	C(15)-N-C(12)	110.5	O(21)-C(2)-C(1)-O(11)	85.6
H-C(13)	1.079	H-C(13)-N	109.5	C(13)-N-C(12)-C(11)	−175.1
H-C(14)	1.077	H-C(14)-N	107.9	C(14)-N-C(12)-C(11)	65.2
H-C(15)	1.081	H-C(15)-N	107.8	C(15)-N-C(12)-C(11)	−55.2
H-O(31)	0.967	H-O(21)-C(2)	110.3	H(13A)-C(13)-N-C(12)	176.9
C(3)-O(31)	1.453	O(31)-C(3)-C(2)	111.1	H(13B)-C(13)-N-C(12)	56.4
N-C(13)	1.510	H-O(31)-C(3)	106.9	H(13C)-C(13)-N-C(12)	−63.3
N-C(14)	1.522	H-C(3)-C(2)	106.8	H(14A)-C(14)-N-C(12)	164.0
N-C(14)	1.518	H-C(3)-C(2)	110.7	H(14B)-C(14)-N-C(12)	44.2
				H(14C)-C(14)-N-C(12)	−76.7
				H(15A)-C(15)-N-C(12)	−168.7
				H(15B)-C(15)-N-C(12)	72.5
				H(15C)-C(15)-N-C(12)	−49.6
				O(31)-C(3)-C(2)-C(1)	−44.7
				H-O(31)-C(3)-C(2)	72.9
				H(3A)-C(3)-C(2)-C(1)	77.8
				H(3B)-C(3)-C(2)-C(1)	−163.5

Table 3.24: Geometrical parameters for GPC_B.

bond length ($\AA$)		bond angle (deg.)		dihedral angle (deg.)	
O(13)-P	1.492	O(14)-P-O(13)	124.6	O(14)-P-O(13)-O(11)	−127.5
O(14)-P	1.458	O(12)-P-O(11)	98.3	O(13)-P-O(14)-O(12)	−126.7
O(12)-P	1.630	C(11)-O(12)-P	118.6	α_1	144.5
O(11)-P	1.626	C(1)-O(11)-P	121.7	α_2	−167.6
C(11)-O(12)	1.437	C(12)-C(11)-O(12)	109.1	α_3	49.1
C(1)-O(11)	1.455	C(2)-C(1)-O(11)	108.3	α_4	−127.2
C(12)-C(11)	1.519	H-C(11)-O(12)	110.0	α_5	68.7
C(2)-C(1)	1.524	H-C(1)-O(11)	109.4	H(11A)-C(11)-O(12)-P	−4.2
H-C(11)	1.077	N-C(12)-C(11)	115.9	H(11B)-C(11)-O(12)-P	114.3
H-C(1)	1.078	H-C(12)-C(11)	109.6	H(1A)-C(1)-O(11)-P	−95.5
H-C(12)	1.078	H-C(2)-C(1)	108.3	H(1B)-C(1)-O(11)-P	24.9
H-C(2)	1.078	C(3)-C(2)-C(1)	111.7	H(12A)-C(12)-C(11)-O(12)	−51.2
N-C(12)	1.531	O(21)-C(2)-C(1)	107.5	H(12B)-C(12)-C(11)-O(12)	−171.6
H-C(3)	1.081	C(13)-N-C(12)	107.3	H(2A)-C(2)-C(1)-O(11)	153.3
H-O(21)	0.967	C(14)-N-C(12)	112.0	C(3)-C(2)-C(1)-O(11)	30.9
C(2)-O(21)	1.452	C(15)-N-C(12)	111.1	O(21)-C(2)-C(1)-O(11)	−87.5
H-C(13)	1.079	H-C(13)-N	108.8	C(13)-N-C(12)-C(11)	173.9
H-C(14)	1.076	H-C(14)-N	107.8	C(14)-N-C(12)-C(11)	−66.5
H-C(15)	1.080	H-C(15)-N	107.9	C(15)-N-C(12)-C(11)	53.9
H-O(31)	0.966	H-O(21)-C(2)	110.9	H(13A)-C(13)-N-C(12)	179.8
C(3)-O(31)	1.439	O(31)-C(3)-C(2)	111.7	H(13B)-C(13)-N-C(12)	−60.3
N-C(13)	1.507	H-O(31)-C(3)	106.5	H(13C)-C(13)-N-C(12)	60.0
N-C(14)	1.529	H-C(3)-C(2)	106.6	H(14A)-C(14)-N-C(12)	−163.3
N-C(14)	1.520	H-C(3)-C(2)	110.0	H(14B)-C(14)-N-C(12)	−43.1
H-C(13)	1.079			H(14C)-C(14)-N-C(12)	77.7
H-C(14)	1.076			H(15A)-C(15)-N-C(12)	170.2
H-C(15)	1.082			H(15B)-C(15)-N-C(12)	−71.2
				H(15C)-C(15)-N-C(12)	51.0
				O(31)-C(3)-C(2)-C(1)	43.5
				H-O(31)-C(3)-C(2)	−59.6
				H(3A)-C(3)-C(2)-C(1)	−78.5
				H(3B)-C(3)-C(2)-C(1)	160.0

E (RHF) = −2305.799857 hartree

Table 3.25: A comparison of theoretical and experimental results for the main torsional angles in single GPE.

Conformation	angles (deg.) [1]	angles (deg.)	difference (deg.) [3]
	$\alpha_1 = -120$	$\alpha_1 = -174$	54
	$\alpha_2 = -111$	$\alpha_2 = -81$	-30
	$\alpha_3 = -49$	$\alpha_3 = -81$	32
$\alpha_1 - \alpha_5$	$\alpha_4 = -100$	$\alpha_4 = 164$	96
$-$ac $-$ac $+$sc $-$ac $-$sc	$\alpha_5 = 71$	$\alpha_5 = 55$	16
	$\theta_1 = 192$	$\theta_1 = 166$	33
	$\theta_2 = -52$	$\theta_2 = -89$	37
	$\theta_3 = -54$	$\theta_3 = -67$	13
	$\theta_4 = -172$	$\theta_4 = 180$	8

[1] [2] [3] have the same meanings as in Table 3.20.

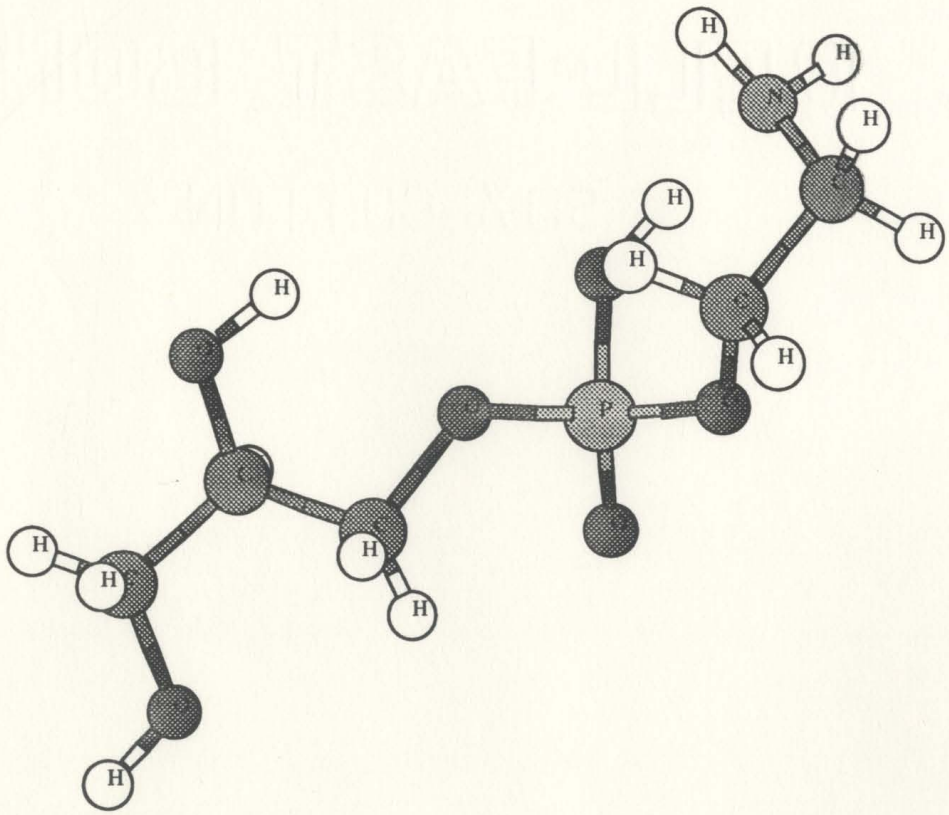

Figure 3.11 The structure of GPE.

Table 3.26: Geometrical parameters for GPE.

bond length ($\AA$)		bond angle (deg.)		dihedral angle (deg.)	
O(13)-P	1.552	O(14)-P-O(13)	118.56	O(14)-P-O(13)-O(11)	−121.9
O(14)-P	1.450	O(12)-P-O(11)	102.99	O(13)-P-O(14)-O(12)	−126.0
O(12)-P	1.591	C(11)-O(12)-P	125.47	α_1	−120.5
O(11)-P	1.586	C(1)-O(11)-P	124.19	α_2	−110.7
C(11)-O(12)	1.448	C(12)-C(11)-O(12)	109.33	α_3	−49.0
C(1)-O(11)	1.471	C(2)-C(1)-O(11)	105.87	α_4	−100.1
C(12)-C(11)	1.526	H-C(11)-O(12)	106.59	α_5	71.3
C(2)-C(1)	1.518	H-C(1)-O(11)	110.45	H(11A)-C(11)-O(12)-P	141.4
H-C(11)	1.080	N-C(12)-C(11)	111.16	H(11B)-C(11)-O(12)-P	23.0
H-C(1)	1.076	H-C(12)-C(11)	110.12	H(1A)-C(1)-O(11)-P	0.3
H-C(12)	1.082	H-C(2)-C(1)	106.82	H(1B)-C(1)-O(11)-P	121.5
H-C(2)	1.082	C(3)-C(2)-C(1)	110.83	H(12A)-C(12)-C(11)-O(12)	−46.8
N-C(12)	1.492	O(21)-C(2)-C(1)	109.82	H(12B)-C(12)-C(11)-O(12)	−165.0
H-C(3)	1.082	H-N-C(12)	111.07	H(2A)-C(2)-C(1)-O(11)	70.5
H-O(21)	0.967	H-O(21)-C(2)	110.40	C(3)-C(2)-C(1)-O(11)	−160.8
C(2)-O(21)	1.436	H-O(31)-C(3)	111.75	O(21)-C(2)-C(1)-O(11)	−51.9
H(NA)-N	1.007	H-C(3)-C(2)	109.01	H(NA)-N-C(12)-C(11)	81
H(NB)-N	1.009	O(31)-C(3)-C(2)	105.52	H(NB)-N-C(12)-C(11)	−33.5
H(NC)-N	1.676			H(NC)-N-C(12)-C(11)	−155.0
H-O(31)	0.967			H-O(21)-C(2)-C(1)	48.1
C(3)-O(31)	1.436			O(31)-C(3)-C(2)-C(1)	−53.6
				H-O(31)-C(3)-C(2)	−178.9
				H(3A)-C(3)-C(2)-C(1)	66.6
				H(3B)-C(3)-C(2)-C(1)	−174.9

E (RHF) = −1036.481618 hartree

3.5.3 GPE

A full geometry optimization was also performed for GPE. Major torsional angles are summarized in Table 3.25. The molecular conformation is shown in Figure 3.11. The complete set of geometrical parameters for this molecule is given in Table 3.26. Table 3.25 shows that, in contrast to the GPC, the torsional angles on an α chain exhibit large differences ranging from $8° - 96°$. In addition as shown in Figure 3.11,

one of the hydrogens attaches to one of the oxygens in phosphate group (similar to what has been observed for compound III). This result will change with the addition of water molecules (see chapter 4).

3.5.4 Summary

In this subsection, we compare molecular parameters for phospholipid models, GPE and GPC. The changes in intermolecular and intramolecular interactions result in changes in the geometrical parameters. For example the P−N distance changes from 3.03 $\AA$ in compound III to 3.34 $\AA$ in hydrated compound III (with four water molecules), to 3.51 $\AA$ in GPE, to 3.73 $\AA$ in hydrated GPE and to 3.94 $\AA$ in GPC (the hydrated cases will be discussed in chapter 4). This indicates that intermolecular and intramolecular interactions play an important role in determining stable structures of these molecular systems. Other molecular parameters are given in Table 3.27.

Table 3.27: The summary of some of the molecular parameters for compound III−V.

compound	molecular area ($\AA^2$)	thickness of polar region ($\AA$)	thickness of the headgroup ($\AA$)	total dipole moment (debye)
III	7−54		5.2	8.15
V(GPC)	15−82	8.1	5.9	15.24
2 GPC	15−68	7.4	5.0	29.07
GPE	20−77	10.1	6.8	7.80
III + $4H_2O$	16−62		7.0	4.48
GPE +$6H_2O$	17−79	10.3	8.0	9.66

Chapter 4

Structure of Hydrated Phospholipid Headgroups

The physical state of the hydrated phospholipid bilayer membranes partially depends on the properties of the polar headgroups, the concentration of the solvent and the temperature. The conformations of the esterified phosphate group will be greatly influenced by the hydration force in solution and by intermolecular ionic linkages, especially at low water concentration. A related question is how do the strong interactions between the phospholipid and water molecules affect the packing of the bilayer membranes? Numerous theoretical and experimental works have tried to answer these questions[14, 15, 16, 17, 18]. In recent years, NMR and x-ray diffraction experiments have been successful in answering qualitatively some of these questions. However, detailed structural studies of the hydrated polar heads, such as GPE and GPC, at the molecular level are still lacking.

What is the hydration force? Hydration force is defined as the hydrogen bond between the hydrogen that belongs to water and another element (not a hydrogen) that belongs to the molecular system studied [19]. The existence of the hydration force has been experimentally observed when water was removed from between membranes or molecular surfaces. The hydration force brings the neutral bilayers together. It is also a repulsive force that can be strong enough to prevent contact between membranes. For example it is observed when lipid bilayers can be brought closer together than $20-30$ $\mathring{A}$ in water[21]. The hydration force is used to explain why water molecules are more ordered when they are near the headgroups

of phospholipid molecules[21]. The hydrogen bond is one type of weak intermolecular bonding that is just slightly stronger than the intermolecular van der Waals forces present in condensed matter systems. Although the hydrogen bond is not a strong bond it can significantly determine the properties of substances. Because of its small bonding energy, it allows the associated molecular system to be reactive at normal temperatures. Atoms such as N, O, F and P are strongly electronegative so that they often form hydrogen bonds. That is, the X and Y positions in the structure of hydrogen bond X−H...Y, are of the type O...H−O or O−H...P etc.[20]. The length of the hydrogen bond is defined as the distance between X and Y. Since the hydrogen bond is stronger than the van der Waals interaction, the distances between X...H...Y in hydrogen bond are shorter than the "bonding" distance of the van der Waals bonds[20]. However due to the weak bonding energy relative to covalent or ionic bonds, the bond distances are sensitive to their environment. The x-ray diffraction experiments show that in the case of ice, the O...H distances in the hydrogen bonds O−H...O are about 1.2 $\mathring{A}$ longer than the free O−H bond (1.00−1.05 $\mathring{A}$)[20]. On the other hand, the distances such as O−H in the bondings of O−H...O are closely related to the distances of O...O. The hydrogen bonds formed in the molecular system change the geometrical structure of water and the phospholipid molecules.

The study of the hydrogen bond occurring between the phospholipids and water molecules is useful in revealing the possible mechanisms of the stability of the bilayer system. The surface atoms of polar headgroup interact with the water molecules via electrostatic interaction. They act like a bridge that links with the headgroups of phospholipid molecules at the two layers. This forms a hydrogen-bonded system. Some water molecules are also located between the phosphate oxygens of two lipid molecules. Other water molecules link with lipid phosphates and the neighboring

water molecules. This kind of hydrogen bond increases stability of the system since they resemble more closely the strong hydration bonds that exist in the bulk water. The interaction between water and lipids affects the system in two important ways: water molecules in the interfacial region become more ordered and the headgroups of lipids change their orientations and geometries. Thus, the presence or lack of hydration bonds can be directly related to the phase transition temperature of lipids[34]. Our studies on the hydrated headgroups included: hydrated compound III and hydrated GPE. Both of these compounds have shown anomalous structures when treated as isolated systems. We also note that in the calculations of the hydrated models, discussed below, we did not systematically search for the lowest energy structure (since this would be very time consuming at the ab initio level) by starting the calculations with different initial water placements. In this part of the thesis we are investigating general features of the hydrated systems. Detailed conformational analysis of hydrated phospholipids will be the subject of the future studies.

4.1 Hydrated Compound III (in the Global Minimum Conformation)

In chapter 3, we described complete geometry optimization for compound III. We have found that isolated compound III forms a (unexpected) distorted structure. It is our belief that this result is due to the fact that the hydration force was not taken into account. In order to test this hypothesis we performed geometry optimization of compound III in the presence of four water molecules. We began our calculations with four water molecules randomly distributed around compound III which was initially in the global minimum structure. The waters placed themselves close to the phosphate group and ammonium group. The complete geometry optimization for compound III + $4H_2O$ was performed using the HF/3-21G* basis set (as in

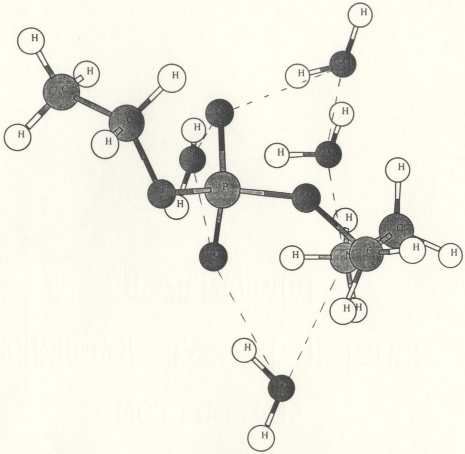

Figure 4.1 The lowest energy conformation for compound III + $4H_2O$. (The hydrogen bonds are indicated by dashed lines.) The lengths of the hydrogen bonds are as follows:

O(1)...O(14): 2.93 Å, O(1)...O(13): 2.76 Å,

O(2)...O(13): 2.63 Å, O(2)...O(3): 2.67 Å,

O(3)...N: 2.58 Å, O(4)...N: 2.79 Å

O(4)...O(14): 2.67 Å,

Table 4.1: Geometrical parameters for compound III+ $4H_2O$.

bond length $\AA$		bond angle (deg.)		dihedral angle (deg.)	
O(13)-P	1.501	O(14)-P-O(13)	114.8	O(14)-P-O(13)-O(11)	−125.4
O(14)-P	1.506	O(12)-P-O(11)	104.0	O(13)-P-O(14)-O(12)	−120.4
O(12)-P	1.590	C(11)-O(12)-P	126.0	α_1	76.7
O(11)-P	1.571	C(1)-O(11)-P	124.2	α_2	122.0
C(11)-O(12)	1.455	C(12)-C(11)-O(12)	110.6	α_3	127.1
C(1)-O(11)	1.464	C(2)-C(1)-O(11)	110.1	α_4	72.0
C(12)-C(11)	1.531	H-C(11)-O(12)	108.0	α_5	−81.7
C(2)-C(1)	1.525	H-C(1)-O(11)	106.9	H(11A)-C(11)-O(12)-P	−51.2
H-C(11)	1.077	N-C(12)-C(11)	110.9	H(11B)-C(11)-O(12)-P	−169.4
H-C(1)	1.077	H-C(12)-C(11)	110.2	H(1A)-C(1)-O(11)-P	−44.6
H-C(12)	1.078	H-C(2)-C(1)	111.0	H(1B)-C(1)-O(11)-P	−162.8
H-C(2)	1.083	H-N-C(12)	110.1	H(12A)-C(12)-C(11)-O(12)	35.7
N-C(12)	1.516	H^A_{W1}-O(14)-P	73.1	H(12B)-C(12)-C(11)-O(12)	158.5
H^A_N-N	1.070	O_{W1}-H^A_{W1}-O(14)	92.3	H^A_2-C(2)-C(1)-O(11)	174.0
H^B_N-N	1.032	H^B_{W1}-O_{W1}-H^A_{W1}	105.4	H^B_2-C(2)-C(1)-O(11)	53.7
H^C_N-N	1.023	O_{W2}-H^A_N-N	103.7	H^C_2-C(2)-C(1)-O(11)	−66.5
H^A_{W1}-O(12)	2.731	H^A_{W2}-O_{W2}-H^A_N	158.0	H^A_N-N-C(12)-C(11)	146.9
O_{W1}-H^A_{W1}	0.979	H^B_{W2}-O_{W2}-H^A_{W2}	111.0	H^B_N-N-C(12)-C(11)	32.3
H^B_{W1}-O_{W1}	0.967	O_{W3}-H^B_N-N	64.2	H^C_N-N-C(12)-C(11)	−82.1
O_{W2}-H^A_N	3.101	H^A_{W3}-O_{W3}-H^B_N	97.1	H^A_{W1}-O(14)-O(13)-O(11)	122.3
H^A_{W2}-O_{W2}	0.963	H^A_{W3}-O_{W3}-H^A_{W3}	105.8	O_{W1}-H^A_{W1}-O(14)-P	171.0
H^B_{W2}-O_{W2}	0.994	O_{W4}-H^C_N-N	111.3	H^B_{W1}-O_{W1}-H^A_{W1}-O(14)	25.9
O_{W3}-H^B_N	2.852	H^A_{W4}-O_{W4}-H^A_N	147.2	O_{W2}-H^A_N-N-C(12)	−42.9
H^A_{W3}-O_{W3}	0.984	H^B_{W4}-O_{W4}-H^A_{W4}	110.7	H^A_{W2}-O_{W2}-H^A_N-N	114.9
H^B_{W3}-O_{W3}	0.986			H^B_{W2}-O_{W2}-H^A_{W2}-H^A_N	169.4
O_{W4}-H^C_N	2.252			O_{W3}-H^A_N-N-C(12)	110.4
H^A_{W4}-O_{W4}	0.964			H^A_{W3}-O_{W3}-H^A_N-N	−93.1
H^B_{W4}-O_{W4}	0.982			H^B_{W3}-O_{W3}-H^A_{W3}-H^A_N	77.3
				O_{W4}-H^B_N-N-C(12)	88.6
				H^A_{W4}-O_{W4}-H^B_N-N	163.1
				H^B_{W4}-O_{W4}-H^A_{W4}-H^B_N	137.5

E (RHF) = −1151.285553 hartree

chapter 3). In this case, compound III + $4H_2O$ converged quickly to a stable structure. The NH_3^+ group remained intact, (i.e. the hydrogen covalent bond between phosphate and hydrogen was not formed). The conformation is displayed in Figure 4.1 and full geometry parameters are given in Table 4.1. In Figure 4.1, the stabilizing hydrogen bonds are displayed. We note that in the calculations of the hydrated models we did not systematically search for the lowest energy structure (since this would be very time consuming at the ab initio level) by starting the calculations with different initial water placements.

4.1.1 The Effect of Water on Molecular Stability in Compound III

The main effect of water molecules on compound III was that in the hydrated compound III, all of the N and H atoms remained covalently bonded. The reason for this is that the water molecules have a screening effect on the intramolecular interaction between the ammonium cation and phosphate anion, thereby preventing strong interactions between N−H and ionic oxygens on the phosphate group. Thus, the ammonium hydrogen atoms are not attracted by the oxygens of the phosphate group. The hydration force is predominantly formed between the oxygens of the phosphate group and water molecules. X-ray diffraction experiments have illustrated that there is, at least, one water molecule between the oxygens bonded by the phosphate in one phospholipid and the hydrogens bonded to the nitrogen in another phospholipid molecule.

This results in generating a large lipid and water complex in the crystalline state. Molecular mechanics studies on the phospholipid systems have also shown that stable structures are obtained when three to five water molecules are placed around the NH_3^+ group for a given molecular model. The distribution of hydrogen bonds will strongly depend on the size of the system. Different patterns of hydrogen bonds will

result in different changes in the geometrical parameters (such as the bond length (P−O, P=O, N−H) and the bond angles in the α−chain) of the lipid molecules. This in turn has an effect on the physical properties of lipid molecules such as average molecular areas, the thickness of polar regions etc. These properties are associated with the phase behavior of lipid bilayers and their transport capabilities. In summary, our calculations for compound III reveal the importance of solvent in reducing strong intramolecular interactions.

4.1.2 The Effect of Compound III on Water Molecules

The structures of water molecules between the lipid bilayer differs from that in the free bulk water. In Table 4.1, we list the geometrical parameters of the water molecules in the lipid-water system. The four water molecules have four different molecular structures. The corresponding H−O−H bond angles are 111.69°, 110.57°, 107.32° and 105.31° respectively. The biggest bond angles have been observed close to the phospholipid. Their O−H bond lengths exhibit 0.03 $\AA$ fluctuations (0.964−0.995 $\AA$). The largest change in the bond length is observed when water is closest to the headgroup. Clearly, water molecules change their bulk free water structure in the presence of the phospholipids. That is the lipid-water interaction mutually perturbes both of their geometries.

As shown in Figure 4.1, seven hydrogen bonds are formed in this water and compound III cluster. Distances between the oxygen atoms in water and the oxygen and nitrogen atoms in the headgroup range from 2.63−2.93 $\AA$. These distances are smaller than the van der Waals radii found in ice (3.04 $\AA$). The hydrogen bonds can be divided into three types: water...oxygen of the phospholipid, water...NH_3^+ group and water...water. In the hydration process, which was fully geometry optimized we have seen that some water molecules which were far away from the phospholipid

were attracted closer to phospholipid and some water molecules which were too close to the phospholipid were repelled farther away. The number of water molecules was larger than the smallest number determined by the x-ray experiment. However we can not say if the compound III has reached the saturation limit found by x-ray diffraction for the crystal. We have found three kinds hydrogen bonds and their distances are also in reasonable agreement with experimental values (see Figure 4.1). It is expected that the structure of water molecules will depend on the total number of the water molecules in the system. We emphasize that water molecules in our studies were placed randomly around the phospholipid headgroup to begin with. There were no constraints on their positions during geometry optimization since we were interested in investigating the effect of hydration field on the structure of the phospholipid molecule.

4.2 Hydrated Compound III (in the First Local Minimum Conformation)

In this section, we present the results for a similar calculation as discussed above with the exception that the starting conformation of compound III is its first local minimum structure. The geometrical parameters for this system given in Table 4.2 and their structures are shown in Figure 4.2. As discussed in section 4.1, the structure of compound III in this case also resembled more accurately the structure found in phospholipids. The torsional angles in $\alpha-$chain are closer to the experimental values. Again we have found seven similar hydrogen bonds. They are listed in Figure 4.2. Among them, the hydrogen bonds, O(1)...O(13), O(2)...O(3), O(4)...O(14), are exactly the same as found in the previous calculation. The hydrogen bonds, O(1)...O(14), O(2)...O(13), and O(4)...N are 0.01 $\AA$ longer than the corresponding values in section 4.1. The hydrogen bond of O(3)...N are 0.06 $\AA$ longer than the

repetitive value in the global minimum compound III + $4H_2O$ system. These longer hydrogen bonds increase the energy of the system relative to the previous conformation. This hydration pattern illustrates that the formation of hydrogen bonds is sensitive to the conformation of the phospholipid. From the point of phospholipid molecule, the number of hydrogen bonds remained the same as before. The atoms O(13) and O(14) formed two hydrogen bonds with two water molecules each. The hydrogen bond distance between O(2)...O(3) remained the same. In solution, as discussed previously, the phospholipid displays a large flexibility. At room temperature they are always in motion. These movements will in turn produce changes in hydrogen bonds. These induce changes in the physical and biochemical properties of the bilayer. In summary the comparison of two hydrated systems of compound III indicates that the hydrogen bonds in the hydrated phospholipid-water molecule are sensitive to the conformational changes in the phospholipid molecules.

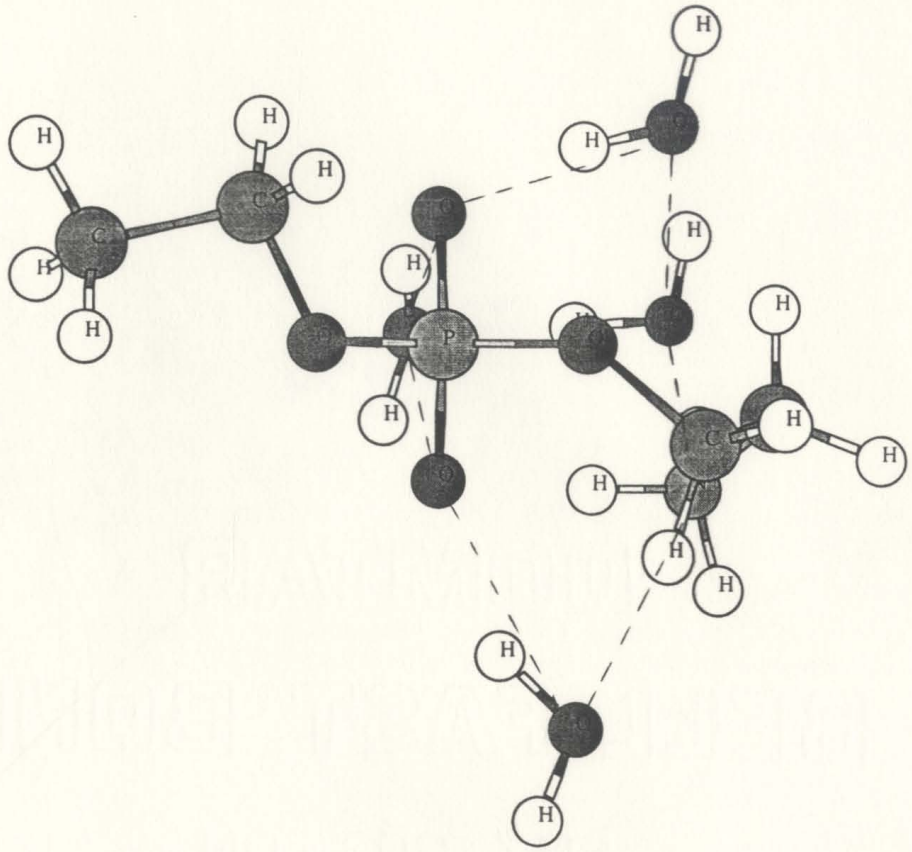

Figure 4.2 The second lowest energy (first local minimum) conformation of compound III + $4H_2O$. (The hydrogen bonds are indicated by dashed lines.)

We have found the following hydrogen bonds:

O(1)...O(14): 2.94 $\mathring{A}$, O(1)...O(13): 2.76 $\mathring{A}$

O(2)...O(13): 2.64 $\mathring{A}$, O(2)...O(3): 2.67 $\mathring{A}$

O(3)...N: 2.64 $\mathring{A}$ O(4)...N: 2.80 $\mathring{A}$

O(4)...O(14): 2.67 $\mathring{A}$,

Table 4.2: Geometrical parameters of the first local minimum conformation for compound III+ $4H_2O$.

bond length $\AA$		bond angle (deg.)		dihedral angle (deg.)	
O(13)-P	1.500	O(14)-P-O(13)	115.7	O(14)-P-O(13)-O(11)	−125.8
O(14)-P	1.504	O(12)-P-O(11)	104.5	O(13)-P-O(14)-O(12)	−120.6
O(12)-P	1.594	C(11)-O(12)-P	125.7	α_1	152.8
O(11)-P	1.571	C(1)-O(11)-P	124.8	α_2	87.0
C(11)-O(12)	1.455	C(12)-C(11)-O(12)	111.1	α_3	129.1
C(1)-O(11)	1.464	C(2)-C(1)-O(11)	106.9	α_4	68.6
C(12)-C(11)	1.532	H-C(11)-O(12)	108.1	α_5	−82.5
C(2)-C(1)	1.521	H-C(1)-O(11)	108.2	H(11A)-C(11)-O(12)-P	−53.6
H-C(11)	1.077	N-C(12)-C(11)	110.3	H(11B)-C(11)-O(12)-P	−172.9
H-C(1)	1.079	H-C(12)-C(11)	110.3	H(1A)-C(1)-O(11)-P	31.7
H-C(12)	1.078	H-C(2)-C(1)	109.1	H(1B)-C(1)-O(11)-P	−87.0
H-C(2)	1.082	H-N-C(12)	109.9	H(12A)-C(12)-C(11)-O(12)	35.3
N-C(12)	1.520	H^A_{W1}-O(14)-P	72.6	H(12B)-C(12)-C(11)-O(12)	157.8
N-C(12)	1.520	H^A_{W1}-O(14)-P	72.6	H(12B)-C(12)-C(11)-O(12)	157.8
H^A_N-N	1.071	O_{W1}-H^A_{W1}-O(14)	90.9	H^A_2-C(2)-C(1)-O(11)	178.5
H^B_N-N	1.035	H^B_{W1}-O_{W1}-H^A_{W1}	105.3	H^B_2-C(2)-C(1)-O(11)	58.3
H^C_N-N	1.012	O_{W2}-H^A_N-N	105.0	H^C_2-C(2)-C(1)-O(11)	−61.2
H^A_{W1}-O(12)	2.753	H^A_{W2}-O_{W2}-H^A_N	159.2	H^A_N-N-C(12)-C(11)	147.1
O_{W1}-H^A_{W1}	0.978	H^B_{W2}-O_{W2}-H^A_{W2}	110.8	H^B_N-N-C(12)-C(11)	32.1
H^B_{W1}-O_{W1}	0.967	O_{W3}-H^B_N-N	63.2	H^C_N-N-C(12)-C(11)	−82.6
O_{W2}-H^A_N	3.104	H^A_{W3}-O_{W3}-H^B_N	98.7	H^A_{W1}-O(14)-O(13)-O(11)	120.4
H^A_{W2}-O_{W2}	0.964	H^A_{W3}-O_{W3}-H^A_{W3}	106.4	O_{W1}-H^A_{W1}-O(14)-P	173.2
H^B_{W2}-O_{W2}	0.994	O_{W4}-H^C_N-N	109.5	H^B_{W1}-O_{W1}-H^A_{W1}-O(14)	24.4
O_{W3}-H^B_N	2.873	H^A_{W4}-O_{W4}-H^A_N	151.0	O_{W2}-H^A_N-N-C(12)	114.5
H^A_{W3}-O_{W3}	0.982	H^B_{W4}-O_{W4}-H^A_{W4}	110.3	H^A_{W2}-O_{W2}-H^A_N -N	168.8
H^B_{W3}-O_{W3}	0.987			H^B_{W2}-O_{W2}-H^A_{W2}-H^A_N	110.6
O_{W4}-H^C_N	2.259			O_{W3}-H^A_N-N-C(12)	−91.6
H^A_{W4}-O_{W4}	0.964			H^A_{W3}-O_{W3}-H^A_N-N	78.1
H^B_{W4}-O_{W4}	0.981			H^B_{W3}-O_{W3}-H^A_{W3}-H^A_N	90.0
				O_{W4}-H^B_N-N-C(12)	169.5
				H^A_{W4}-O_{W4}-H^B_N-N	145.5
				H^B_{W4}-O_{W4}-H^A_{W4}-H^B_N	

E (RHF) = −1151.285046 hartree

4.3 The Effect of Two Compounds III on Water Molecules

The system investigated in this section consists of two compounds III and four water molecules. The geometries of compounds III are not relaxed in this calculation (the parameters are taken as given in Table 4.2). As before, four water molecules were placed randomly at the beginning of this computation. Also the relative position of two compounds III is allowed to vary. The structures of water molecules were fully optimized. Thus, a partial geometry optimization was performed in this section. The results of this calculation, as related to positions and structures of the four water molecules, are summarized in Table 4.3. The complete system is shown in Figure 4.3.

Table 4.3: Geometrical parameters for four water molecules for the system that consists of two compounds III and $4H_2O$

bond length $\AA$		bond angle (deg.)		dihedral angle (deg.)	
H^A_{W1}-O_{12}	2.79	H^A_{W1}-O_{14}-P	69.5	H^A_{W1}-O_{13}-P-O_{11}	121.1
O_{W1}-H^A_{W1}	0.97	O_{W1}-H^A_{W1}-O_{14}	113.2	O_{W1}-H^A_{W1}-O_{14}-P	177.0
H^B_{W1}-O_{W1}	0.97	H^B_{W1}-O_{W1}-H^A_{W1}	109.8	H^B_{W1}-O_{W1}-H^A_{W1}- O_{14}	149.6
O_{W2}-H^A_N	3.22	O_{W2}-H^A_N-N	104.1	O_{W2}-H^A_N-N-C_{12}	−40.2
H^A_{W2}-O_{W2}	0.96	H^A_{W2}-O_{W2}-H^A_N	153.4	H^A_{W2}-O_{W2}-H^A_N-N	82.5
H^B_{W2}-O_{W2}	0.99	H^B_{W2}-O_{W2}-H^A_{W2}	111.2	H^B_{W2}-O_{W2}-H^A_{W2}-H^A_N	133.0
O_{W3}-H^B_N	2.95	O_{W3}-H^B_N-N	63.4	O_{W3}-H^A_N-N-C_{12}	107.6
H^A_{W3}-O_{W3}	0.98	H^A_{W3}-O_{W3}-H^B_N	97.9	H^A_{W3}-O_{W3}-H^A_N-N	−89.6
H^B_{W3}-O_{W3}	0.98	H^A_{W3}-O_{W3}-H^A_{W3}	106.2	H^B_{W3}-O_{W3}-H^A_{W3}-H^A_N	83.1
O_{W4}-H^C_N	3.87	O_{W4}-H^C_N-N	73.7	O_{W4}-H^B_N-N-C_{12}	149.0
H^A_{W4}-O_{W4}	0.97	H^A_{W4}-O_{W4}-H^A_N	95.3	H^A_{W4}-O_{W4}-H^B_N-N	40.7
H^B_{W4}-O_{W4}	0.98	H^B_{W4}-O_{W4}-H^A_{W4}	104.8	H^B_{W4}-O_{W4}-H^A_{W4}-H^B_N	66.4

Hydrogen bonds for the system consisting of two compound III and $4H_2O$ are very similar to hydrogen bonds observed for one compound III and $4H_2O$ (see section 4.2). In this geometry optimization, it is interesting to note that the second compound III greatly adjusted its orientation relative to the first compound III. However, the positions of the four water molecules relative to the first compound III

changed very little. This phenomenon suggests that the hydration of the phospholipids exhibits a basic pattern. The hydrogen bonds formed with one phospholipid molecule will not change very much when a bilayer or a multi−layer system is produced. Of course, two compounds III are not enough to construct a realistic model of a bilayer system and to illustrate its hydration properties. In addition, it is clear that four water molecules do not provide adequate hydration forces for two compound III. We suspect that at least six other water molecules are needed to form the hydrogen bonds such that link oxygen atoms of water to $O(13)_2$, $O(14)_2$, N_1 and N_2. Therefore, we suggest that a future study should involve ten water molecules instead of four.

Next we compare the parameter lists in Tables 4.2 and 4.3 with the corresponding bulk water parameters. In general, the O−H bond length in the case of hydrated compounds III differ from the standard bond lengths of O−H bond in bulk water (differ by $\sim 0.002 - 0.003\mathring{A}$). The bond angles are also different relative to the standard values for bulk water by $6-8\ \mathring{A}$. The hydration forces change geometries of the water molecules from those observed in bulk water. It has been observed experimentally[34] that these changes in structure of H_2O molecules will decay exponentially as the distance between the bilayer increases.

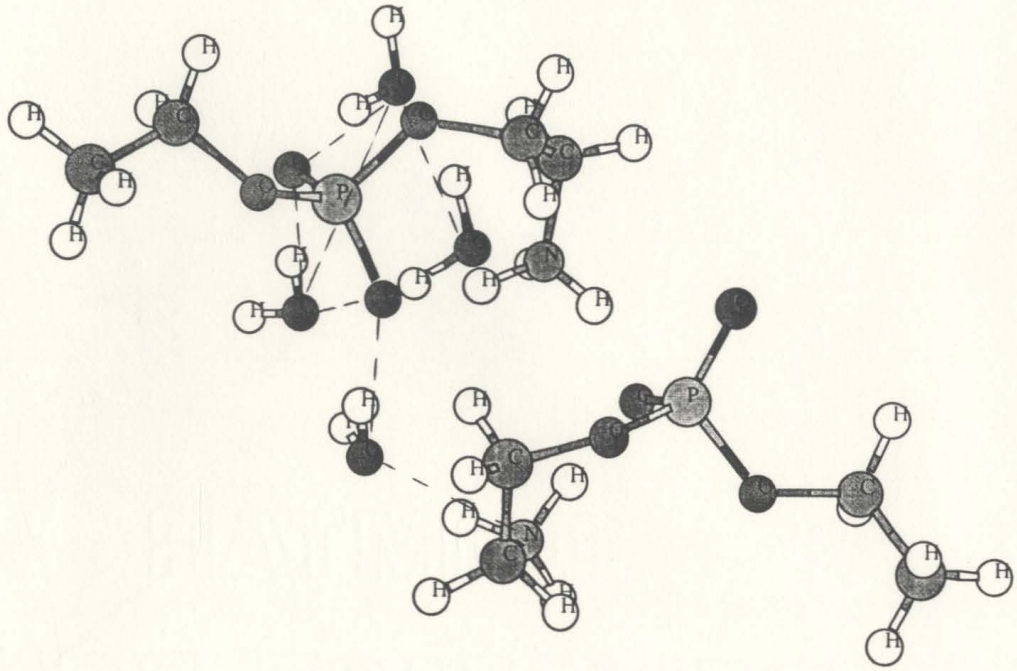

Figure 4.3 Two compounds III + $4H_2O$.

The following hydrogen bonds have been found:

O(1)...O(14): 2.98 $\AA$, O(1)...O(13): 2.75 $\AA$

O(2)...O(13): 2.64 $\AA$, O(2)...O(1): 2.71 $\AA$

O(3)...N(1): 2.63 $\AA$, O(2)...O(3): 2.68 $\AA$

O(4)...O(14): 2.61 $\AA$, O(4)...N_2 : 2.64 $\AA$

4.4 Hydrated GPE

The structure of an isolated GPE molecule has been studied in chapter 3 (see Figure 3.11). Similar to the optimized structure for GPE displayed the behavior of breaking one of the N−H bonds and forming an extra O−H bond with one of the oxygens attached to phosphate. In the case of compound III, this unexpected result was overcome by hydrating the compound. In this section the results of a hydrated GPE calculation will be discussed. The starting geometry for GPE was taken from the experimental data[4]. Six water molecules were placed around the GPE. Thus, greater hydration level was employed in this case than in the previous system. A complete geometry optimization was performed for the system consisting of the GPE and six water molecules. As before, basis set, HF/3-21G* was employed in the optimization. We begin by first analyzing the conformation of the hydrated GPE. Table 4.4 compares experimental and computational findings for the major torsional angles of the α−chain.

Table 4.4: A comparison of theoretical and experimental torsional angles for hydrated GPE.

system	angles (deg.) (calculated)	angles (deg.) (experimental)	difference (deg.) (calculated - experimental)
	$\alpha_1 = 141$	$\alpha_1 = -174$	−45
	$\alpha_2 = -50$	$\alpha_2 = -81$	31
$GPE+6H_2O$	$\alpha_3 = -79$	$\alpha_3 = -81$	2
$\alpha_1 - \alpha_5$	$\alpha_4 = 240$	$\alpha_4 = 164$	76
+ac −sc −sc −ac +sc	$\alpha_5 = 54$	$\alpha_5 = 55$	−1
	$\theta_1 = 170$	$\theta_1 = 166$	4
	θ_2 =-72	θ_2 =-89	17
	$\theta_3 = -64$	$\theta_3 = -67$	3
	$\theta_4 = 178$	$\theta_4 = 180$	−2

In Table 4.4, the second column gives the theoretical results for the hydrated GPE. The third column lists corresponding experimental data. The fourth column

gives differences between the second and third columns.

In Table 4.5 a complete set of geometrical parameters for hydrated GPE is given. Clearly there are many differences between the isolated GPE (see Table 3.26) and hydrated GPE (see Table 4.5). In this section we focus on the differences between dihedral angles. From Table 4.4 it is clear that the differences between the theoretical and the experimental data decreased significantly in the presence of water molecules. This is particularly true for the torsional angles α_3 and α_5. The hydrated system resembles the experimental result more closely. The torsional angle α_5 greatly depends on the hydration environment. It is this correction that disconnects the phosphate group and ammonium groups. It should be noted that all of the values of torsional angles, θ's, in the $\alpha-$chain are closer to the experimental values although the majority of water molecules are far away from the region determined by the θ values. Again, this indicates that the structure of GPE is equally determined by both the intermolecular and intramolecular interactions.

We also calculated the molecular parameters such as area, the thickness of polar region, the thickness of the head group and the total molecular dipole moment. The molecular area is $17-79$ $\mathring{A}^2$, the thickness of polar region is 10.3 $\mathring{A}$, the thickness of the head group is 8.0 $\mathring{A}$. All of these are slightly larger than those of GPE without the presence of hydration forces. The total dipole moment is 9.66 debye (it is 2.15 debye larger than for the isolated GPE). This larger dipole implies stronger polarization of the system containing water. From Mulliken population analysis, six water molecules have net charges of -0.80, -0.83, -0.82, -0.81, -0.82 and -0.83 respectively. Such nonzero net charges are caused by water molecules interacting with phospholipid model compound. One of the important changes in the net charges has been observed for the NH_3^+ group whose charge becomes $+0.36$ in water in comparison to -0.16 without water. Also, the distance between the atom

P and N increases to 3.73 $\AA$ from 3.51 $\AA$ in the presence of water. Therefore, the net effect of hydration is to increase the size of the molecule. Under this condition, the molecule is more reactive and more susceptible to outside influences.

The hydrogen bonds: O(1)...O(13), O(2)...O(13), O(2)...O(3), O(4)...O(14) and O(4)...N have similar values to those obtained in the hydrated compound III. The hydrogen bonds are of two types: water...phospholipid and water...water and are listed below.

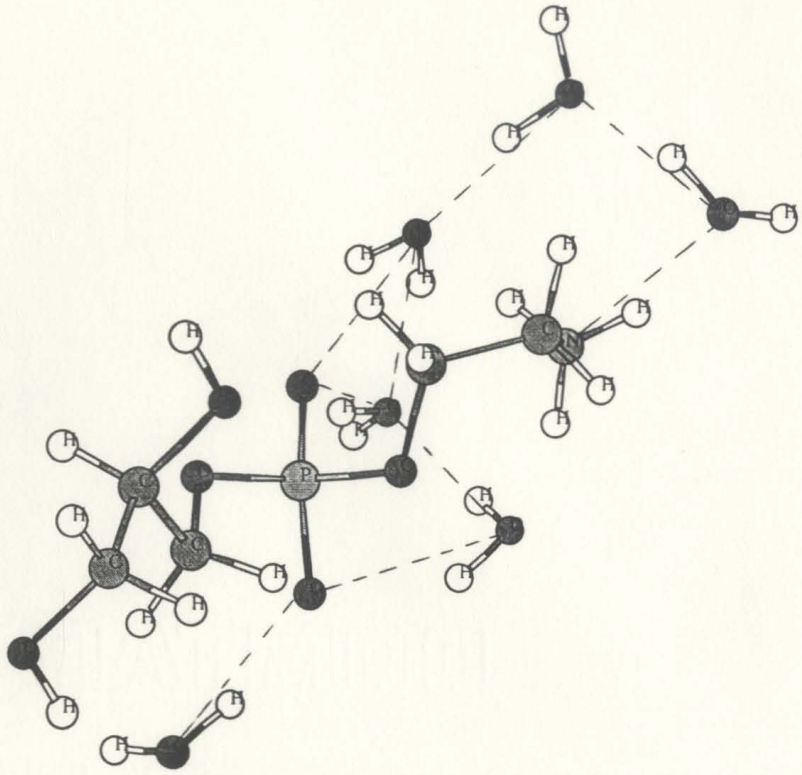

Figure 4.4 The structure of GPE + $6H_2O$. (The hydrogen bonds are indicated by dashed lines).

Hydrogen bonds:		Mulliken population:			
O(1)...O(13):	2.62 Å,	P	1.61	O(W1)	−0.02
O(1)...O(2):	2.66 Å	O(14)	−0.76	O(W2)	0.01
O(2)...O(13):	2.67 Å,	O(13)	−0.76	O(W3)	0.01
O(2)...O(3):	2.65 Å,	O(12)	−0.74	O(W4)	0.01
O(3)...O(4):	2.60 Å,	O(11)	−0.74	O(W5)	0.03
O(1)..O(5):	2.81 Å,	C(11)	0.36	O(W6)	0.01
O(6)...O(14):	2.74 Å,	C(1)	0.38		
O(4)...N:	2.63 Å,	C(12)	0.25		
O(5)...O(14):	2.86 Å,	C(2)	0.22		
O(5)...N:	2.70 Å	N	0.22		

Table 4.5: Geometrical parameters for hydrated GPE.

bond length $\AA$		bond angle (deg.)		dihedral angle (deg.)	
O(13)-P	1.460	O(14)-P-O(13)	124.6	O(14)-P-O(13)-O(11)	−132.8
O(14)-P	1.488	O(12)-P-O(11)	99.2	O(13)-P-O(14)-O(12)	−120.5
O(12)-P	1.640	C(11)-O(12)-P	117.5	α_1	141.1
O(11)-P	1.622	C(1)-O(11)-P	120.2	α_2	−50.3
C(11)-O(12)	1.434	C(12)-C(11)-O(12)	109.3	α_3	−79.2
C(1)-O(11)	1.452	C(2)-C(1)-O(11)	108.4	α_4	−120.0
C(12)-C(11)	1.519	H-C(11)-O(12)	110.2	α_5	54.1
C(2)-C(1)	1.519	H-C(1)-O(11)	109.5	H(11A)-C(11)-O(12)-P	120.2
H-C(11)	1.078	N-C(12)-C(11)	116.0	H(11B)-C(11)-O(12)-P	1.4
H-C(1)	1.078	H-C(12)-C(11)	109.6	H(1A)-C(1)-O(11)-P	−96.7
H-C(12)	1.080	H-C(2)-C(1)	108.1	H(1B)-C(1)-O(11)-P	22.8
H-C(2)	1.084	C(3)-C(2)-C(1)	110.6	H(12A)-C(12)-C(11)-O(12)	−65.3
N-C(12)	1.531	O(21)-C(2)-C(1)	107.9	H(12B)-C(12)-C(11)-O(12)	175.4
H-C(3)	1.080	H-N-C(12)	108.5	H(2A)-C(2)-C(1)-O(11)	49.4
H-O(21)	0.967	H-O(21)-C(2)	110.4	C(3)-C(2)-C(1)-O(11)	170.6
C(2)-O(21)	1.454	H-O(31)-C(3)	107.3	N-C(12)-C(11)-O(12)	54.1
H-N	1.007	H-C(3)-C(2)	106.7	O(21)-C(2)-C(1)-O(11)	−71.5
H-O(31)	0.970	O(31)-C(3)-C(2)	111.2	H^A_N-N-C(12)-C(11)	170.2
C(3)-O(31)	1.454	H^A_{W1}-O(13)-P	119.5	H^B_N-N-C(12)-C(11)	53.5
H^A_{W1}-O(14)	3.112	O_{W1}-H^A_{W1}-O(14)	59.0	H^C_N-N-C(12)-C(11)	−62.9
O_{W1}-H^A_{W1}	0.966	H^B_{W1}-O_{W1}-H^A_{W1}	107.2	H-O(21)-C(2)-C(1)	156.8
H^B_{W1}-O_{W1}	0.981	O_{W2}-H^A_N-N	101.1	O(31)-C(3)-C(2)-C(1)	−64.1
O_{W2}-H^A_N	3.122	H^A_{W2}-O_{W2}-H^A_N	150.9	H-O(31)-C(3)-C(2)	81.2
H^A_{W2}-O_{W2}	0.962	H^B_{W2}-O_{W2}-H^A_{W2}	111.5	H(3A)-C(3)-C(2)-C(1)	59.6
H^B_{W2}-O_{W2}	0.986	O_{W3}-H^B_N-N	108.4	H(3B)-C(3)-C(2)-C(1)	177.1
O_{W3}-H^B_N	2.905	H^A_{W3}-O_{W3}-H^B_N	72.3	H^A_{W1}-O(14)-O(13)-O(11)	18.3
H^A_{W3}-O_{W3}	0.994	H^A_{W3}-O_{W3}-H^A_{W3}	110.9	O_{W1}-H^A_{W1}-O(14)-P	96.5
H^B_{W3}-O_{W3}	0.963	O_{W4}-H^C_N-N	160.1	H^B_{W1}-O_{W1}-H^A_{W1}-O(14)	−8.2
O_{W4}-H^C_N	1.735	H^A_{W4}-O_{W4}-H^A_N	118.0	O_{W2}-H^A_N-N-C(12)	−100.8
H^A_{W4}-O_{W4}	0.975	H^B_{W4}-O_{W4}-H^A_{W4}	108.2	H^A_{W2}-O_{W2}-H^A_N − N	89.9
H^B_{W4}-O_{W4}	0.974	H^A_{W5}-O(13)-P	114.7	H^B_{W2}-O_{W2}-H^A_{W2}-H^A_N	102.5
H^A_{W5}-O(13)	1.690	O_{W5}-H^A_{W5}-O(13)	156.4	O_{W3}-H^A_N-N-C(12)	108.4
O_{W5}-H^A_{W5}	0.989	H^B_{W5}-O_{W5}-H^A_{W5}	111.6	H^A_{W3}-O_{W3}-H^A_N-N	−166.5
H^B_{W5}-O_{W5}	0.965	H^A_{W6}-O(13)-P	151.5	H^B_{W3}-O_{W3}-H^A_{W3}-H^A_N	135.4
H^A_{W6}-O(13)	1.852	O_{W6}-H^A_{W6}-O(13)	138.8	O_{W4}-H^B_N-N-C(12)	126.9
O_{W6}-H^A_{W6}	0.979	H^B_{W6}-O_{W6}-H^A_{W6}	104.8	H^A_{W4}-O_{W4}-H^B_N-N	−106.7
H^B_{W6}-O_{W6}	0.980			H^B_{W4}-O_{W4}-H^A_{W4}-H^B_N	−118.4
				H^A_{W5}-O(13)-P-O(12)	109.1
				O_{W5}-H^A_{W5}-O(13)-P	−107.4
				H^B_{W5}-O_{W5}-H^A_{W5}-O(13)	−170.9
				H^A_{W6}-O(13)-P-O(12)	−2.3
				O_{W6}-H^A_{W6}-O(13)-P	81.8
				H^B_{W6}-O_{W6}-H^A_{W6}-O(13)	39.2

Chapter 5

Summary and Conclusions

In this chapter we summarize the main results presented in chapters 3 and 4 and give some conclusions.

We found that the minimal basis set, STO-3G, is not appropriate for predicting the geometry of a phospholipid molecule. The error in bond lengths was at the order of 0.1 $\AA$ and in bond angles was of the order of 4 °. Including the diffuse functions in basis set did not change the geometries significantly. The HF/6-31G* results showed little improvement over the HF/3-21G* basis set. Thus, taking into account CPU time savings, the HF/3-21G* basis set was chosen for our calculations.

The preferred structure for compound I had the +sc/+sc conformation for the torsional angles α_2/α_3. The corresponding conformational energy differences were 4.98 and 9.20 kcal/mol for the +sc/ap and ap/ap conformations indicating that compound I is very flexible. The conformation +sc/+sc as described by torsional angles α_2/α_3 is the most stable conformation in all model compounds considered. They vary from 75° to 60° as the size of model compounds increases.

Esterified oxygens form single and double bond respectively in compound I and II. The bond lengths and bond angles, P-O(13) and P-O(14), O(11)-P-O(13) and O(12)-P-O(14), remained unchanged in compound I and II. Extending compound II to include nitrogen atom breaks the symmetry of the model compounds.

The relative conformational energies for compound II show little difference. The

maximum conformational energy difference is 9.2 kJ/mol. This implies that a number of different conformations could exist in solution at room temperature. Compound II (similar to compound I) is very flexible.

The inclusion of water molecules in the geometry optimization of compound III has a dramatic effect of stabilizing its structure. The minimum energy for compound III and GPE showed an unusual hydrogen bond on one of the esterified oxygens. This illustrates that the stabilities of compound III and GPE in a membrane system depend significantly on the intermolecular interaction and hydration forces. The structures of compound III and GPE do not differ very much, once again showing that adding C(3), O(21) and O(31) does not lead to large changes in the corresponding part of GPE. Also, GPE and GPC have similar structures. The values of major torsional angles tend to cluster in a narrow range.

Preliminary results of the hydration calculations indicate that presence of water increases the molecular area of phospholipid molecules.

The important dihedral angles for a single GPC molecule obtained from the ab initio geometry optimization agree with the experimental crystallographic values to within 10° to 20°. The differences can be accounted for by noting that both intermolecular interactions and hydration effects are not included in the single molecule calculation. The stability of GPC suggests that it is mainly determined by intramolecular forces. The calculation for hydrated compound III and GPE indicate that four waters are sufficient to provide adequate shielding of the strong attractive interaction between the P and the N groups. The inclusion of water generates conformations similar to those obtained in x-ray crystalline diffraction experimental studies. The calculations reveal the important role of water in reducing strong intramolecular (electrostatic) interactions.

The calculations in this work were restricted by a number of factors: (1) They

were not in bulk water, thus they did not illustrate exactly the properties of the molecule in aqueous solution. Adding a few water molecules gave some indication of the effect of hydration force on the structure phospholipids. Actually, the physical state and phase behavior of the phospholipid greatly depend on the concentration of the solution (i.e. on the hydrated level) and length of the β and γ hydrocarbon chains. (2) The intermolecular interactions arising from the presence of other phospholipid molecules were not taken into account. These will have an effect on both hydrogen bonds and the conformation of the phospholipid molecules. (3) The hydration forces would change the energy of preferred conformations of the phospholipid. Our conformational analysis sampled only the energetics of isolated molecules. Some molecular mechanics calculations show that in bulk water, the influence of solvent results in a greater conformational flexibility (i.e. leads to smaller conformational energy differences and lower rotational barriers). It would appear from the results obtained in work and the available comparison with experimental crystallographic data that ab initio calculations can be use to simulate the crystalline structures of phospholipids. In some case though (e.g. GPE), depending on the polarizability of the headgroup the inclusion of few water molecules may be essential in order to obtain accurate crystal structures of phospholipids. Finally, we would like to emphasized that these calculations have been carried out without the presence of the alkaline chains. It is not clear at this point how the presence of chains would affect the molecular structure of the headgroups. The primary role of the chains is in building of the stable macroscopic structures such as bilayers etc., thus we suspect that their presence would not change the molecular structure of the headgroups very much.

Bibliography

[1] Brian L. Silver. *The Physical Chemistry of Membranes.* Creative and Services, Inc., NY, 1985.

[2] Gregor Cevc and Derek Marsh. *Phospholipid Bilayers.* John Wiley and Sons, Inc., USA, 1987.

[3] K.V. Damodaran and Kenneth M. Merz Jr. *Reviews in Computational Chemistry*,Vol. 5 Chapter 14, edited by Kenny B.Lipkowitz and Donald B. Boyd VCH publishers, Inc, New York, (1994).

[4] Irmin Pascher and Max Lundmark and Per-Georg Nyhom. *Biochimica et Biophysica Acta.*, **1113**:339, 1992.

[5] Michel Roux and Jean-Michel Neumann and Robert S.Hodges and Philippe F.Devaux and Myer Bloom. *Biochemistry*, **28**:40, 1989.

[6] Francesca M. Marassi and Peter M. Macdonald. *Biochemistry*, **30**:10558, 1991.

[7] B.A. Lewis and D.M. Engelman. *J.Mol.Biol*, **166**:211, 1983.

[8] Bernard Pullman and Héléne Berthod *FEBS letters*, **44**:266, 1974.

[9] Congxin Liang and Carl S.Ewig and Terry R.Stouch and Arnold T.Hagler. *J.Am.Chem.Soc.*, **115**:1537, 1993.

[10] Thomas B and Woolf and Benoit Roux. *J.Am.Chem.Soc.*, **116**:5916-5926, 1994.

[11] Bernard Pullman and Héléne Berthod and Nouhad Gresh. *FEBS letters.*, **53:2**:199, 1975.

[12] J.B. Lagowski and I.G. Csizmadia and G.J. Vancso *J. Quantum Chemistry*, **43**:595, 1992.

[13] J.B. Lagowski and G.J. Vancso *J. Quantum Chemistry*, **46**:271, 1993.

[14] H. Berthod and A. Pullman and N. Gresh. *Chemical Physics Letters.***33:1**:11,15 1975.

[15] Giuliano Alagona and Caterina Ghio and Peter Kollman. *J. Am. Chem.Soc*, **105**:5226, 1983.

[16] David G Gorenstein and Debojyoti Kar. *J. Am. Chem.Soc*, **99:3**:672, 1977.

[17] B. Jayaram and M. Mezei and D.L. Beveridge. *J. Am. Chem.Soc*, **110**:1691-1694, 1988.

[18] Giuliano Alagona and Caterina Ghio and Peter Kollman. *J. Am. Chem.Soc*, **107**:2229, 1985.

[19] R.P. Rand and V.A. Parsegian. *Biochimica et Biophysica Acta*, **988**:351 , 1989.

[20] N.W. Alcock. *Bonding And Structure.* Ellis Harwood, Inc., 1990.

[21] Max L.Berlowitz and K.Raghavan. *Langmuir*, **7**:1042-1044, 1991.

[22] H. Frischleder, S. Gleichmann and R. Krahl. *Chemistry and Physics of Lipids.*, **19**:144,1977.

[23] Hideo Akutsu and Toshiaki Nagamori. *Biochemistry*, **30**:4510-4516, 1991.

[24] Roland Kjellander and Stjepan Marcelja. *Chemical Physics Letters*, **1204,5**:393, 1985.

[25] Garret Vanderkooi. *Biochemistry* **30**:10760, 1991.

[26] Richard W.Pastor and Richard M.Venable and Martin Karplus. *Proc. Natl.Acad.Sci.USA*, **88**:892, 1991.

[27] H.Frischleder. *Chemistry and Physics of Lipids*, **27**:83, 1980.

[28] G. Peinel and H. Frischleder. *Chemistry and Physics of Lipids*, **24**:277 , 1979.

[29] A.E. Blaurock. *Biochimica et Biophysica Acta*, **650**:167 , 1982.

[30] Hideo Akutsu and Toshiaki Nagamori. *Biochemistry*, **30**:4510, 1991.

[31] L.J. Lis and M. Mcalister and N. Fuller and R.P. Rant. *Biophysical Journal*, **37**:657, 1982.

[32] Warren J. Hehre and Leo Radom and Paul R. Schleyer and John A.Pople. *Ab Initio Molecular Orbital Theory,* Chapter 3, John Wiley and Sons, Inc., USA, 1986.

[33] Attila Azabo and Neil S. Ostlund, *Modern Quantum Chemistry.* Macmillan,Inc.,USA, 1982.

[34] Gregor Cevc and Derek Marsh. *Phospholipid Bilayers.* John Wiley and Sons, Inc., USA, 1987.

[35] James B. Foresman and Eleen Frisch. *Exploring Chemistry with Electronic Structure Methods; A Guide to Using Gaussian*, Gaussian, Inc., USA, 1993.